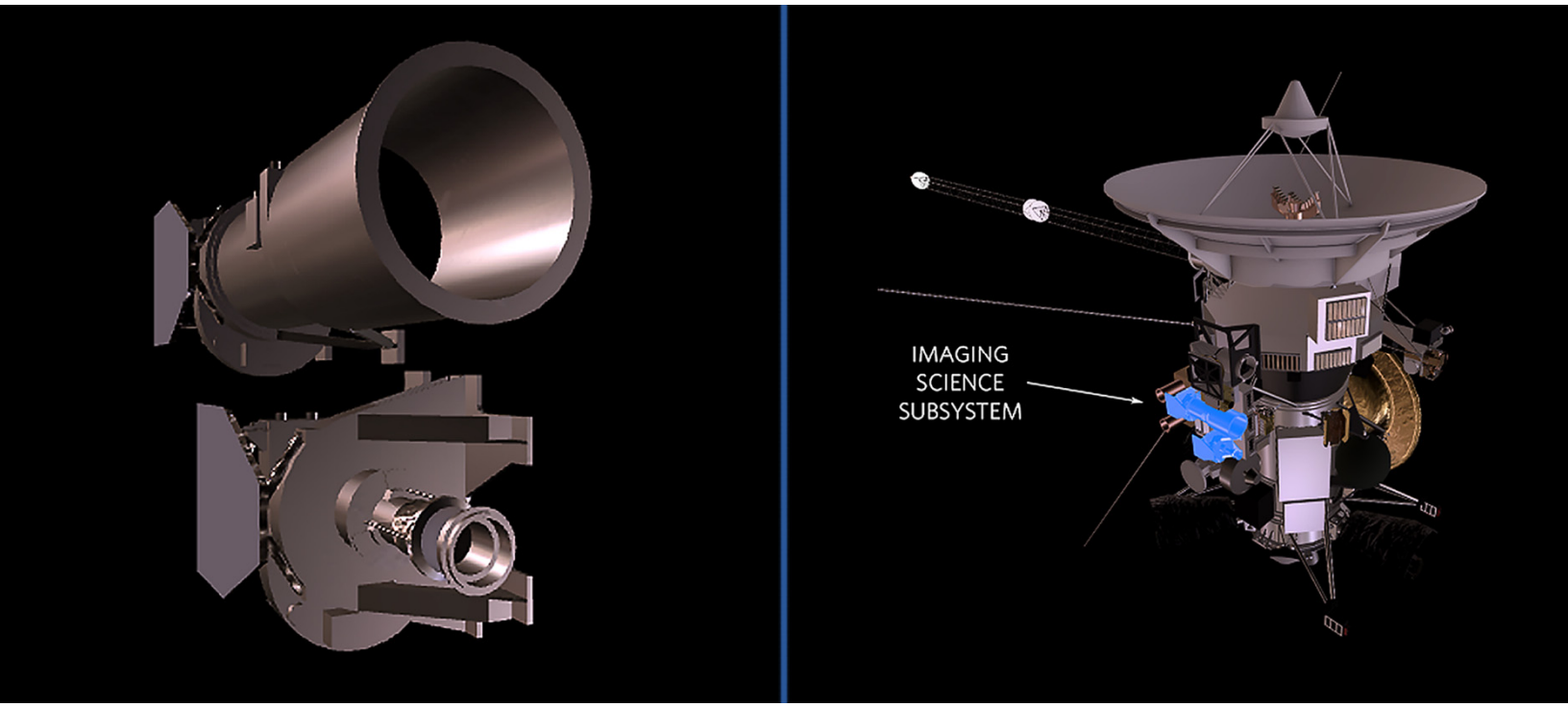

Imaging Science Subsystem

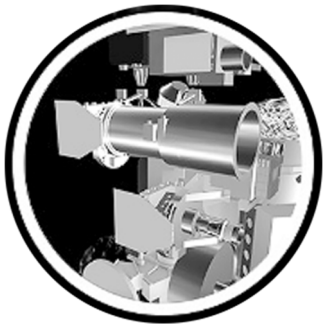

The Imaging Science Subsystem (ISS) consisted of both a wide-angle and a narrow-angle digital camera specifically designed for exploring the Saturn system. The **science objectives** included capturing lightning, investigating three-dimensional cloud structure and meteorology of Saturn's and Titan's atmospheres, imaging the surfaces of icy satellites, determining the composition and structure of Saturn's enormous ring system, and peering through the hazy Titan atmosphere to study its surface. The two cameras were able to capture beautiful images of the Saturn system as well, which inspired the public. In addition to acquiring scientific images, the cameras were also used for optical navigation to refine the knowledge of the spacecraft's trajectory and the position of the satellites.

Each camera included optics, two filter wheels, a shutter and detector head, plus their electronics. The cameras were sensitive to visible wavelengths of light and to some infrared and ultraviolet wavelengths. The filters for each camera were mounted on wheels to select the wavelengths to be sampled in each image. They were also capable of filtering for linear polarization.

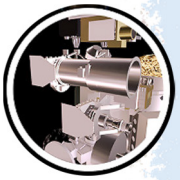

CONTENTS

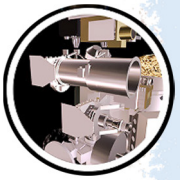

Figures

Tables

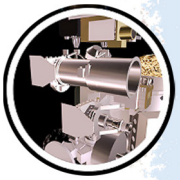

EXECUTIVE SUMMARY

The Cassini Imaging Science Subsystem (ISS) was the highest resolution imaging device on the Cassini mission and was specifically designed to image the bodies in the Saturn system. In its photometric sensitivity, linearity, dynamic range, spectral range—from near-ultraviolet (UV) to near-infrared (IR)—filter complement, resolving power, and variety of data collection and compression modes, it represented a significant advance over its predecessor carried on the Voyager spacecraft to Saturn in 1980 and 1981. The ISS was also the instrument used for optical navigation of the spacecraft.

The Cassini Imaging Science Subsystem (ISS) was the highest resolution imaging device on the Cassini mission and was specifically designed to image the bodies in the Saturn system.

The range of scientific objectives addressed by the ISS, as set forth early on by the Imaging Science team, included surveys of new phenomena and new moons/moonlets, as well as deeper characterization of known phenomena and features, throughout the Saturnian system out to the orbit of Iapetus, though seminal scientific results were obtained in a late-mission study of Saturn's irregular satellites, lying well beyond Iapetus. Among the specific goals of the ISS team were: determining the life-cycle of eddies and storms, and measuring wind speeds and photometric properties, in the Saturn atmosphere; revealing the geomorphology of the surface of Titan, searching for liquid hydrocarbons on the moon's surface, and characterizing the meteorology of the moon's atmosphere and its interactions with the surface; revealing at very high-resolution the architecture and dynamics of Saturn's rings; and mapping the surfaces of Saturn's ring-region and main icy satellites at high-resolution, including a search for plumes spouting from the surface of Enceladus.

This document summarizes the results of the imaging investigations conducted at Jupiter during Cassini's flyby of that planet on the eve of the year 2001, and at Saturn between the years 2004 and 2017. A perfectly engineered Jupiter flyby and several extensions that added nine years to the prime four-year Cassini mission at Saturn, the outstanding technical skill of the mission designers and the exquisite accuracy and richness of the 13-year Saturn orbital tour they produced, the commitment of the spacecraft flight team, the excellent performance of both the ISS and the spacecraft, and the perseverance, intelligence and sheer love of exploration of the imaging science team and the operations staff that supported it, together ensured the unqualified success of the ISS investigations at Saturn and Jupiter.

ISS INSTRUMENT SUMMARY

The ISS As-Built description is documented in Porco et al. [2004]. What follows in this section are excerpts from that paper.

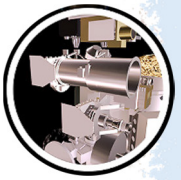

The Cassini ISS consists of two fixed focal length telescopes called cameras. The narrow-angle camera is 95 cm long and 40 cm × 33 cm wide (Figure ISS-1); the wide-angle camera is 55 cm long and 35 × 33 cm wide (Figure ISS-2). Both camera systems together have a mass of 57.83 kg. They sit on the remote sensing palette, fixed to the body of the Cassini orbiter, between the Visual and Infrared Mapping Spectrometer (VIMS) and the Composite Infrared Spectrometer (CIRS), and above the Ultraviolet Imaging Spectrometer (UVIS). The apertures and radiators of both telescopes are parallel to each other.

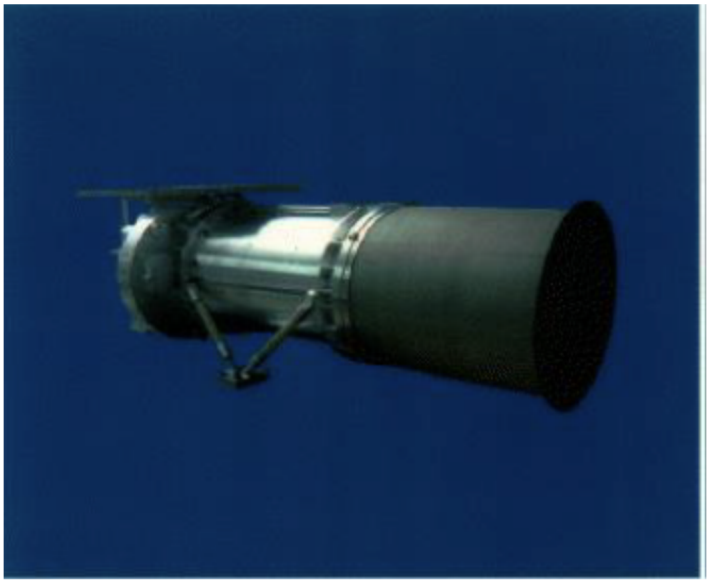

Figure ISS-1. Cassini ISS narrow-angle camera.

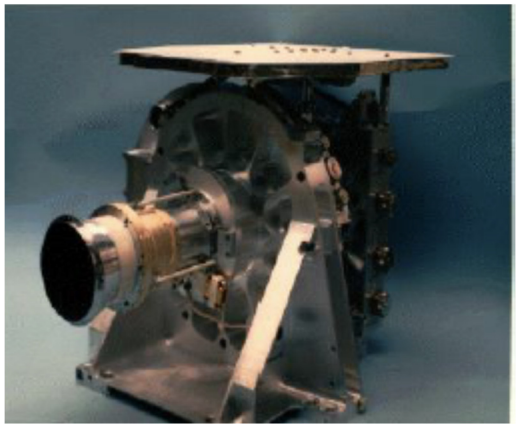

Figure ISS-2. Cassini ISS wide angle camera.

Each camera has its own set of optics, mechanical mountings, charge coupled device (CCD), shutter, filter wheel assembly, temperature sensors, heaters, various control electronics, engineering flight computer, and bus interface unit (BIU) to the central spacecraft command & data system (CDS). The electronics that control each camera consist of two parts: sensor head subassembly and the main electronics subassembly. The sensor head electronics supports the

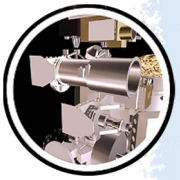

operation of the CCD detector and the preprocessing of the pixel data. The main electronics provide the power and perform all other ISS control functions, including generating and maintaining internal timing which is synchronized to the CDS timing of 8 Hz, control of heaters, and the two hardware data compressors. The Cassini engineering flight computer (EFC) is a radiation-hardened version of IBM's standard, general purpose MIL-STD-1750A 16-bit computer and is the ISS processor that controls the timing, internal sequencing, mechanism control, engineering and status data acquisition, and data packetization.

The narrow angle camera (NAC) is an f/10.5 reflecting telescope with an image scale of ~6 µrad/pixel, a 0.35° × 0.35° field of view (FOV), and a spectral range from 200 nm–1100 nm. Its filter wheel subassembly carries 24 spectral filters: 12 filters on each of two wheels. The optical train of the wide-angle camera (WAC), a Voyager flight spare, is an f/3.5 refractor with a ~60 µrad/pixel image scale and a 3.5° × 3.5° FOV. The refractor objective lens transmission limits the lower end of the spectral range on the WAC which is 380 nm–1100 nm. The WAC filter subassembly carries 9 filters in each of two filter wheels, for a total of 18 filters. In both cameras, images are acquired through two filters, one on each wheel, allowing in-line combinations of filters for greater flexibility, i.e., polarizers in line with other spectral filters, new band-passes created by the overlap of two spectral filters, etc.

KEY OBJECTIVES FOR ISS INSTRUMENT

The Cassini ISS instrument is designed to perform multispectral imaging of Saturn, Titan, rings, and icy satellites to observe their properties. Specific science objectives are as follows:

Cassini Early Mission (2004–2010)

Saturn and Titan atmospheres

1. Motions and dynamics.
    a. Basic flow regime (Titan).
    b. Poleward flux of momentum (u′v′).
    c. Poleward flux of heat (with CIRS).
    d. Life cycles and small-scale dynamics of eddies.
    e. Radiative heating for dynamical studies.
2. Clouds and aerosols.
    a. Cloud and haze stratigraphy (strongly couples with wind studies).

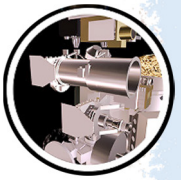

b. Particle optical properties.

c. Particle physical properties.

d. Auroral processes and particle formation.

e. Haze microphysical models.

3. Lightning (related to water clouds on Saturn, unknown for Titan).

4. Auroras (H and H_2 emissions on Saturn, N and N_2 emissions on Titan).

Titan surface

a. Map the surface of Titan in haze-penetrating spectral regions.

b. Search for bodies of liquid hydrocarbons (morphology, glints, etc.).

c. Determine surface/atmospheric interactions.

Rings

a. Ring architecture/evolution—azimuthal, radial, temporal variations across tour.

b. New satellites—orbits, masses/densities, effects on rings; complete inventory of Saturn's ring-region moons.

c. Search and characterize material potentially hazardous to Cassini—diffuse rings, arcs, Hill's sphere material, etc.

d. Orbit refinement of known satellites; temporal variations; resonant effects.

e. Particle/disk properties—vertical disk structure; particle physical properties and size distribution; variations across disk.

f. Spokes—formation timescales/process; periodic variations.

g. Diffuse rings (E-ring, G-ring)—structure, characterize particle properties.

Icy satellite objectives

a. Determine the general characteristics and geological histories of the satellites.

b. Define the mechanisms of crustal and surface modifications, both external and internal.

c. Investigate the compositions and distributions of surface materials, particularly dark, organic rich materials and low melting point condensed volatiles.

d. Constrain models of the satellites' bulk compositions and internal structures.

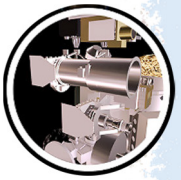

e. Investigate interactions with the magnetosphere and ring systems and possible gas and particle injections into the magnetosphere.

f. Search for plumes erupting from the surface of Enceladus.

Cassini Solstice Mission (2010–2017)

The ISS objectives for Cassini's late mission, or Solstice Mission, have been captured, by discipline, in a series of matrices outlined in the section entitled Science Objectives and Traceability Matrices.

ISS Science Assessment

The ISS Science Assessment describes if and how well ISS observations met the objectives listed in the sections entitled Key Objectives for ISS Instrument and Science Objectives and Traceability Matrices. Evaluation of the objectives are highlighted below. The Cassini Solstice Mission evaluation is given in the section entitled Science Objectives and Traceability Matrices.

Saturn and Titan Atmospheres

1. Motions and dynamics.

   a. Basic flow regime (Saturn and Titan). This goal was met on Saturn and Titan (see Porco et al. [2005a, 2005b] and subsequent ISS papers on Saturn's dynamics). ISS images confirm the discovery by the CIRS team that Titan's zonal flow has a pole location that is offset by a few degrees from Titan's solid body rotation pole [Roman et al. 2009; West et al. 2016].

   b. Poleward flux of momentum ($u'v'$). This goal was met for Saturn [Del Genio et al. 2007].

   c. Poleward flux of heat (with CIRS). This goal has not yet been met for Titan or Saturn. The appropriate ISS data were obtained but the analysis is not complete. However, there have been new global circulation models for Titan constrained by Cassini data [Lora et al. 2015].

   d. Life cycles and small-scale dynamics of eddies. This goal was partially met for Saturn (see Porco et al. [2005a]; Antuñano et al. [2018] and parts of other ISS papers on Saturn's clouds and dynamics).

   e. Radiative heating for dynamical studies. This goal was met [Li et al. 2011, 2013, 2015; Li et al. 2018].

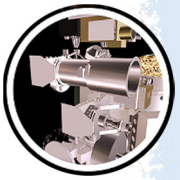

2. Clouds and aerosols.

    a. Cloud and haze stratigraphy (strongly couples with wind studies). This goal was partially met [West et al. 2009, 2016].

    b. Particle optical properties. This goal was met for a restricted latitude band on Saturn [Pérez-Hoyos et al. 2016]. Appropriate data were obtained for other latitudes but the analysis is not complete.

    c. Particle physical properties. This goal has not yet been met. The appropriate data were obtained but the analysis is not complete.

    d. Auroral processes and particle formation. The goal was met for Saturn [Dyudina et al. 2010, 2015].

    e. Haze microphysical models. This goal has not yet been met. The appropriate data were obtained but the analysis is not complete.

3. Lightning (related to water clouds on Saturn, did not know what to expect for Titan). Lighting on Saturn was detected and studied. It was found correlated with Saturn Electrostatic Discharges (see Porco et al. [2005a] and subsequent ISS papers). No lightning was detected for Titan.

4. Auroras (H and H_2 emissions on Saturn, N and N_2 emissions on Titan). Auroras on Saturn were studied [Dyudina et al. 2010, 2015]. Airglow on Titan was discovered [West et al. 2012; Lavvas et al. 2014].

Titan Surface

a. Map the surface of Titan in haze-penetrating spectral regions. The goal was met, providing a global albedo map of Titan [McEwen et al. 2005a, 2005b; Turtle et al. 2009, 2011a, 2011b, 2011c, 2013, 2018a; Perry et al. 2005, 2007; Stephan et al. 2009]. Reprocessing using the complete ISS dataset for much improved signal/noise is underway [Karkoschka et al. 2017a, 2017b].

b. Search for bodies of liquid hydrocarbons (morphology, glints, etc.). The goal was met, with the ISS discovery of the largest lakes and seas in both the south and northern polar regions, from morphology [http://ciclops.org/view.php?id=1161; http://ciclops.org/view.php?id=1194; http://ciclops.org/view.php?id=2607; http://ciclops.org/view.php?id=2631] and temporal changes [Turtle et al. 2009; Turtle et al. 2011b, 2011c, 2018a] and by searching for glints [Fussner et al. 2005], although no glints were found at ISS wavelengths.

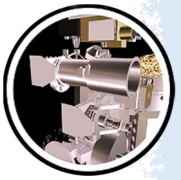

c. Determine surface/atmospheric interactions. The goal was met [Porco et al. 2005b], especially via co-analysis of ISS with other datasets [Turtle et al. 2009, 2011a, 2011b, 2011c, 2018a, 2018b; Barnes et al. 2013; Birch et al. 2017].

Rings

a. Ring architecture/evolution—azimuthal, radial, temporal variations across tour. This goal was met, with substantial discoveries about the azimuthal, radial, and temporal characteristics of the rings [Porco et al. 2005c]. See reviews by Cuzzi et al. [2018]; Murray and French [2018]; Nicholson et al. [2018].

b. New satellites: orbits, masses/densities, effects on rings; complete inventory of Saturn's inner moons. This goal was met. See Porco et al. [2005c] and subsequent papers reporting discovery of Daphnis, Aegaeon, Methone, Pallene, Anthe, Polydeuces; and a survey that verified the non-existence of shepherd moons in most of the gaps within the main rings [Spitale 2017].

c. Search and characterize material potentially hazardous to Cassini—diffuse rings, arcs, Hill's sphere material, etc. This goal was met, with substantial discoveries about current resonant characteristics and long-term evolution of satellite orbits [Porco et al. 2005c; Jacobson et al. 2006a, 2006b, 2008; Lainey et al. 2017], as well as an unexpected sudden change in the orbit of Daphnis [Jacobson 2014].

d. Orbit refinement of known satellites; temporal variations; resonant effects. This goal was met, with substantial discoveries about current resonant characteristics and long-term evolution of satellite orbits [Porco et al. 2005c; Jacobson et al. 2006a, 2006b, 2008; Lainey et al. 2017], as well as an unexpected sudden change in the orbit of Daphnis [Jacobson 2014].

e. Particle/disk properties—vertical disk structure; particle physical properties and size distribution; variations across disk. This goal was met, with substantial discoveries about particle and disk properties [Porco et al. 2005c]. See reviews by Cuzzi et al. [2018]; Estrada et al. [2018]; Murray and French [2018]; Spahn et al. [2018]; Spilker et al. [2018].

f. Spokes—formation timescales/process; periodic variations. This goal was met, with detailed studies of the workings of spokes [Mitchell et al. 2006, 2013].

g. Diffuse rings (E-ring, G-ring): structure, characterize particle properties. This goal was met, with substantial discoveries about the structure and particle properties of diffuse rings [Porco et al. 2005c]. See review by Hedman et al. [2018].

Icy Satellites

a. Determine the general characteristics and geological histories of the satellites. These goals were met [Porco et al. 2005d; Porco et al. 2006]. See comprehensive reviews

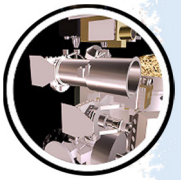

and references therein: Patterson et al. [2018]; Schenk et al. [2018]; Verbiscer et al. [2018]; Postberg et al. [2018]; Kirchoff et al. [2018]; Goldstein et al. [2018]; Thomas et al. [2018]; Spencer et al. [2009]; Matson et al. [2009]; Jaumann et al. [2009a]; Roatsch et al. [2009a]; Dones et al. [2009].

b. Define the mechanisms of crustal and surface modifications, both external and internal. This goal was partially met [Porco et al. 2005d; Porco et al. 2006; Patterson et al. 2018; Schenk et al. 2018; Thomas et al. 2018; Kirchoff et al. 2018; Postberg et al. 2018; Wagner et al. 2006, 2007, 2009, 2010; Matson et al. 2009; Dones et al. 2009].

c. Investigate the compositions and distributions of surface materials, particularly dark, organic rich materials and low melting point condensed volatiles. This goal was partially met [Porco et al. 2005d]. See comprehensive reviews and references therein: Verbiscer et al. [2018]; Schenk et al. [2018]; Thomas et al. [2018].

d. Constrain models of the satellites' bulk compositions and internal structures. This goal was met [Porco et al. 2006; Thomas et al. 2007a, 2016, 2018; Thomas 2010; Castillo-Rogez et al. 2018].

e. Investigate interactions with the magnetosphere and ring systems and possible gas and particle injections into the magnetosphere. This goal was partially met [Thomas et al. 2018; Verbiscer et al. 2014; Annex et al. 2013; Verbiscer et al. 2018; Schenk et al. 2017; Spencer and Denk 2010].

f. Search for plumes emerging from the surface of Enceladus. This goal was met [Porco et al. 2006; Porco et al. 2014].

ISS Saturn System Science Results

Titan

Imaging of Titan's surface, with global mapping at 4 km or better resolution, shows the distribution and wide variety of surface features, including first sighting of a hydrocarbon lake in the south polar region (Ontario Lacus) [http://ciclops.org/view.php?id=1161; http://ciclops.org/view.php?id=1194], the first sighting of Titan’s largest sea in the north polar region (Kraken Mare) [http://ciclops.org/view.php?id=2607; http://ciclops.org/view.php?id=2631], both confirmed as liquid-filled later by other Cassini instruments and Titan's largest impact crater (Menrva). Analysis of the entire equatorial dataset acquired over the duration of the mission indicates surface albedos range from 0.25 in the dunes to 0.9 at Hotei Arcus [Porco et al. 2005b; Perry et al. 2005, 2007; McEwen et al. 2005a, 2005b; Turtle et al. 2009; Stephan et al. 2009; Karkoschka et al. 2017a, 2017b].

Strategies have been developed for effective imaging of Titan's atmosphere and surface as well as image processing techniques to achieve as high signal-to-noise ratio from the surface as

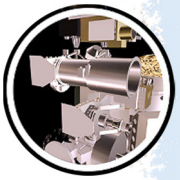

possible. [Porco et al. 2005b; Perry et al. 2005, 2007; Fussner et al. 2005; McEwen et al. 2005a, 2005b; Turtle et al. 2009, supplementary material; Karkoschka et al. 2017a, 2017b].

Features ISS has identified and mapped on the surface include:

- Equatorial dune fields and Xanadu, impact craters, polar lakes and seas, and undifferentiated mid-latitude plains [Porco et al. 2005b; McEwen et al. 2005a, 2005b; Turtle et al. 2009; Lopes et al. 2016].
- Possible shoreline changes at Titan lakes [Turtle et al. 2009, 2011c].
- Identification of a bright surface deposit at Titan's North Pole [Turtle et al. 2013].
- Joint analyses of surface processes and features, including Hotei Arcus; Tui Regio; surface modification associated with seasonal rainfall; and polar lakes, seas, and implications for Titan hydrology [Barnes et al. 2005, 2006; Turtle et al. 2009, 2011b, 2011c; Hayes et al. 2011; Jaumann et al. 2009b].

Surface darkening was observed from Titan rainstorms at Arrakis Planitia in 2004-2005 [Turtle et al. 2009] and at ~30° south latitude, including Concordia Regio, Adiri, in 2010–2011 [Turtle et al. 2011b, 2011c] as well as subsequent isolated brightening [Turtle et al. 2011b; Barnes et al. 2013].

Titan's main haze is almost featureless but shows hemispheric contrast that changes with season. This was known from Voyager images. Work with Cassini images [Roman et al. 2009] showed that the pole of rotational symmetry determined by the shape of the contrast boundary is displaced from Titan's solid body rotational pole by a few degrees, and corroborates the finding of pole displacement by Achterberg et al. [2008]. This finding opens up a new mystery about Titan's atmospheric dynamics.

The behavior of the detached haze provides new information to test and improve Titan dynamical models of the mesosphere and upper stratosphere.

Titan's detached haze, first seen in Voyager images, was again seen in Cassini images, but at altitudes that depend on season [Porco et al. 2005b; West et al. 2011, 2018]. West et al. [2011] showed that the detached haze underwent rapid descent centered around the northern spring equinox in 2009. It reached the same altitude as seen in Voyager images (near 350 km) one Titan year after the Voyager images were obtained. From about mid-2012 to early 2016 the detached haze was not seen in ISS images. It emerged in early 2016 but was weak, and showed irregular variations in latitude and time. The behavior of the detached haze provides new information to test and improve Titan dynamical models of the mesosphere and upper stratosphere.

In 2012, a distinct cloud was observed at an altitude of 300 km near Titan's south pole [West et al. 2016]. Spectral measurements by the VIMS instrument indicate an HCN ice composition [de Kok et al. 2014]. ISS measured altitude, morphology, texture, and motions of the cloud and showed that the atmospheric rotation at 300 km altitude is around a pole that is offset from Titan's solid

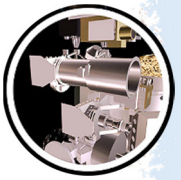

body rotational pole. Texture suggests that the cloud is undergoing open-cell convection, an unusual configuration for high-altitude clouds initiated by downwelling.

ISS documented the distribution, morphology, speeds, and seasonal behavior of Titan's tropospheric clouds starting on approach in April 2004 (late southern summer on Titan) through September 2017 (after the northern summer solstice in May 2017), as well as implications for atmospheric general circulation models and Titan's methane cycle including sub-surface reservoirs. During Titan's late southern summer, extensive convective cloud systems were common over Titan's south pole, and in the case of a large cloud in October 2004 led to substantial precipitation. Starting in 2007 as the Sun rose in Titan's north, clouds began to appear at northern latitudes >55° N and were relatively common until the equinox when northern cloud activity dropped off precipitously. The expectation from atmospheric models had been that cloud activity would increase at high northern latitudes as northern summer approached. However, only small isolated cells were seen near Titan's north pole, leaving the mystery of when/if north polar cloud systems form during northern summer. [Porco et al. 2005b; Turtle et al. 2009, 2011a, 2018a, 2018b; Mitchell et al. 2011].

In addition to polar clouds, Titan exhibited a preference for mid-latitude clouds, at ~40° S early in the mission during late southern summer, and gradually drifting poleward to ~60° S by equinox and beyond [Porco et al. 2005b; Turtle et al. 2009, 2011a]. After equinox, similar mid-latitude clouds were expected in the northern hemisphere but were not observed with any regularity until early 2016 (first at ~50° N and drifting poleward to 60° N). These cloud bands imply a seasonal Hadley circulation with rising motion at these latitudes, a feature that can only be predicted by models that include methane moist convection. However, the timing of the transition from the southern summer to the northern summer configuration is observed to be several Earth years later than predicted by the models [Turtle et al. 2018b]. Similar clouds appeared with lower frequency near ~15° S earlier in the mission and ~30° N late in the mission.

Spectral dependence of detection of some north-polar cloud features was observed starting in 2016, with VIMS detecting features at 2.1 μm that are not seen by ISS at 938 nm [Turtle et al. 2016, 2018a, 2018b] or by VIMS at wavelengths both shorter and longer than 2.1 μm.

Atmospheric airglow observations were made while Titan was in Saturn's shadow. [West et al. 2012; Lavvas et al. 2014].

Enceladus

Early ISS observations of Enceladus and its plume yielded many new discoveries, all refined in subsequent papers. Only the major highlights from these papers are presented next.

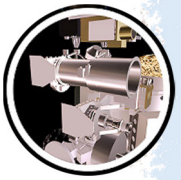

Plume

- A plume of fine, icy particles was discovered erupting from the south polar region of Enceladus in images taken in January and February 2005 [Porco et al. 2006]. In November 2005 the plume was resolved into discrete jets, or geysers, that eject the particles that eventually supply Saturn's E-ring, carried aloft by water vapor in the jets.
- The first argument is presented that the jetting activity at the South Pole is the result of venting from subsurface reservoirs of liquid water [Porco et al. 2006].
- Cassini's revised estimates of the bulk density of Enceladus and the inferred rock mass fraction suggest that radiogenic heating is not the dominant source of heat within the moon, compared with estimates of tidal heating via the Dione:Enceladus 2:1 resonance [Porco et al. 2006].
- In a multi-year high-resolution imaging survey of the south polar terrain (SPT), ~100 discrete geysers were found erupting from the four main fractures crossing the SPT [Porco et al. 2014]. A later claim—that the majority of the jet detections were not real and rather the result of observational bias [Spitale et al. 2015]—was refuted [Porco et al. 2015].
- Anomalously hot regions observed by CIRS at low resolution were found to be coincident with the SPT fractures [Porco et al. 2006; Spitale and Porco 2007]. At very high-resolution, very small scale (~10 m) hot spots reported by VIMS were found coincident with the surface locations of individual discrete geysers [Porco et al. 2014]. This correlation, along with the small size estimates of the hot spots derived from the observations of other instruments, strongly suggests that the source of the surface warmth is not shear heating but latent heat from the condensation of vapor onto the near-surface walls of the vents [Porco et al. 2014], allowing for a deep source of the venting materials.
- The plume that is formed from the geysers varies diurnally due to the varying extensional tidal stresses across the surface, with a phase lag of ~45° (or ~4.5 hours) compared to simple tidal models that assume an elastic ice shell [Nimmo et al. 2014]. The origin of the phase lag is not yet clear. Notable is the observation that the plume never goes to zero strength. Behounkova et al. [2015] showed the variation is best described by the cyclical variation in the normal stresses across the fractures, averaged over the SPT, and simulated the viscoelastic tidal response of Enceladus with a full 3-D numerical model. The delay in eruption activity may be a natural consequence of the viscosity structure in the south-polar region and the size of the putative subsurface ocean.
- Individual geysers were observed to be time variable, turning on and/or off on timescales that were not comparable to the diurnal cycling of stresses [Porco et al. 2014]. This was taken as an indication that condensation of ice in the vents leads to the stochastic clogging of the vents and consequently the shutoff of geysers, but

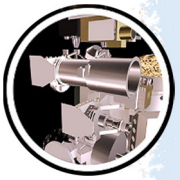

averaged across the SPT, the plume is continuous in time while variable in strength. The estimated timescale for the clogging process is months to a couple of years [Porco et al. 2006].

- Models of vapor arising by sublimation from the walls of the cracks and then condensing to make ice particles [Ingersoll and Pankine 2010] yield ice mass fractions no greater than 1.3%, confirming an earlier argument [Porco et al. 2006] that ice/vapor ratios of order unity favor a liquid source rather than sublimating ice.
- Observations by ISS of plume brightness at scattering angles ranging from 2.25° to 5.30°, which are only possible when the spacecraft is in Saturn's shadow, yield estimates of the particle size distribution in the plumes [Ingersoll and Ewald 2011]. The best-fitting distributions have a median mass-weighted radius r0 = 3.6 μm and differential power laws of r1 and r-3 for r << r0 and r >> r0, respectively. If the particles were solid ice spheres, the ice/vapor ratio is in the range 0.35–0.70, which would favor a liquid source.
- The ISS observations at scattering angles of 2.25–5.30° yield estimates of 51 ±18 kg s^{-1} for the mass leaving the vents and 9% for the fraction that escapes into the E-ring [Ingersoll and Ewald 2011]. The implied lifetime of particles in the E-ring is then ~8 years, but this assumes the particles are solid ice spheres. The estimate would be longer if the particles were fluffy aggregates rather than solid ice.
- Modeling the particles as irregular aggregates of spherical monomers yields ice/vapor ratios of 0.07 ±0.01 for the plume [Gao et al. 2016]. Therefore, a vapor-based origin for the plume particles cannot be ruled out if plume brightness is the only criterion.
- Comparison of ISS measurements of plume particle number density with those taken by other Cassini instruments has significantly reduced initial differences among them (factors of 10–20) by accounting for the temporal variability of the plume and the differing times and geometries of the different observations [Porco et al. 2017]. These results remove the need to assume low-density particle aggregates [Gao et al. 2016] to bring about agreement among all Cassini measurements. The preferred exponent in a differential size distribution was q = 3 at an altitude of 50 km.
- During the early years of the Cassini mission, 2006–2010, the computed diurnally averaged ice mass production rate that reproduces ISS observations of plume mass at 50 km altitude was 29 ±7 kg/s [Porco et al. 2017]. This new value is likely a lower limit as it does not account for heavier ice particles that don’t make it up to 50 km altitude. Because of the time-varying behavior of the plume, comparison of quantities of interest must be made at the same time and geometries, or nearly so. Utilizing a diurnally averaged estimate from other Cassini instruments of vapor production rate for the same time period, a solid to vapor ratio > 0.06 was computed. At 50 km altitude, the plume’s peak optical depth during the same time period was ~10^{-3}; by 2015, it was ~10^{-4}.

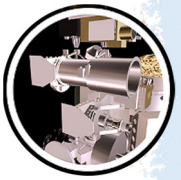

- Analysis of ISS observations from 2005–2015 reveals a decrease of plume brightness by roughly a factor of two [Ingersoll and Ewald 2017]; suggested explanations included a long-period tide (the decreasing phase of an 11-year cycle in orbital eccentricity), clogging of vents over time, or seasonal thermal effects. (The observations are from 47 individual days, usually with many observations per day, and document in great detail the four-fold to five-fold variation with orbital phase.)
- Thousands of ISS observations of the plume extending over the entire Cassini mission, through late 2017 [Porco et al. 2018], showed, after a multi-year decline in plume brightness, a resurgence to a brightness level exceeding that earlier in the mission. The analysis of this result confirmed previous suggestions [Nimmo et al. 2016] that the plume is varying on three time periods associated with the Dione/Enceladus 2:1 orbital resonance (diurnal, ~4 years and ~11 years) and that secular clogging and seasonal effects can be dismissed. The brightness of the secondary peak at MA ≈55°, near mission's end, declined substantially from its early-mission and mid-mission levels.
- A model of flow of vapor in vertical cracks yields estimates of crack width in the range 0.05–0.075 m [Nakajima and Ingersoll 2016]. A wider crack would yield an unacceptably high ratio of escaping vapor compared to that condensing on the walls as inferred from the observed radiated power.
- A model of the liquid-filled cracks introduces the concept of controlled boiling, in which backpressure limits the rate of evaporation [Ingersoll and Nakajima 2016]. The backpressure arises from frictional stress of the walls on the upward-flowing vapor, and leads to a steady state in which the evaporation rate is proportional to the width of the crack divided by its depth.
- The average geothermal flux into the sea beneath Enceladus' SPT was estimated to be comparable to that of the average Atlantic, of order 0.1 W/m^2 [Porco et al. 2017]. Based on this value, microbes could be present on Enceladus and concentrations at its seafloor hydrothermal vents could be comparable to those on Earth, ~10^5 cells/mL. Bubble-scrubbing, a process well-known to marine microbiologists, could enhance microbial concentrations over native ocean values by up to factors of 1000's in the Enceladus' plume. Estimates of microbial concentrations that might be collected in future missions of various designs were given.

Body and surface

- Fracturing and tectonic modification of Enceladus' surface is much more pervasive than predicted from Voyager imaging—tectonic resurfacing has likely played a major role in shaping youthful appearance of Enceladus. Intensely modified expanses are regionally divided by diverse styles of tectonic features among which are deep rifts, horst-and-graben terrains, folded ridges, braided or vermicular

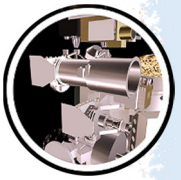

networks of grooves, and curvilinear ridges and fractures [Helfenstein et al. 2005a; Rathbun et al. 2005; Porco et al. 2006].

- An ubiquitous spidery network of sub-parallel, curvilinear, high-angle cracks appear to dissect topographic structures into vertical slabs. Numerous impact craters have been modified by cracks, the orientations of which appear to have a radial component, indicating that the extensional stress field that caused the fractures was influenced by stresses due to the craters themselves [Helfenstein et al. 2005a; Rathbun et al. 2005].
- A network of kilometer-scale ridges (now called Dorsa) and linear arrays of rounded domes are present on the trailing hemisphere of Enceladus and they appear to have extruded through preexisting surface fractures. Some wrinkled, flow-like features with lobate margins are found near the ridge and dome features. New details of viscously-relaxed craters, first seen by Voyager, include central dome features with structurally breached summits [Helfenstein et al. 2005a].
- A geologically active province at the south pole of Saturn's moon Enceladus is circumscribed by south-facing scarps and a chain of folded ridges and troughs at ~55° S latitude. The terrain southward of this boundary is distinguished by its albedo and color contrasts, elevated temperatures, extreme geologic youth, and narrow tectonic rifts that exhibit coarse-grained ice and coincide with the hottest temperatures measured in the region [Porco et al. 2006].
- The placement, morphology, and orientations of the SPT boundary is consistent with its interpretation as a convergent tectonic boundary arising from global deformation due to axial shortening along Enceladus' spin axis. Youthful systems of N-S tending fractures extending from Y-shaped discontinuities (i.e., a Y-shaped tectonic pattern of scarps and confined arcuate ridges that interrupt the SPT boundary) are also consistent with this deformation mechanism [Porco et al. 2006; Helfenstein et al. 2006; Helfenstein 2014].
- Flexural uplift along the ~3.5 Ga aged Harran Sulci rift zone in the tectonically resurfaced trailing hemisphere of Enceladus indicates that, at the time of formation, the mechanical lithospheric thickness was 2.5 km with heat fluxes comparable to average values measured in the active south polar region [Giese et al. 2008b].
- Tiger stripe fractures fall into a family of gradational morphological types. Smooth Flank formations coincide with volcanically active sections. The highest-resolution images (<10 m/pixel) show ice blocks up to tens of meters in size that are widely but non-uniformly distributed over a variety of terrain units. The upraised flanks and valley walls are mantled in places by smooth fluffy-looking deposits, most likely accumulations of coarse-grained plume fallout. Peculiar narrow lenticular ridges (now called shark fins), perhaps emplaced by extrusion or as icy pyroclastic deposits, rise from tens to hundreds of meters along the medial fissures of some tiger stripes. The Smooth Flank formations grade into Platy Flank formations near the ends of the tiger stripes. Platy Flank formations are notably less covered by

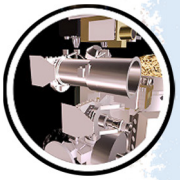

smooth materials giving a somewhat armored surface that reveals small surface cracks. Relict tiger stripe materials exist at the segmented, distal ends of tiger stripes and in at least one large system of parallel ridges and medial troughs eastward of Damascus Sulcus that are superficially similar in appearance and scale to the tiger stripes, but with smooth, strongly muted topography [Helfenstein et al. 2008; Spencer et al. 2009].

- The active Tiger Stripe rifts are separated by a system rounded, platy-textured, elongate hills and a conspicuous system of quasi-parallel ropy ridges and grooves that have spacings and dimensions comparable to the tiger stripe flanks themselves (now called funiscular terrain) [Porco et al. 2006; Helfenstein et al. 2008; Spencer et al. 2009].
- Enceladus' shape deviates slightly from a nominal equilibrium ellipsoid and has a south polar basin with a depth of ~0.4 km [Porco et al. 2006; Thomas et al. 2007a; Thomas 2010; Nimmo et al. 2011].
- The leading hemisphere of Enceladus has distinct geological provinces that exhibit diverse tectonic styles and different cratering histories. The highly tectonized terrains are bounded by a prominent broad annulus of grooved and striated terrains that ranges from about 60 km to over 140 km in width. It surrounds a complex arrangement of tectonic structures, including a conspicuous province near 30° N, 90° W of curvilinear massifs and roughly orthogonal-trending ridged-troughs that define a crudely radial and concentric pattern relative to a point near 25° N, 125° W. This angular sector, about 65° in width, may be the partial remains of an ancient impact basin with a diameter of about 180 km. It could also be the surface expression of an ancient, large diapir. Peculiar quasi-radial ridged-troughs superficially resemble extinct, topographically degraded examples of tiger stripes seen elsewhere on Enceladus. While these features may have a different fracture origin from tiger stripes, their comparable morphology suggests that long ago they may have expressed a similar style of fissure volcanism. Among our other significant findings is a region near 10° S, 60° W of rounded, rope-like sub-parallel ridges similar to ropy (funiscular) plains materials previously found only in the SPT region near active tiger stripes [Helfenstein 2010].
- The topography of a ~1 km high, 250 km wide bulge on the leading side of Enceladus has undergone strong resurfacing and has distinct boundaries to surrounding lower lying cratered terrains; it is consistent with the presence of convection-related warm ice at depth in isostatic equilibrium with surrounding non-convecting cooler ice. [Giese et al. 2010b].
- Tectonic deformation is a major source of blocky-ice features in the SPT. Impact cratering as well as mass wasting, perhaps triggered by seismic events, cannot account for a majority of ice-block features within the inner SPT [Martens et al. 2015; Giese et al. 2010a].

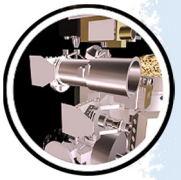

- Geologically young cycloidal fracture segments are found over a variety of different locations on the surface of Enceladus, including the SPT. These features likely have initiated as tension cracks with their form being controlled by diurnal variation of tides, as suggested for Europa. Such a mechanism requires that the ice be mechanically weak and, to allow for sufficient tidal amplitude, there must be a fluid layer below the icy surface. Thus, rather than being confined to just southern latitudes, our observations hint at the presence of fluid layers beneath other areas on Enceladus, potentially at a global sub-surface ocean in recent times [Giese et al. 2011a].
- Geysers emplaced along the three most active tiger stripe fractures (Damascus Sulcus, Baghdad Sulcus, and Cairo Sulcus) occur in local groupings with relatively uniform nearest-neighbor separation distances (~5 km). Their placement may be controlled by uniformly spaced *en echelon* Riedel-type shear cracks originating from left-lateral strike-slip fault motion inferred to occur along tiger stripes. The spacing would imply a lithosphere thickness of ~5 km in the vicinity of the tiger stripes [Helfenstein and Porco 2015].
- The orientations of tilted geyser jets are not randomly distributed; rather their azimuths correlate with the directions either of tiger stripes, cross-cutting fractures, or else fine-scale local tectonic fabrics. Periodic changes of plume activity may be significantly affected by crosscutting fractures that open and close at different times than the tiger stripes that they intersect [Helfenstein and Porco 2015].
- Geyser jets and their associated local hot-spots have the capacity to alter the morphology of surrounding icy geological features, possibly through ablation and sublimation-aided erosion, but also through condensation (which is the source of the heat) and the creation of vent plugs. Plausible morphological examples of ablation and sublimation-erosion include formations of pinnacles along the ridge crests surrounding active areas on and near tiger stripes fractures, possible scour marks or dust trails surrounding active vents, and the excavation of circular pit-like enlargements of active fracture troughs [Helfenstein and Porco 2015].
- Enceladus has a global subsurface ocean which was detected by multi-year imaging observations of forced librations in Enceladus' rotation [Thomas et al. 2016].

Geyser jets and their associated local hot-spots have the capacity to alter the morphology of surrounding icy geological features, possibly through ablation and sublimation-aided erosion, but also through condensation … and the creation of vent plugs.

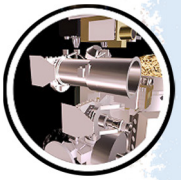

- An exceptionally high-standing (1750 m), 100 km long sawtooth-shaped ridge in the Samarkand Sulci fault band likely initiated by rift flank-uplift caused by extension followed by sinistral shear and compression 3.7 ±0.7 Ga ago, emplacing small-scale fragments sticking out of the surface and creating a (previously enigmatic) pattern of black spots on the sun-facing side of the ridge [Helfenstein et al. 2005a]. The estimated effective elastic lithospheric thickness is ~0.36 km at the time of formation compared to a present-day lower limit of 1.5 km obtained from lithospheric loading modelling [Giese et al. 2017; Wagner et al. 2017; Roatsch et al. 2016].
- A global chain of topographic depressions on Enceladus indicate that this synchronously locked moon has likely undergone True Polar Wander by ~55° about the tidal axis, from an early orientation in which the present terrain near (77° W, 40° N) would have been located at the paleo north pole [Tajeddine et al. 2017a].
- The large collection of high-resolution Cassini ISS images of Enceladus has provided a complete global photomosaic Enceladus base map at 100 m/pixel resolution [Roatsch et al. 2008a; Becker et al. 2016].

Main Icy Satellites (except Enceladus)

Mid-sized icy moons overview

- Accurate values for fundamental whole-body physical properties of the moons were obtained. These include mean radii, densities, shapes, etc., for example, Thomas [2010]; Thomas et al. [2018]; Castillo-Rogez et al. [2018], and also photometric quantities like geometric albedo, the phase integral, or Hapke photometric model parameters [Verbiscer et al. 2018].
- The sizes and shapes of the six mid-sized icy satellites were measured from ISS data. Mimas, Enceladus, Tethys, Dione and Rhea are well described by triaxial ellipsoids; Iapetus is best represented by an oblate spheroid [Thomas et al. 2007a].
- Global photomosaic base maps (ISS CL1:CL2 filter) were completed at better than ~400 m/pxl over the surfaces (Mimas to Rhea; ~800 m/pxl for wide parts of Iapetus) [Roatsch et al. 2009a; Roatsch et al. 2006, 2008a, 2008b, 2009b, 2012, 2013; Schenk et al. 2011; Schenk et al. 2018].
- Images of selected or serendipitous targets at very high-resolution (up to ~3 m/pxl) included bright-ray crater Inktomi (Rhea), fracture networks on Tethys, Dione, and Rhea, equatorial spots on Rhea, parts of Iapetus's ridge (Toledo Montes), etc.
- Almost complete stereo imaging was acquired for all mid-sized icy satellites from Mimas to Rhea (and > 50% for Iapetus), and global topographic maps are now essentially complete for each of the five moons [Schenk et al. 2018].

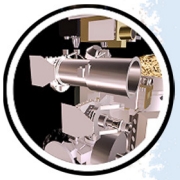

- Impact craters dominate the surfaces and provide the primary means of estimating terrain ages as well as many other properties of the surfaces [Dones et al. 2009; Kirchoff and Schenk 2010; Schenk et al. 2018; Kirchoff et al. 2018].
- However, crater saturation (crater density has reached a point where the formation of new craters erases the same area of older craters, and crater density has reached an equilibrium) is found on probably most, if not all, heavily cratered terrains on the mid-sized icy moons [Dones et al. 2009; Kirchoff et al. 2018].
- A predicted apex-antapex asymmetry in crater density is not observed at all on the Saturnian moons. Non-synchronous rotation is considered unlikely as the cause [Kirchoff et al. 2018].
- Secondary craters have been identified [Schmedemann et al. 2017; Schenk et al. 2018].
- None of the unusual crater landforms (like multi-ring basins or shallow distorted craters on the Galilean moons) seen on icy worlds that have confirmed internal oceans are seen on the mid-sized moons. However, this does not preclude possible oceans [Schenk et al. 2018].
- Global mapping has revealed geologically complex worlds. All (except perhaps Iapetus) have been tectonically deformed to different degrees. Almost all tectonic landforms are interpreted as extensional structures [Schenk et al. 2018].
- The trailing sides of Tethys and Dione and to a lesser degree of Rhea are darker than the respective leading sides. This is due to E-ring material infalling preferentially on the leading sides and has originally been discovered in Voyager data. The colors of the trailing sides are also redder than the leading sides of these moons.
- Potential endogenic processes acting on Saturn's mid-sized moons are cryovolcanism, tectonism, and viscous relaxation, see Kirchoff et al. [2018] and numerous references therein.
- Smooth plains were observed on Tethys and Dione by Voyager, and Cassini mapping confirmed that these are the only moons with such plains [Jaumann et al. 2009b].
- Wispy terrains, discovered on the trailing hemispheres of Dione and Rhea by Voyager, are rather recent and relatively pristine fracture networks. Their morphology and distribution are similar on these two moons [Schenk et al. 2018].
- The orbits and masses of the mid-sized moons have been largely improved.

Mimas

- Mimas was globally mapped at 216 m/pxl [Roatsch et al. 2013].

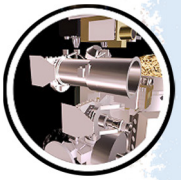

- It is a heavily cratered object with little evidence of endogenic resurfacing [Schmedemann et al. 2015].
- There was no targeted Mimas flyby of Cassini. Closest approach occurred on February 13, 2010 during rev 126, and the best images obtained at this flyby have a spatial resolution of ~93 m/pxl.
- There is morphologic evidence for a highly degraded impact basin of ~153 km diameter northeast of crater Herschel [Schmedemann and Neukum 2011].

Tethys

- Tethys was globally mapped at 292 m/pxl [Roatsch et al. 2009b].
- The highest definition view of Tethys' surface has a spatial resolution of 18 m/pxl and was obtained during the targeted flyby in rev 15 on September 24, 2005.
- Rugged topography of overlapping craters is typical for wide parts of Tethys [Schenk et al. 2018].
- Large 425 km-wide impact basin Odysseus is one of the largest well-preserved basins in the Saturnian system. Flat-floor deposits (as commonly found in large craters on the Moon and Mercury) are lacking, suggesting that impact melt ponding did not occur in large quantities. This lack of large melt sheets is characteristic of all craters in the Saturn system [Schenk et al. 2018].
- Tectonic structures on Tethys are all extensional [Schenk et al. 2018].
- Ithaca Chasma is the dominant tectonic feature. It is a giant rift zone already identified by Voyager, 1,800 km in length and subtending at least 270° of arc, between 70 km and 110 km in width, and 2–5 km deep. It predates the Odysseus basin and thus should not have been formed by this impact feature [Giese et al. 2007].
- Red streaks were only found on Tethys and are very enigmatic. They show an enhanced color signature in the near-IR which is a very unusual color for features on Saturn's icy satellites. No associated surface deformation is visible even at image resolutions of 60 m/pxl [Schenk et al. 2015].

Red streaks were only found on Tethys and are very enigmatic.

- Tethys's equatorial albedo band, first seen in Voyager images, was analyzed in several ISS NAC wavelengths. The band is symmetric 15° on either side of the equator and extends from 0° to 160° W that is, almost centered on the leading edge of Tethys. There is no evidence that the band is topographically-based; margins are gradational and there is no visible difference in underlying geology [Elder et al. 2007].

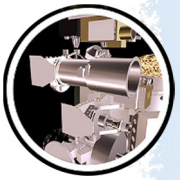

- ISS NAC polarization images found no evidence for surface textural variations on size-scales comparable to individual geological features, like crater walls and floors—on these size scales, the surface texture of Tethys appears to be uniform. However, a banded pattern on the surface was found and that likely originates in the subtle albedo variations tied to Tethys equatorial band [Elder et al. 2007] and thermally anomalous terrain [Helfenstein et al. 2005b].

Dione

- Dione was globally mapped at 153 m/pxl [Roatsch et al. 2013].
- Some Dione images taken from very close range are formally better than 6 m/pxl (rev 129 on April 7, 2010 and rev 220 on August 17, 2015), but these are somewhat smeared because of the large speed of the spacecraft.
- Dione is the geologically most-complex of the mid-sized moons except Enceladus.
- Although the Magnetometer (MAG) instrument detected a small mass loading from Dione toward space, ISS did not detect plumes or jets like those on Enceladus.
- The 345 km-wide Evander basin, discovered in Cassini images (this area was not covered by Voyager) features a prominent central peak ~4 km high, surrounded by a nearly complete peak ring. Unlike Odysseus on Tethys, Evander is strongly relaxed, with the floor nearly elevated up to the ground level. Despite this, relief of up to 4 km is preserved within the basin. Outside the rim, low topographic lobes radiate out from Evander ~1 crater radius from the rim [Schenk et al. 2018].
- Dione's most dramatic tectonic features are a distributed network of linear walled depressions interpreted as normal-fault-bound graben and half graben, for example, Wagner et al. [2006, 2009]. The so-called wispy terrain (associated directly with these extensional tectonic structures) might reflect exposures of clean water ice along normal fault scarps [Stephan et al. 2010; Beddingfield et al. 2016].
- There are only few positive-relief tectonic landforms on Dione. The most obvious is Janiculum Dorsa, a single ridge ~900 km long that trends approximately north-south in the moon’s leading hemisphere. Most other positive-relief landforms are related to impact craters, for example, Wagner et al. [2006].
- At the center of the smooth plains on the leading side of Dione is a pair of oblong craters (named Murranus and Metiscus). They are 45 to 70 km across, but only ~1 km deep. Their irregular shapes and the central mounds do not resemble the circular conical relaxed craters elsewhere on Dione [White et al. 2017]. It is suggested that Murranus and Metiscus might be volcanic craters. If so, these irregular craters were the only evidence for explosive or collapse-forming volcanism on Saturn's icy moons [Schenk et al. 2018].

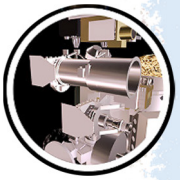

Rhea

- Rhea was globally mapped at 416 m/pxl [Roatsch et al. 2012].
- The best-resolved images of Rhea were acquired from rev 143 (January 11, 2011) and show details as small as ~5 m in size.
- The largest of the bright ray craters found in the Saturn system, the 49 km diameter Inktomi, is a flat-floored crater with a ray system radiating several hundred kilometers from the crater rim. It was imaged by ISS in August 2007 in 3 colors at resolutions up to 32 m/pxl and in stereo. The images are the best for a pristine crater in the Saturnian system and reveal a rugged landscape. Most of the ejecta and floor is essentially free of small craters [Wagner et al. 2011; Schenk et al. 2018].
- Many of the tectonic lineaments are normal faults and graben, for example, Wagner et al. [2007, 2010]. Most of this is concentrated in the trailing hemisphere as two major rift zones (Galunlati and Yasmi Chasmata) that trend roughly northeast–southwest and that are up to 3 km deep. These rifts are morphologically similar to those on Dione.
- The blue pearls (bluish spots; discovered with ISS) are a series of near-IR-dark irregular patches located at the crests of the highest ridges or massifs located along the equator of Rhea. Their origin is speculated to be related to infalling or collapse of a former orbiting debris ring [Schenk et al. 2011]. A dedicated search with ISS showed that present Rhea has no ring system [Tiscareno et al. 2010a].
- The blue pearls are not associated with any tectonic feature along its length or in near proximity. Instead, they appear to be associated with steep slopes (e.g., crater rims). The lack of any constructional artifacts associated with these color patterns on Rhea implies that they are due to regolith disruption [Schenk et al. 2011].

Iapetus

- About 75% of the surface of Iapetus was mapped at better than ~500 m/pxl [Schenk et al. 2018]. The scale of the global map from Roatsch et al. [2009b] is 802 m/pxl.
- Iapetus's unusual shape is best represented by an oblate spheroid; it supports a fossil bulge of ~34 km [Thomas et al. 2007a; Castillo-Rogez et al. 2007].
- A total of 10 basins larger than 300 km have been identified on Iapetus (despite the lack of resolved imaging in some locations), but only four on Rhea. Dione, Tethys, and Mimas are similarly depleted [Schenk et al. 2018].
- These three points show that there must be something fundamentally different between Iapetus and the inner mid-sized moons.
- Global and regional topography is much less smooth than for the other mid-sized icy moons [Thomas et al. 2007a].

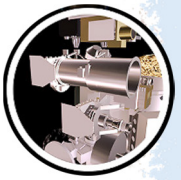

- The close targeted flyby in September 2007 revealed many properties of the anti-Saturn and the trailing hemisphere at high spatial resolution. The best-resolved images have resolutions of 10 m/pxl and show parts of the equatorial ridge within the dark terrain on the anti-Saturn side near 165° W longitude [Denk et al. 2008].
- ISS data show numerous impact craters down to the resolution limit [Denk et al. 2010].
- Iapetus's global albedo dichotomy, first described by the spacecraft's eponym Jean-Dominique Cassini in 1677 and unexplained since then, has been solved through Cassini CIRS and ISS data [Spencer and Denk 2010].
- Dust from Phoebe or possibly from other retrogradely-orbiting irregular moons has likely been painting the surface of Iapetus, forming the newly-detected global color dichotomy of Iapetus [Denk et al. 2010], which triggered the evolution of low-latitude and mid-latitude parts of the leading side into the stark bright and dark patterns we see today as the global albedo dichotomy [Spencer and Denk 2010].
- The global color dichotomy is identified as a fuzzy margin located approximately at the boundary between the leading and the trailing hemisphere; it is consistent with infalling material from Phoebe or the other irregular moons, while the boundary of the global albedo dichotomy is sharp, abrupt, irregular, and somewhat lens-shaped with equatorial parts extending from the leading to the trailing side and completely avoiding the polar areas. The global albedo dichotomy is not consistent with infalling material, but with thermal migration of water ice [Denk et al. 2010].
- A major property of the global color dichotomy is that dark material on the leading side is redder than dark material on the trailing side, and that bright material on the leading side (mainly at high latitudes) is also redder than bright material on the trailing side [Denk et al. 2010].
- Observations of small, bright-ray craters within the dark terrain indicate that the dark material corresponds to a blanket of a few meters or less in thickness [Denk et al. 2010], a finding also supported by Titan Radar Mapper (RADAR) data and consistent with the thermal migration model of Spencer and Denk [2010]. Bright ice, excavated through an impact, presumably sublimates away quickly; fading down to about twice the brightness of the dark surroundings happens within some ~107 years [Denk et al. 2008, 2010].
- While the global albedo dichotomy was known for centuries, Cassini ISS data showed that the stark dark-bright contrast is also a local phenomenon. The surface is either bright or dark, but almost never gray, even in the transition zone between the dark Cassini Regio and the bright Roncevaux Terra and Saragossa Terra [Denk et al. 2008].
- At mid-latitudes on the leading side and also low-latitudes on the trailing side, most of the equator-facing crater walls are covered by dark material, while

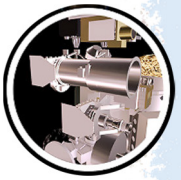

poleward-facing walls are mostly bright. Thermal segregation of water ice is again the explanation [Denk et al. 2008].

- The crater size-frequency distribution of Iapetus could be measured over almost four orders of magnitude (from > 60 m to ~600 km) [Denk et al. 2010].
- Iapetus's equatorial ridge—a huge and enigmatic ridge located exactly at the equator was discovered in ISS images [Porco et al. 2005d; Denk et al. 2005a, 2005b]. In places, this ridge is up to 20 km high and 70 km across, and it spans almost 75% of the moon's circumference [Porco et al. 2005d; Denk et al. 2008; Giese et al. 2008a; Singer and McKinnon 2011].
- While the ridge is mainly continuous on the leading side (Toledo Montes), it separates into the isolated mountains of the Carcassone Montes which were already discovered in Voyager data (and thus sometimes dubbed Voyager mountains) [Denk et al. 2000]. In general, it shows a wide range of cross-sections and heights at different longitudes [Denk et al. 2008; Singer et al. 2012]. Singer and McKinnon [2011] did not find potential hints for tectonic or volcanic origin.
- Defying any obvious explanation, numerous endogenic and exogenic formation mechanisms were proposed—for example, see short review of them by Damptz et al. [2018]. None of them can be favored over the others at this point.
- ISS NAC CL1:GRN-filter polarization images of Iapetus's highly contrasting terrains demonstrate that the degree linear polarization correlates almost linearly with the terrain albedo, thus verifying that Umov's Law broadly holds for all terrains visible in our Iapetus images even though there are stark albedo contrasts across the boundary of Cassini Regio and adjacent high-albedo regions. Thus, at sub-centimeter size scales, Iapetus's regolith most likely has a fairly uniform surface texture [Burleigh et al. 2010].

Satellite Orbits (including OpNav) and Orbital Evolution

Determination of gravitational mass (GM) for Mimas using an analysis of its resonant motion with Tethys and its effect on Methone [Jacobson et al. 2006a].

Pioneering use of systematic ISS astrometric observations (including OpNav images), including the use of mutual events, to improve the orbits of the Saturnian satellites [Spitale et al. 2006; Jacobson et al. 2008; Tajeddine et al. 2013; Cooper et al. 2014; Tajeddine et al. 2015].

The discovery and orbital dynamics of Polydeuces, establishing that it is an L5 co-orbital of Dione [Murray et al. 2005a].

The discovery and orbital dynamics of Anthe, establishing that Anthe is librating in the 11:10 resonance with Mimas: the first known example of a planetary satellite in a coupled inner Lindblad

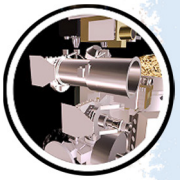

resonance (ILR) / co-rotation-eccentricity resonance (CER), leading to a new determination of the GM of Mimas [Cooper et al. 2008].

Association of Anthe's libration with the structure of its newly-discovered ring arc, in accordance with theory [Hedman et al. 2009b].

The discovery and orbital dynamics of Aegaeon in the G-ring, establishing that Aegaeon is also librating in a coupled first-order ILR/CER, in common with Anthe and Methone [Hedman et al. 2010b].

Improved orbits of the inner satellites and demonstration that the motion of Atlas is chaotic and can be modelled using the CoraLin theory applied to the 54:53 Lindblad and co-rotation resonances with Prometheus [Cooper et al. 2015; Renner et al. 2016].

The first determination of Saturn's tidal parameters incorporating Cassini astrometric data, including the tidal dissipation number Q and the Love number k_2, with confirmation that Q has previously been overestimated by a factor of 10. Important consequences for tidal heating of Enceladus [Lainey et al. 2017].

Small Satellites

Six new moons were discovered in Cassini images …

Six new moons were discovered in Cassini images: Daphnis, Aegaeon, Anthe, Pallene, Methone, and Polydeuces [Murray et al. 2005a; Cooper et al. 2008; Hedman et al. 2009b; Hedman et al. 2010b].

Cassini showed small satellites in the rings had a two-step origin. The innermost ones—Daphnis, Pan, Atlas, even Prometheus and Pandora—are likely not homogenous bodies and must have formed through aggregation of material around a denser core [Porco et al. 2007]. Pan and Atlas later developed equatorial ridges from late-stage accretion from the rings [Charnoz et al. 2007].

The inner small satellites of Saturn have distinctive physical properties and surface morphologies in each of several dynamical niches [Thomas et al. 2013].

Cassini image monitoring of Janus and Epimetheus revealed forced libration for Epimetheus which placed limits on any inhomogeneous mass distribution [Tiscareno et al. 2009].

Cassini showed that small (< 5 km) solid bodies can assume hydrostatic equilibrium ellipsoid shapes [Thomas et al. 2013].

The chaotically rotating satellite Hyperion has unique sponge-like topography that may reflect sublimation of species more volatile than water ice [Thomas et al. 2007b].

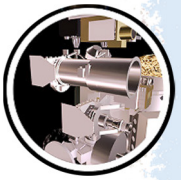

The chaotic rotation of Hyperion was analyzed using data from three flybys. The Lyapunov timescale was found to be approximately 100 days [Harbison et al. 2011].

Cassini images showed some small satellites had surface grooves, and the morphology and patterns of some of these were consistent with tidal effects [Morrison et al. 2009].

Phoebe and the Irregular Satellites

Phoebe

- June 11, 2004—only close flyby of Cassini-Huygens at Phoebe.
- ISS obtained images at better than 2 km pxl^{-1} over slightly more than three Phoebe rotations. The highest resolution ISS images have a pixel scale of 12.3 m.
- A global map was produced and delivered to the United States Geological Survey (USGS). Scale: 1:1,000,000; resolution: 8 pxl deg^{-1} or 233 m pxl^{-1} [Roatsch et al. 2006].
- Phoebe's global shape is close to an oblate spheroid, with a = b to within the uncertainties of the data [Thomas 2010; Castillo-Rogez et al. 2012; Thomas 2010].
- Mean radius: 106.4 ±0.4 km; Ellipsoidal radii (a × b × c):
  109.3 ±0.9 km × 108.4 ±0.4 km × 101.8 ±0.2 km [Thomas et al. 2018].
- Mean density: 1.642 ±0.018 g cm^{-3} [Thomas 2010].
- Even if the porosity of Phoebe were zero, its density would be 1σ above that of the regular icy Saturnian satellites. Therefore, Phoebe appears to be compositionally different from the mid-sized regular satellites of Saturn, ultimately supporting the evidence that it is a captured body [Johnson and Lunine 2005].
- Numerous impact craters are visible on the surface; they range in diameter from the lower limit imposed by the ISS image resolution up to ≈100 km [Porco et al. 2005d].
- Phoebe's topography, relative to an equipotential surface, is within the range of other small objects and is much higher than that for clearly relaxed objects [Thomas 2010].
- Digital terrain model (DTM) and orthoimage of the surface were produced from ISS data [Giese et al. 2006].
- J2000 spin-axis was found at Dec = 78.0° ±0.1°; RA = 356.6° ±0.3°, substantially different from the former Voyager solution [Giese et al. 2006].
- Two ISS observations from remote were designed to obtain light-curves at low and high phase angles [Denk et al. 2018].
- The Phoebe dust ring, discovered from Earth, has also been observed with the ISS WAC [Tamayo et al. 2014].

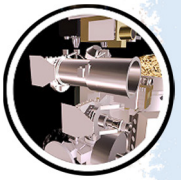

Other irregular satellites

- The irregular-moon observation campaign with ISS was the first use of an interplanetary spacecraft for a systematic photometric survey of a relatively large group of solar-system objects. They were not part of the original science goals of Cassini ISS.
- With 38 known members, the outer or irregular moons constitute the largest group of satellites in the Saturnian system. Except Phoebe, all were discovered between 2000 and 2007 from Earth (Cassini itself did not discover an irregular moon).
- Due to the large distance to the Cassini orbiter and the small sizes of the objects, the irregulars except Phoebe were always smaller than the size of a NAC pixel. The goal of the observations was thus to obtain light curves. The information for this sub-section stems from the summary chapter on irregular moons from Denk et al. [2018].
- All 9 known prograde plus 16 of the known 29 retrograde irregular moons were successfully observed with ISS, mainly with the NAC. Rotational periods could be derived for most of them (from light curve phasing), and also minimum ratios of the equatorial axes (from light curve amplitudes).
- Due to the position of the spacecraft inside the orbits of the moons, a large range of phase angles was available (and used) for the ISS observations.
- Most measured light curves show either four or six extrema (2-maxima/2-minima or 3-maxima/3-minima patterns), indicative that the objects have quite different shapes.
- All but Phoebe's light curves are primarily shape-driven, as expected for such small bodies.
- Average rotational period of 22 objects is 11.4 ±0.1 h (spin rate 2.10 ±0.02 d^{-1}). This is quite slow compared to main-belt asteroids of similar size range (~4 to ~45 km), but maybe not much different from the Jupiter Trojans, Hildas, or objects beyond Saturn's orbit.
- The fastest measured period is 5.45 h (Hati). This is the fastest reliably known rotational period of all moons in the solar system.
- However, the Hati period is much slower than the fastest rotations of asteroids, indicating that the outer moons may have rather low densities, possibly as low as comets.
- The slowest measured period is slightly longer than three days (Tarqeq).
- All light curves of moon Kiviuq show large amplitudes and are relatively symmetric. This makes Kiviuq a potential candidate for a binary or contact-binary object.
- The spin of Tarqeq is only ~0.5% off the 1:5 orbit resonance of Titan.

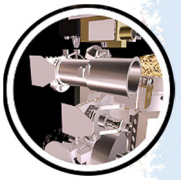

- Siarnaq and Ymir show very distinct 3-maxima/3-minima light curves. Convex-shape models of these moons resemble triangular prisms.
- Siarnaq and Ymir light curves from color filters do not show measurable deviations from the clear-filter light curves, indicating that their surfaces are not colorful at regional scales.
- Siarnaq's pole axis points to low ecliptic latitudes, indicating that this moon experiences strong seasons similar to the regular Uranian moons.
- Contrary to this, the pole axes of Phoebe and Ymir point close to one of the ecliptic poles.
- Most rotational periods of the prograde moons were found to be longer than those of the retrograde moons.
- Most rotational periods of the moons on higher tilted orbits were found to be longer than those on lower tilted orbits.
- Most rotational periods of the moons closer to Saturn were found to be longer than those of the moons farther away.
- Most rotational periods of the larger moons were found to be longer than those of the smaller moons.

Saturn

Cloud top zonal winds in Saturn's equatorial region were documented to be ~100 m s^{-1} weaker than those measured by Voyager, while winds outside the equatorial region were shown to be stable over this same time interval [Porco et al. 2005a; Pérez-Hoyos and Sánchez-Lavega 2006; Sánchez-Lavega et al. 2007; Li et al. 2013]. Stratospheric winds appear to vary over the Cassini mission, perhaps affecting the semi-annual equatorial oscillation [Li et al. 2011; Sánchez-Lavega et al. 2016].

The first direct measurements of vertical wind shear on Saturn showed that the equatorial zonal wind decreases sharply with increasing altitude, suggesting that the observed decrease in cloud top winds since Voyager may be a combination of time variation in the wind itself and time variation in the altitude of the equatorial cloud top [Porco et al. 2005a; Sayanagi and Showman 2007; Garcia-Melendo et al. 2010].

A giant long-lived dragon storm at 35° S appeared in 2004 and was found to be correlated with repeatable Saturn electrostatic discharges (SEDs), implying that the cloud feature is indeed an organized convective disturbance and that the origin of the SEDs is lightning discharges [Porco et al. 2005a; Dyudina et al. 2007; Fischer et al. 2007]. This in turn implies that Saturn's water abundance at depth must not be substantially less than Earth's.

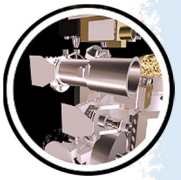

An even larger and longer-lasting giant storm was discovered by ISS at 33° N in 2010. This storm eventually encircled the entire latitude band, was also accompanied by SEDs, and created the largest tropospheric vortex ever seen on Saturn. The storm originated from the string of pearls feature previously discovered by VIMS. The string of pearls was found to be accompanied by a chain of dark cyclonic spots [Fischer et al. 2011, 2014; Sánchez-Lavega et al. 2011; Garcia-Melendo et al. 2013; Sayanagi et al. 2014]. The giant storm has a non-negligible effect on Saturn's global reflected sunlight and emitted thermal radiation [Li et al. 2015].

The first direct detection of lightning flashes on Saturn was made by ISS at the dragon storm latitude in the southern hemisphere [Dyudina et al. 2010]. This was followed by a similar direct lightning detection at the latitude of the giant northern hemisphere storm [Dyudina et al. 2013]. The lightning originates at a depth 125–250 km below the cloud tops, consistent with it being generated by water convective cloud systems.

The quasi-periodic occurrence of giant storms on Saturn on time scales of decades may be explained as the result of suppression of moist convection by the relatively high molecular weight of water in a hydrogen-helium atmosphere [Li and Ingersoll 2015].

Vortices occur preferentially in latitude bands containing westward jets, preferentially on the anticyclonic side of the jet maximum but sometimes on the cyclonic side. Most vortices last for less than a year, but the largest one observed has lasted for at least four years. The southern hemisphere has more vortices than the northern hemisphere [Vasavada et al. 2006; del Rio-Gaztelurrutia et al. 2010; Trammell et al. 2014, 2016].

Horizontal eddy momentum fluxes are directed into eastward jet cores and away from westward jet cores, converting eddy kinetic energy to zonal kinetic energy [Del Genio et al. 2007; Del Genio and Barbara 2012], as on Jupiter. Deep convective clouds exist at all latitudes but preferentially at cyclonic latitudes, as on Jupiter. This behavior is consistent with the idea that the rising branch of the mean meridional circulation occurs at cyclonic shear latitudes and the sinking branch at anticyclonic shear latitudes, implying that the jets are maintained by eddies due to instabilities of the large-scale flow [Del Genio et al. 2009].

Zonal winds weaken with increasing altitude in the cores of eastward jets [Garcia-Melendo et al. 2009, 2011a] and strengthen on either side of the jet core, implying that the jets broaden with increasing altitude [Del Genio and Barbara, 2012]. Eddy momentum fluxes weaken with altitude on the flanks of the jets, consistent with the broadening with altitude and suggesting that the eddy source is near or below cloud level [Del Genio and Barbara 2012].

Inferences about meridional circulation and convective storms from ISS images were found to be consistent with some of the spatial variations in ammonia abundance derived from Cassini RADAR radiometer [Laraia et al. 2013].

Objective analysis of cloud types in ISS continuum and methane band images suggests that dynamically, there are three distinct types of latitude bands on Saturn: 1) deep convectively

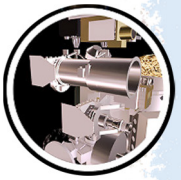

disturbed cyclonic shear regions poleward of the eastward jets; 2) convectively suppressed regions near and surrounding the westward jets; and 3) baroclinically unstable regions near eastward jet cores and in anti-cyclonic regions equatorward of them. These are roughly analogous to Earth's tropics, subtropics, and mid-latitudes [Del Genio and Barbara 2016].

Saturn has distinct vortices at both poles, with cyclonic winds, a warm core and cloud clearing near the pole, and high eyewall clouds surrounding the core. This feature resembles polar vortices found on several other planets [Dyudina et al. 2008, 2009; Sánchez-Lavega et al. 2006; Sayanagi et al. 2017].

The Saturn ribbon feature embedded in the 47° N eastward jet has properties in common with meandering western boundary currents in Earth's oceans such as the Gulf Stream and may be explained by a nonlinearly saturated shear instability [Sayanagi et al. 2010].

The ~78° N polar hexagon first seen by Voyager has persisted through the Cassini era [Sánchez-Lavega et al. 2014; Antuñano et al. 2015, 2018]. Simulations suggest that stable meandering polygonal structures resembling the hexagon can emerge without forcing when dynamical instabilities in a shallow eastward jet nonlinearly equilibrate. The wavenumber of the feature and its phase speed depend on the wind speed both at the cloud level and at the base of the flow [Morales-Juberías et al. 2011, 2015].

Stratospheric haze in Saturn's atmosphere produces photometric and polarimetric signatures that are most apparent in the short (near-UV and blue) wavelengths, in methane absorption bands at 619, 727, and 889 nm, and in polarization at visible and near-IR wavelengths. When Cassini arrived at Saturn in 2004, and earlier during the cruise phase, the northern high latitudes were blue, indicating an atmosphere with little haze content, emerging from a long period of little or no photochemical activity. During the course of the mission the northern high latitudes became exposed to sunlight, leading to photochemical haze formation and a trend toward redder colors [Fletcher et al. 2018]. Hemispheric differences in cloud feature contrast and decreases in contrast in the northern hemisphere over the course of the Cassini mission occur as a result [Del Genio et al. 2009; Del Genio and Barbara 2016].

Most latitudes on Saturn show little polarization, a consequence of reflection from an optically thick layer of large (relative to the observation wavelength), nonspherical ammonia ice or ammonia ice crystals mixed with an unknown component (since the near-infrared spectral feature of ammonia ice is rarely observed for Saturn). Cassini polarization images show enhanced polarization, enhanced forward scattering and darker particles in the region contained within the north polar hexagon [West et al. 2015; Pérez-Hoyos et al. 2016; Sayanagi et al. 2018]. These features indicate that, like Jupiter's poles, auroral input to the high atmosphere leads to the breakup of methane molecules and the subsequent

ISS made the first detection of Saturn's aurora at visible wavelengths in both hemispheres.

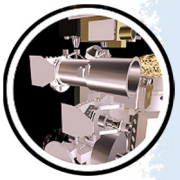

formation of heavier hydrocarbons leading to formation of a UV-dark haze of aggregate particles [Sayanagi et al. 2018].

ISS made the first detection of Saturn's aurora at visible wavelengths in both hemispheres. The color of the aurora varies with altitude and contains a distinct H-alpha line. The auroras form as bright arcs that sometimes spiral around the poles and sometimes form double arcs. The period of the north aurora is close to that of the Saturn Kilometric Radiation [Dyudina et al. 2015].

Rings

Discovery of many new ring phenomena, and more detailed observations of known phenomena, occurred very early in the Cassini mission in ISS observations [Porco 2005], all refined or extended in subsequent papers:

- Moonlets in the F-ring.
- New moons, Methone, Pallene and Polydeuces, among the mid-sized satellites, and estimates of their orbital elements,
- Refined orbits and sizes of ring region satellites Janus, Epimetheus, Prometheus, Pandora, Atlas, and Pan.
- High-resolution images of the edge of the Encke gap revealing in clear detail the edge waves created by Pan.
- Wakes created by Pan seen at large distances from the moon and the inference of low damping, and importance of self-gravity and collective effects, in the rings.
- Many previously undetected spiral waves, Atlas 5:4, 9:8, and 10:9, and Pan 7:6, producing estimates of ring and satellite properties in some cases.
- A wave in the middle of the narrow eccentric Maxwell ringlet.
- A wave in the Huygens ringlet.
- Very fine scale (~0.1 to 1 km) in high optical depth regions in the inner and outer B-ring, attributed to pulsation instabilities (or overstabilities).
- Mottled, ropy, and straw-like structure in the rings at fine scales (few km), indicative of particle clumping.
- New diffuse but relatively narrow tenuous rings between the A-ring edge and the F-ring, and within gaps (Encke, Huygens and Maxwell) in the main rings.
- Spikes and wisps, sharp and broad structures, that extend into the Keeler gap from its outer edge, predicting the presence of an embedded moon (which was discovered later to be Daphnis).
- Spectrophotometric results on the rings.

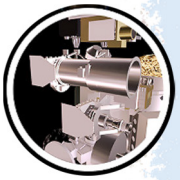

Discovery of characteristic gravitational signature of Prometheus in the F-ring core [Porco 2005].

Discovery of mirroring of F-ring core structure at opposite ansae confirming the effect of eccentricity/periapse perturbations [Porco 2005].

Discovery that the apparent multiple strands of the F-ring are kinematic spirals due to Keplerian shear following collisions [Charnoz et al. 2005].

Detailed understanding of how the gravitational perturbations from Prometheus combined with Keplerian shear produce the characteristic streamer and channel structures visible in the F-ring core [Murray et al. 2005b].

First observation of spokes with Cassini, confirming (with theoretical explanation) that they are a seasonal phenomenon [Mitchell et al. 2006].

Discovery of small moons embedded in the mid A-ring via the propeller-shaped disturbance they create in the ring [Tiscareno et al. 2006a].

First understanding of the complex morphology of spiral density waves due to the co-orbital moons Janus and Epimetheus, tracing their history as recorded in the rings and deriving ring surface mass density values for wave locations [Tiscareno et al. 2006b].

Discovery that the D-ring has undergone substantial changes in the 25 years between Voyager and Cassini [Hedman et al. 2007a].

Discovery of a vertical corrugation in the D-ring with a wavelength that decreases with time, interpreted as a winding spiral due to differential nodal regression after the ring was initially very slightly tilted in the early 1980s [Hedman et al. 2007a].

Discovery of a denser arc within the G-ring, confirming initial indications from Cassini Magnetospheric Imaging Instrument (MIMI). The ISS images are dominated by dust, but the MIMI absorptions must be due to a population of meter-sized objects [Hedman et al. 2007b].

Discovery that the G-ring arc material is trapped in a 7:6 corotation eccentricity resonance with Mimas [Hedman et al. 2007b].

Detailed understanding of spiral density waves and other radial structure from Cassini images taken during Saturn orbit insertion (SOI), deriving surface mass density and ring viscosity values for many locations within the rings with much higher fidelity than pre-Cassini measurements [Tiscareno et al. 2007].

New upper limit on the vertical thickness of the ring, 3–5 meters in the Cassini Division, 10-15 meters in the inner A-ring [Tiscareno et al. 2007].

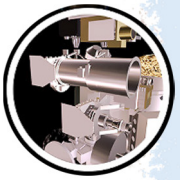

Detailed understanding of propellers in the Propeller Belts of the mid A-ring from analysis of ~150 objects seen in Cassini images [Tiscareno et al. 2008].

Discovery of moonlets embedded in the F-ring core and that the combined gravitational and collisional effects of Prometheus and small satellites produces the F-ring's unusual morphology [Murray et al. 2008].

In studies of the azimuthal asymmetry in Saturn's A-ring, the coefficient of restitution of the particles was found to be ~3.5 times lower than previously assumed, suggesting that particle collisions in the A-ring are more lossy than previously expected, possibly due to particle surface roughness, a regolith, and/or a large degree of porosity [Porco et al. 2008].

Discovery of the time variability of the outer edge of the A-ring due to the 7:6 inner Lindblad resonance with Janus and the effect of the Janus-Epimetheus orbital swap in January 2006 [Spitale and Porco 2009].

Detailed understanding of the relationship between the mass of a moon in a gap and the amplitude of the wavy edges of that gap, with more accurate measurements of the masses of Pan and Daphnis [Weiss et al. 2009].

Measurement of the inclination of Daphnis' orbit, via measurement of shadow lengths of scalloped gap edges and understanding of how those two quantities are related [Weiss et al. 2009].

Discovery of resonance-sculpted patterns within three dusty ring regions (the G-ring, the D-ring, and the Roche Division) with the latter two linked to periodicities within Saturn [Hedman et al. 2009a].

Discovery of three dusty ring structures at the orbits of three small Cassini-discovered moons (Methone, Anthe, and Pallene) confirming, in the case of Pallene, initial indications from Cassini MIMI. The Methone and Anthe ring structures are arcs centered on their moon and are associated with Mimas resonances, while the Pallene ring is circumferential and does not appear to be associated with any strong resonance [Hedman et al. 2009b].

Discovery of the mechanism by which perturbations from Prometheus produce gravitational instabilities in the F-ring core leading to moonlet formation and evolution [Beurle et al. 2010].

Discovery of unforced 1-lobed, 2-lobed, and 3-lobed self-excited patterns in the outer edge of the B-ring, in addition to the previously known 2-lobed pattern forced by Mimas, which implies the importance of viscous overstability in sculpting this region of the rings [Spitale and Porco 2010].

Discovery of localized structures, up to 3.5 km in vertical height, near the outer edge of the B-ring, implying the presence of embedded massive bodies [Spitale and Porco 2010].

Discovery of a single compact object or structure near the outer edge of the B-ring, designated S/2009 S1, casting a shadow implying a size of ~0.3 km [Spitale and Porco 2010].

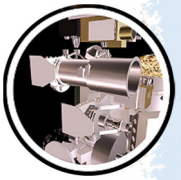

Detailed understanding of the Charming Ringlet, a dusty structure within the Laplace gap of the Cassini Division, as a heliotropic ring whose apoapse always points towards the Sun due to radiation pressure [Hedman et al. 2010a].

Discovery of Aegaeon, a 1 km moon embedded in the G-ring at the heart of the arc in that ring. Determination that Aegaeon is trapped in a strong resonance with Mimas, like Methone and Anthe [Hedman et al. 2010b].

Careful examination of the region around Rhea at both high and low phase angles, with the conclusion that there is no system of rings around that moon, contradicting an earlier report [Tiscareno et al. 2010a].

Discovery of giant propellers and long-term tracking of their orbits [Tiscareno et al. 2010b]. These constitute the first objects in the history of astronomy to have their orbits tracked while they are embedded in a disk, rather than orbiting in free space.

Measurement of shadow lengths for giant propellers during equinox, inferring sizes up to 1-2 km [Tiscareno et al. 2010b].

Discovery of corrugations in the C-ring, like those previously identified in the D-ring, consistent with being caused by an event that occurred in 1983. The identification of such a pattern in the more massive C-ring points to a massive but dispersed cloud of interplanetary debris as the cause [Hedman et al. 2011].

Detailed understanding of the three-dimensional structure of the E-ring, including a radial profile with a local minimum at the location of Enceladus, and variations that correlate with the orientation relative to the Sun [Hedman et al. 2012].

More detailed understanding of the shadow-casting compact object near the B-ring outer edge, S/2009 S1, indicating that it is an unresolved propeller structure and not an isolated embedded moon [Spitale and Tiscareno 2012].

Discovery that, compared to the Voyager epoch, the F-ring core was brighter by a factor two, was three times wider, and had a higher optical depth [French et al. 2012].

The use of geometrical fits of the F-ring core to show the extent of local variability in the orbital elements even though the average values are consistent with those determined from stellar occultations [Cooper et al. 2013]. Discovery of an empirical commensurability between the precession rates of Prometheus and the F-ring.

Discovery and detailed understanding of dusty ringlets in the Encke Gap, one sharing the orbit of Pan and two others on either side, with determination that the radial structure of these ringlets indicates heliotropic behavior as previously described for the Charming Ringlet, while the azimuthal structure constitutes many clumps that are moving with respect to Pan and corotation [Hedman et al. 2013].

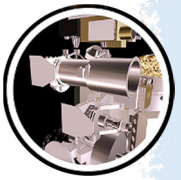

Detailed understanding of the spokes in the B-ring, following their growth and decline as seen in ISS images. Discovery that spokes undergo an active phase during which they grow in size and optical depth, with one edge apparently governed by Lorentz forces and the other edge apparently governed by Keplerian motion. Discovery via light-scattering behavior that spoke particles are irregularly shaped, not spherical. Discovery that spoke activity on both sides of the rings occurs with a period commensurate with the period of northern Saturn kilometric radiation (SKR) emission, though a period commensurate with the southern SKR also seems to be present. Discovery that peak spoke activity is near 200 degrees SLS4, which is divergent from the Voyager value (Mitchell et al. 2013)

Use of the Iapetus—1:0 spiral bending wave to derive a continuous mass density profile for the outer Cassini division and the inner A-ring, in particular finding that the sharp change in optical depth that defines the inner edge of the A-ring does not in fact correspond to any sharp change in surface mass density [Tiscareno et al. 2013a].

Discovery of impact ejecta clouds rising above the rings, and use of those clouds to infer the population of decimeter-to-meter-sized objects in heliocentric orbits near Saturn [Tiscareno et al. 2013b].

Discovery that the exceptionally bright, extended clumps which were common during the Voyager epoch were much rarer in the Cassini era with only two having been seen [French et al. 2014].

Detection and explanation of mini-jets in the F-ring as collisional products due to low velocity impacts with nearby objects [Attree et al. 2012; Attree et al. 2014].

Discovery of an object (Peggy) at the edge of the A-ring. Subsequent tracking of radial discontinuity (probably due to gravitational effect of embedded object) suggests stochastic behavior possibly due to encounters with smaller, nearby objects [Murray et al. 2014].

Discovery of an anti-resonance mechanism which can provide a stabilizing effect to reduce the effect of chaotic evolution of ring particle orbits at the F-ring's location.

Discovery of an anti-resonance mechanism which can provide a stabilizing effect to reduce the effect of chaotic evolution of ring particle orbits at the F-ring's location. The core may be located at a unique location where an anti-resonance and a co-rotation resonance with Prometheus are coincident [Cuzzi et al. 2014].

Detailed understanding of D68, a ringlet in the D-ring, with explication of patterns whose evolution may place important constraints on the ringlet's local dynamical environment and/or the planet's gravitational field [Hedman et al. 2014].

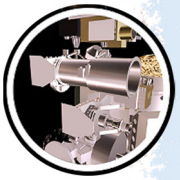

First observation of the Phoebe Ring in visible light, by Cassini images tracing Saturn's shadow as it recedes through that ring, placing new constraints on the properties of Phoebe Ring particles [Tamayo et al. 2014].

Detailed understanding of the tendrils of the E-ring surrounding Enceladus, and the mechanisms by which the E-ring is fed by the Enceladus geysers [Mitchell et al. 2015].

More detailed understanding of corrugations in the D-ring, including a time-variable periodic modulation that likely indicates organized eccentric motions of ring particles, suggesting that the 1983 event that started the spiral had an in-plane component as well as a vertical component, with the vertical component some 2.3 times larger. Mismatch between wavelengths in the D-ring and C-ring may indicate a two-stage initiating event [Hedman et al. 2015].

Detailed understanding of the wide range of viewing geometries available for Cassini ISS photometric measurements of the D-ring and G-ring, and application of the derived functions to understanding similar debris disks around other stars [Hedman and Stark 2015].

Discovery that the Janus-Epimetheus orbital swap in 2010 led to the disappearance of the characteristic 7-lobed pattern as the Janus resonance moved away from the ring edge. Other signatures in the edge pattern could be due to inhomogeneities in Saturn's gravity field [El Moutamid et al. 2016].

Discovery of a new evolving pattern in the D-ring, apparently created by an event that occurred in 2011, possibly debris striking the rings or a disturbance in the planet's electromagnetic environment, with explanation of similar patterns seen by Voyager having possibly resulted from an event that occurred in 1979 [Hedman and Showalter 2015].

Further observations of the Phoebe Ring, yielding a radial profile from 80 to 260 Saturn radii. Evidence of a change in behavior around 110 Saturn radii that may be due to interactions between the dust grains and Iapetus, or to other orbital instabilities. Evidence of material beyond the orbit of Phoebe, which may be due to other moons that contribute material to the ring. Evidence that the Phoebe ring is unusually rich in particles smaller than 20 μm, compared to particles larger than that size, which may be due to a steep size distribution of ejecta or to a subsequent process that preferentially breaks up larger grains [Tamayo et al. 2016].

Detailed understanding of the Huygens ringlet in the C-ring, with each edge modelled separately, finding one 2-lobed pattern forced by a resonance with Mimas as well as a self-excited 2-lobed pattern, and substantial additional structure that is not easily explained [Spitale and Hahn 2016].

Discovery of signs of embedded massive bodies within the Huygens ringlet, especially at two particular co-rotating longitudes [Spitale and Hahn 2016].

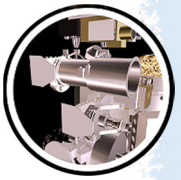

Detailed understanding of the inner edge of the Keeler Gap from ISS images, finding not only strong evidence for a 32-lobed pattern generated by Prometheus, but also 18-lobed and 20-lobed normal modes rising from within the ring. Also, discovery of multiple localized features on eccentric orbits that appear to move at the local Keplerian rate and persist for only a few months. Hypothetical explanations may include differences in how ring particles respond to resonances, and/or unseen embedded objects [Tajeddine et al. 2017b].

Detailed understanding of spiral density waves and their role in holding the ring system in place, using Cassini results for surface mass density and viscosity combined with improved theoretical understanding, demonstration that the A-ring is held in place by many resonances involving at least seven moons [Tajeddine et al. 2017c].

Detailed understanding of spiral density waves and their role in holding the ring system in place, … .

Discovery of a dusty ring that shares the orbit of Prometheus but precesses at a rate characteristic of the F-ring [Hedman and Carter 2017].

Discovery of previously unseen structures in the D-ring and the Roche Division, as well as novel fine-scaled structures in the core of the E-ring, in high-resolution high-phase images obtained during the Ring Grazing Orbits and Grand Finale [Hedman et al. 2017].

Determination that many of the gaps in the C-ring and the Cassini division are not held open by shepherd moons, based on non-detection during intensive Cassini searches for such moons [Spitale 2017].

Discovery of radial variations in the degree of visible clumpiness in the ring, in high-resolution images obtained during the Ring Grazing Orbits and Grand Finale [Tiscareno 2017].

Measurement of the particle-size distribution for small propellers in the Propeller Belts of the mid A-ring, in high-resolution images obtained during the Ring Grazing Orbits and Grand Finale [Tiscareno 2017].

Detailed images of the fine structure of giant propellers, obtained during the Ring Grazing Orbits and Grand Finale [Tiscareno 2017].

Detailed images of impact ejecta clouds in the A-ring and C-ring, with unprecedented color and frequency information, obtained during the Ring Grazing Orbits and Grand Finale [Tiscareno 2017].

Corrected and more complete profile of spiral density in the A-ring [Tiscareno and Harris 2018].

Measurement via spiral density and bending waves of surprisingly low surface density, 25 g/cm^2, in the inner B-ring [Tiscareno and Harris 2018].

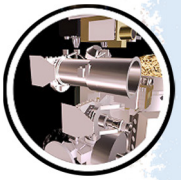

Creation of an atlas of resonant features in Saturn's rings [Tiscareno and Harris, 2018].

Systematic identification of resonant features with moons that drive each wave, and of apparently resonant features with no known driving source [Tiscareno and Harris 2018].

Open Questions for Saturn System Science

Titan (summarized in Nixon et al. [2018])

- What is the timing of the onset of north-polar summer storms?
- Is the weather Cassini observed typical for these seasons on Titan? If so, why does the implied seasonal transition in the mean meridional circulation lag that predicted by models by several Earth years?
- What explains the spectral behavior of some north-polar cloud features visible to VIMS at 2.1 μm but not to ISS at 938 nm or VIMS at other wavelengths (shorter and longer than 2.1 μm)?
- Over what timescale do changes occur in north-polar lakes and seas? And are liquid reservoirs exchanged between the north and south poles, and if so, over what timescale?
- What is the nature of exchange between surface organics and subsurface water? Is there cryovolcanism? Do tectonics facilitate exchange combined with icy mantle convection?
- What are the implications of seasonal behavior of haze for production processes?

Enceladus

- What mechanism(s) produce the phase lag between the maximum normal tidal stresses across the fractures and the maximum plume brightness (and hence mass) over the course of an Enceladus day? Is this phase lag also present in the response of the plume to the 4-year and 11-year periodic variations in tidal stresses across the SPT?
- What processes are occurring in the conduits leading from the ocean to the surface, and how do they change the contents of the plume? How wide are the conduits?
- Does liquid water ever reach the surface?
- How does the magnitude of the flux of curtain-style venting products compare with those of discrete geysers?
- How did the SPT form and how has it evolved with time?

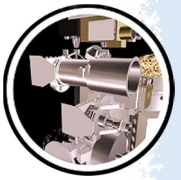

- Was the region of anomalous high thermal flux, presently under the SPT, much more extensive in the past? Did it extend to the equatorial regions on the leading-hemisphere and trailing-hemisphere, where there is widespread evidence for a strongly elevated thermal flux in the past, or where these regions affected by separate hot spots that have diminished over time? Has the activity been constant over time, or does it periodically diminish and return due to tectonic overturn? [Helfenstein 2010].
- To what extent might true polar wander (TPW) have resulted in the formation of tectonic features that are visible today? Are there regions of Enceladus outside the SPT that show evidence of elevated thermal flux due to the lithosphere passing over one or more regional hot spots?
- What does ancient terrain tell us about the early history of Enceladus?
- Are there unique, specific types of local geological structures that discrete geysers deposit or sculp which are diagnostic of their presence, activity, and persistence?
- Can extinct or relict tiger stripe structures be reliably identified outside of the SPT region?
- Are there examples of possibly relict structures other than tiger stripes on Enceladus that have been shaped by some form of ancient venting or cryovolcanism?
- Are the fine, gossamer cracks that slice though terrains throughout the SPT region part of the pervasive system of fine cracks that exist outside of the SPT region? What is their origin and what does it indicate about the mechanical structure of the surface and the nature of stresses that produced them?
- How does the thickness of the icy crust, and its thickness relative to the underlying ocean, vary with location on Enceladus? How has it changed over time?
- What role have tidal interactions played in controlling the evolution of Enceladus' global ocean, lithosphere, tectonism, and water eruptions? [cf. Thomas et al. 2016; Giese et al. 2011b].
- To what extent have plume fallout and accretion of E-ring particles affected the surface physical properties of Enceladus' surface materials [cf. Schenk et al. 2017]? Is there evidence that these interactions have changed over time producing observable records in:
  - Spectral properties and regolith composition?
  - Surface physical properties like regolith porosity and macroscopic texture, particle properties such as grain transparency and particle microstructure?
- Are there observable spectral and/or photometric effects of sintering by thermal hot spots that are diagnostic of the age and persistence of eruptive activity and/or subsurface convection on Enceladus [cf. Helfenstein 2012]?

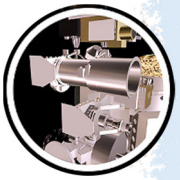

Main icy satellites (except Enceladus)

- What is the absolute timing of all surface-modifying events on the moons?
- How old (or young) is Saturn's satellite system? Based on the hypotheses that orbital instability caused massive collisions within a previous generation of Saturnian mid-sized moons inside the orbit of Titan, it has been speculated that the icy moons (except Iapetus) might be very young relative to the age of the Solar System, maybe just in the order of ~100 Ma [Ćuk et al. 2016]. This possibility is at least not precluded by the geologic record of these mid-sized bodies, but appears to pose major theoretical problems [Schenk et al. 2018]. How likely is it that all moons underwent major formation processes in a short period of time, but look old today? What would be diagnostic signatures of such a scenario? How could kilometer-sized topography of large basins like Evander or Odysseus survive in such a scenario? What is the source of the numerous impact craters?
- Determine the source of the impactors: Is the assumption of heliocentric projectiles (mainly Centaurs/ecliptic comets) as the origin causes of the craters really correct? Or could planetocentric sesquinary impactors (these are secondaries that remained in orbit around Saturn for a while before falling back on a surface) from impacts on the inner moon system and/or from catastrophic break-ups of moons within Titan's orbit [Movshovitz et al. 2015; Ćuk et al. 2016] and/or from the outer irregular moon system (which experienced a violent collisional history, but less likely except for Iapetus and possibly Hyperion because Titan appears to be an effective barrier [Denk et al. 2018] do the job? Alternatively, could there be a completely different impactor population? In case the Ćuk et al. [2016] scenario of a young satellite system is correct, the majority of the craters on the moons inside Titan must come from a planetocentric impactor population.
- How should any early bombardment events be incorporated into the rates? [Kirchoff et al. 2018]. (Only relevant if the moons are old.)
- Crater counts revealed relative paucities of craters with D < ≈10 km on Rhea and Iapetus, and of craters 10–20 km < D < ≈200 km on Mimas, Enceladus, Tethys, and Dione. Cryovolcanism, tectonism, or viscous relaxation are likely not the cause for these differences [Kirchoff et al. 2018]—but what else?
- How have the thermal profiles and physical structure of each satellite evolved over time?
  - How do visible geological and tectonic features record these changes?
- What past or current heating sources ever modified the mid-sized moons of Saturn?
- Why do we see no central pits in craters on these moons, while we do see them on water or ice-bearing bodies like Ceres, Ganymede, Callisto, Europa, Mars, and even examples on Earth?

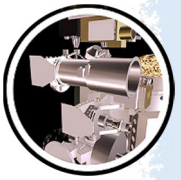

- What is the origin(s) of crater chains on Rhea, Dione, Tethys, and Iapetus? (Are they mostly from secondary cratering, or do split projectiles also form crater chains at Saturn?)
- To what extent have subsurface oceans been present over the geological evolution of each main icy satellite and what role have they played in shaping the present-day surface of each?
  - Is there evidence of tectonism that would require a subsurface water layer?
  - Are there geological features present that are diagnostic of ancient cryovolcanic activity?
  - If such features are present, is there stratigraphic information about their placement in time?
- To what extent have interactions between the outer diffuse rings and the regoliths on the main icy satellites affected the surface physical properties of the regoliths?
  - Spectral properties and regolith composition.
  - Surface physical properties like regolith porosity and macroscopic texture, particle properties such as grain transparency and particle microstructure.
  - Is there any observable evidence that the ring-satellite interactions have changed over time?
- Mimas is similar in size to neighboring, active Enceladus and the closest midsize icy satellite to Saturn, but it is devoid of any but the most rudimentary deformation. Why are these two bodies so different?
- What is the origin of Mimas's trough system?
- Has Mimas an irregularly shaped core or even a sub-surface ocean?
- Did a potential core of Mimas focus seismic energy during the Herschel impact, resulting in the irregular troughs and knobs found antipodal to the crater? (also known as, a scenario somewhat similar to Mercury and the Caloris basin?)
- Why is Tethys so geologically complex despite its very low density (~1 g/cm^3) and the consequently low abundance of radiogenic nuclides?

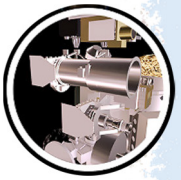

- Are the Odysseus basin and Ithaca Chasma on Tethys genetically linked? Giese et al. [2007] say no, but this has been questioned [Schenk et al. 2018]. What are the relative, what are the absolute ages of these two major features on Tethys?

What is the nature, age, and origin of the enigmatic red streaks on Tethys?

- What is the nature, age, and origin of the enigmatic red streaks on Tethys?
  - Are such spectral features observable on other Saturnian icy satellites? If not, why not?
- Smooth plains emplacement on Tethys and Dione: How did the smooth plains become smooth? The volcanic hypothesis remains, but many challenging questions do so as well: Cassini did not resolve flow fronts on the smooth plains unit—the margins of the smooth terrain grade into heavily cratered highlands over a significant distance, implying that there may be no recognizable discrete contact (boundary) between the two terrains [Kirchoff and Schenk 2010]. Could the smooth plains instead be the result of crater erasure by extremely high heat flow (despite the lack of any cryptic rings representing nearly flattened impact craters)?
- How are thermal anomalies such as those on Tethys and Mimas manifested in terms of surface physical properties of the regolith?
  - Are thermally anomalous features like the Pac-Man terrain observable or more subdued on other main icy satellites of Saturn?
- Does Dione host an ocean [Beuthe et al. 2016]? Difficult to confirm geologically—if the outer shell is on order of 100 km deep as suggested, it may be difficult to fracture.
- Is large basin Evander so much relaxed due to a sub-surface ocean?
- Origin of the wispy terrains (fracture networks) on Dione and Rhea.
- On Rhea, rare high-resolution views (at < 20 m/pixel, e.g., ISS frame N1741547885) reveal occasional isolated fault scarps. Are these far more common than might be guessed from lower resolution global imaging? [Schenk et al. 2018].
- Rhea's blue pearls—on Saturn's mid-sized icy moons, bluish colors are usually associated with young features and fade with time. Thus, we would expect that a color signature like Rhea's equatorial blue spots would also fade with time, implying that it might be a geologically recent phenomenon. Is this really the case? If so, how has a young ring feature formed around Rhea in more recent times? If not, how could the bluish color be preserved?
- Why does Iapetus have so many more large basins and a much more rugged topography than the inner moons? (Was the incoming projectile flux different? Was there a major heating event on the inner moons, erasing the topographic record of early giant impacts? Were the inner moons formed later? Was Iapetus formed elsewhere? ...?)

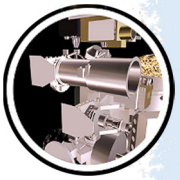

- Iapetus—how did the equatorial ridge form?
- Why is the shape of the cumulative crater size-frequency distribution of Iapetus so close to the size-frequency distribution of the Earth's moon [Denk et al. 2010 Figure 3]?

Satellite orbits and orbital evolution

- Are the orbits of the inner satellites stable in the long-term?
- Did the small inner satellites form from the rings?
- What are the masses of Anthe, Methone, Pallene, Polydeuces and Aegaeon?
- What mechanism determines the secular evolution of the Saturnian satellites, in particular Enceladus?

Small satellites

- Do the mean densities of the satellites restrict possible origin mechanisms?
- Can we assign relative ages to the small satellites and relate those to surface ages of large satellites, or to the age of the main ring system?
- How many types of surface grooves are there, and do any reveal internal structures?
- What are the mechanisms that allow small (few km) objects to assume a hydrostatic shape?

Phoebe and the irregular satellites

- What are the spin rates of the 13 irregular moons not observed by Cassini?
- What are the precise sizes of Saturn's irregular moons?
- How are they looking like? (What are their shapes?)
- What are their exact albedos, how much do they differ between the objects?
- What are their densities? Might they be even lower than ~500 kg/m^3, as indicated by the rotational periods? Are the irregulars indeed rubble piles of cometary nature?
- Are there noticeable albedo variations on the surfaces (other than Phoebe)?
- Is there any irregular moon with color variations on the surface?
- Are there really significant color variations between different objects, as suggested from ground-based observations?
- Is the distribution of pole-axis orientations random, or is there a preferred orientation?

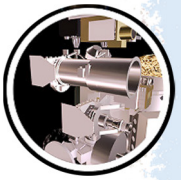

- How are the phase curves looking like, and what will they tell us about the surface properties?
- Do contact-binary irregular moons exist; might they even be common in the Saturn system?
- Do binary moons exist?
- Is there a spin-orbit resonance of Tarqeq with Titan?
- How old are the irregulars that exist today?
- How many progenitor objects were captured by Saturn? When did this happen (when was the first, when the last capture event)? How did Saturn do that? How many of them (or what fraction) were trapped in prograde, in retrograde, in low-tilted, in highly tilted orbits?
- Where in the solar nebula did they originally form? (Inside or outside the Saturn orbit? Were they former asteroids, Hildas, Trojans, Centaurs, Kuiper-Belt objects, comets?)
- Might some of the retrograde moons (especially the Mundilfari and the Suttungr families) be ejecta from large impacts on Phoebe?
- Likely non-random correlations were found between the ranges to Saturn, the orbit directions, the orbit tilts, the object sizes, and the rotation periods. While there are reasonable hypotheses for some of these correlations, a compelling physical cause for size and spin relations to orbital elements is not known.

Saturn

- Does Saturn actually have a much stronger equatorial jet than Jupiter, or are estimates of Saturn's rotation period biased? If Saturn actually has a stronger jet, what makes the two planets different in this regard?
- What is the water abundance at depth on Saturn? If Saturn is wetter than Jupiter, why? Does the water abundance dictate the frequency of major convective storms? Why are giant storms preferentially observed at about the same latitude in both hemispheres?
- Does the sign of the mean meridional circulation at cloud level reverse in the upper troposphere? How does the circulation at cloud level relate to the circulation between cloud level and the water condensation level?
- To what extent do processes deep in Saturn's atmosphere versus processing operating above the water condensation level contribute to the dynamical behavior observed at cloud level? What process provides the energy that drives the eddies at cloud level?
- Why do the north and south poles of Saturn differ in their dynamical behavior?

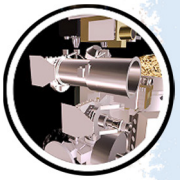

- What explains the lack of coherence between the latitudinal variation of Saturn's visible albedo and the jets at cloud level? Why do cloud features observed at deeper levels by VIMS look different from those observed by ISS at somewhat higher altitude?
- What constituent in Saturn's upper tropospheric haze explains the absence of a near-IR ammonia feature?

Why do cloud features observed at deeper levels by VIMS look different from those observed by ISS at somewhat higher altitude?

Rings

- What causes the C-ring plateaus and sharp optical-depth jumps within the B-ring?
- Are all of the irregular structures in the high optical depth regions of the A-ring and B-ring caused by overstabilities?
- Why are the inner edges of the A-ring and B-ring, and the edges of the C-ring plateaus, sharp only in optical depth, while their mass density profiles are much more gradual?
- What causes the red color of the A-ring and B-ring, and its dramatic increase inwards across the B-ring?
- Why do different ring textures appear in sharp-edged belts that are adjacent to each other? What do these textures tell us about ring particle properties?
- What is the velocity distribution of ring impact ejecta? How does it vary across the radial extent of the rings? How does ballistic transport sculpt the structural and compositional character of the rings?
- What are the kronoseismology waves in the rings telling us about the structure and history of Saturn's interior?
- Are there cyclic, self-limiting processes of growth and disruption of small planetesimal-sized objects, especially in the outer A-ring and F-ring?
- What is the mass of the F-ring?
- Why does the F-ring precess uniformly despite all the local variability? (Collisions? Self-gravity?)
- Is the F-ring in a stable, long-term location or will it eventually dissipate?
- What is the origin and long-term fate of propeller moons? What do they teach us about astrophysical disks?
- Why do propellers have such complex photometry? What do these characteristics tell us about the particles and their properties?

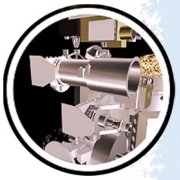

- How was Peggy formed—evolving propeller object or formed from streamline bunching due to 7:6 resonance?)
- What is Peggy's ultimate fate? Will it move inwards, or will it move outwards and escape?
- What forms the spokes?
- How old are the rings?
- How are small dust grains transported, confined and lost throughout the Saturn system?
- What controls the shape and brightness of narrow dusty ringlets within gaps in Saturn's rings?
- What controls the distribution and evolution of bright clumps in the Encke Gap ringlets? Why are such clumps rare in other narrow dusty ringlets?
- What determines the distribution of dust in the D-ring and Roche Division?
- How do the dusty rings respond to seasonal changes in solar radiation forces and magnetospheric asymmetries?
- How much do the dusty rings change over time?

ISS Non-Saturn Science Results

Jupiter Atmosphere and Rings

During a several-month approach to Jupiter, the ISS NAC captured the evolution of a large spot near latitude 65 degrees [Porco et al. 2003]. The lifetime of this UV Great Dark Spot is apparently a few months. A nearly-identical spot was seen in earlier Hubble near-UV images, but only once [West et al. 2004]. Initially the spot resides near System III longitude 180 degrees, coincident with the location Jupiter's deep thermal-IR auroral emission. Over the course of a few months repeated images from Cassini show that the spot morphs and shears, apparently from Jupiter's differential zonal flow field at high latitude. The spot is not visible at wavelengths longer than near-UV, and not seen in methane filters, indicated the absence of particles.

The Cassini ISS took images every ~2 hours as it approached Jupiter starting on October 1, 2000 [Porco et al. 2003]. The phase angle was 20° at the start and passed through 0° in mid-December. In this way, every point on the planet up to ±60° latitude was viewed in sunlight at least once per Jovian day, which is about 10 hours. The images at a given longitude could be played in sequence to make an ~70-day movie with a time step of 10 hours that showed the clouds in motion in Jupiter's atmosphere. This data set was an invaluable aid in measuring the winds, lightning, waves, clouds, turbulence, and discrete features, leading to a greater understanding of the planet's weather.

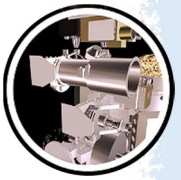

The colored cloud bands that circle Jupiter on lines of constant latitude are an obvious visible feature. The bands are accompanied by zonal winds—the eastward and westward jets that are strongest at the north and south boundaries of the bands. The winds are measured by tracking the positions of clouds in sequences of images, usually with a time step of ~10 hours. The jets are more stable than the cloud colors, and a comparison of jet speeds over the 20-year period from Voyager to Cassini shows almost no change [Porco et al. 2003].

Comparison of data from Cassini, Voyager, and Hubble Space Telescope reveals small changes with a 4–5 year period near the equator [Simon-Miller and Gierasch 2010]. These oscillations are similar to the quasi-biennial oscillation in Earth's atmosphere. The high-speed jet at 24° N varied from 2000 to 2008 [Asay-Davis et al. 2011], but generally the zonal jets are remarkably stable.

Cassini ISS documented changes in the large ovals like the Great Red Spot and the Oval BA. The Red Spot, an anticyclonic vortex that has existed for at least 150 years, was found to be shrinking from 1996–2006 [Asay-Davis et al. 2009; Shetty and Marcus 2010]. The wind speeds in the Oval BA did not change in 2005–2006 when the cloud color became redder [Hueso et al. 2009]. The wind structure around Oval BA is ring-like, and the winds at the periphery strengthened from 1997 to 2007 [Choi et al. 2010; Sussman et al. 2010]. Lifetime is proportional to size. A study of 500 spots over the 70 days of the Cassini movie reveals lifetimes of 3.5 days for convective spots and 16.8 days for all other spots [Li et al. 2004].

Cassini ISS revealed important properties of wave clouds visible in Jupiter's atmosphere. The small-scale (300 km wavelength) gravity waves seen in Voyager and Galileo images were remarkably absent in the Cassini 70-day movie [Arregi et al. 2009]. A chevron-shaped pattern centered on a high-speed (140 m/s) jet at 7.5° S could be an inertia-gravity wave or a Rossby wave [Simon-Miller et al. 2012]. On a larger scale, the equatorial plumes and hot spots seem to form a wave that circles the planet at constant latitude [Li et al. 2006a; Choi et al. 2013]. Hot spots are holes in the clouds, and it is important to understand them if one is to properly interpret the Galileo probe results. Slowly varying westward propagating waves are likely to be Rossby waves, and these were observed in ISS images of the Polar Regions [Barrado-Izagirre et al. 2008].

Around closest approach, Cassini imaged Jupiter over a wide range of phase angles. Cassini ISS observed four clusters of lightning on the night side, where a cluster is a site that produces multiple lightning flashes. Cassini saw lightning flashes that were more than 10 times more powerful than any seen before on Jupiter [Dyudina et al. 2004]. Brightness versus phase angle revealed scattering properties, color, and number of chromophores of the clouds [Ordonez-Etxeberria et al. 2016]. Jupiter provided surface truth for use in interpreting exoplanet phase curves [Dyudina et al. 2016]. The phase angle dependence was useful in inferring vertical structure in Jupiter's clouds [Li et al. 2006b; Garcia-Melendo et al. 2011b; Sato et al. 2013; Dyudina et al. 2016].

> Cassini ISS confirmed a result from Voyager that the eddies, … , are accelerating the zonal jets … .

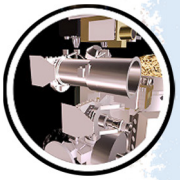

The high-resolution and dense coverage of the Cassini ISS images made possible a number of fundamental statistical studies of turbulence, eddies, and eddy mean flow interaction. Cassini ISS confirmed a result from Voyager that the eddies, which are transient structures ranging in size up to a few thousand km, are accelerating the zonal jets [Salyk et al. 2006]. Other processes, invisible to Cassini, must be decelerating the jets in order to maintain a steady state.

Other fundamental properties of the flow include the scale and power spectrum of the motions [Barrado-Izagirre et al. 2009, 2010; Choi and Showman 2011], for which one often uses brightness variations as a proxy for the wind itself. When the spatial resolution is good enough, as it is with Cassini ISS, one can use the derived velocity field to get the kinetic energy spectrum. The spectral slope implies an inverse cascade of kinetic energy from small scales to the scale of the zonal jets [Galperin et al. 2014; Young and Read 2017]. The velocity field derived from the Cassini movie was used to derive the transport barriers to horizontal mixing [Hadjighasem and Haller 2016].

The basic dynamical features (the zonal wind profile versus latitude, the flow around the large ovals, and their time-dependent behavior) become the target quantities that numerical models try to reproduce. Thus the published zonal wind profiles from Voyager and Cassini were used to compute potential vorticity, which is an important dynamic quantity in modeling studies [Read et al. 2006]. Specific features of the flow within the Red Spot were matched with numerical models to solve for uncertain atmospheric parameters [Morales-Juberias and Dowling 2013]. Finally, the general features of the zonal jets were used to address the basic question of whether the flow is shallow or deep [Heimpel et al. 2005].

Cassini images of the Jovian main ring sampled a broad range of wavelengths and viewing geometries over a period of 37 days during the Jupiter flyby [Porco et al. 2003]. The ring's phase curve was found to be flat from low to medium phase angles.

The color of the Jupiter ring is indicative of the parent bodies' intrinsic color, and not an effect of scattering by small dust grains [Throop et al. 2004]. The main ring is composed of a combination of small grains with a normal optical depth of ~4.7×10^{-6}, and larger bodies of optical depth ~1.3×10^{-6}. The ring's flat phase curve between 1° and 130° confirms the irregular-sized, rather than spherical, particles.

Jupiter/Exoplanet Studies

Disk-integrated reflected light curves derived from Cassini images indicate that for gas giant exoplanets, an assumption that they behave as Lambertian scatterers will underestimate stellar absorption and thus equilibrium temperature of the atmosphere. Saturn-size rings can be confused for a larger planet size, but produce an asymmetry in the phase curve that may help to resolve the ambiguity [Dyudina et al. 2005, 2016].

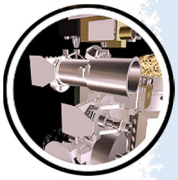

Jupiter Satellites

Discovery of previously unseen ~400 km high plume over the north pole of Io. Joint Galileo imaging showed that the location of the vent was Tvashtar Catena [Porco et al. 2003].

Spatially resolved images of Europa in eclipse show that its visible aurorae are brightest around the limb, indicating an atmospheric rather than surface source [Porco et al. 2003].

First disk resolved imaging of a Jovian outer satellite. The measured size range of Himalia is four to six NAC pixels indicating that it is not spherically shaped. These values correspond to a diameter of 150 ±10 km × 120 ±5 km, if the principal axes (or diameters close to them) were measured. From this size, the surface albedo is calculated as 0.05 ±0.01 [Porco et al. 2003].

The fitted orbital parameters of the inner satellites Amalthea and Thebe confirm the relatively high inclinations of these satellites, equivalent to maximum vertical displacements from the equatorial plane consistent with current estimates of the half-thickness of the Amalthea and Thebe gossamer rings [Cooper et al. 2006]. This supports the conclusion that these satellites are sources of the ring material.

There are no undiscovered satellites between 2.6 R_J and 20 R_J with inclinations < 1.6°, eccentricities < 0.0002 and visual magnitudes (as seen from 40 million km) brighter than 14.5 [Porco et al. 2003].

Observations of auroral emissions in Io's atmosphere throughout the duration of eclipse indicate that the atmosphere must be substantially supported by volcanism [Geissler et al. 2004].

Open Questions for Non-Saturn Science

Jupiter's atmosphere

- Are the zonal winds shallow, or do they extend downward thousands of km along cylinders concentric with the rotation axis? This question applied immediately after Cassini's encounter with Jupiter in 2000. It may have been answered since then by Juno observations of Jupiter and Cassini observations of Saturn.
- What powers the eddies, given that the eddies seem to be powering the zonal jets? The possibilities are: horizontal gradients of temperature due to excess sunlight absorbed at the equator, and unstable vertical gradients due to internal heat from below.
- What limits the speed of Jupiter's zonal jets compared to the higher speeds of the zonal jets of the other giant planets?
- How does the Red Spot maintain itself against turbulent friction? Does it cannibalize smaller spots? Why is the Red Spot shrinking?

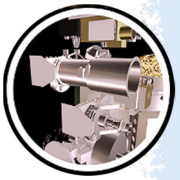

- What caused the three white ovals to merge into the single Oval BA after almost 60 years of separate existence?
- What generates the waves seen in the Jovian clouds? Can one feature act as an obstacle to the flow and generate lee waves? Can an energetic transient event generate waves radiating off to infinity? What role do breaking waves play in redistributing energy and momentum? The question applies to each wave type separately.
- What are the visible clouds made of, and what gives them their color?
- What does lightning tell us about the atmosphere below the cloud tops? Does lightning imply water, or could charge separation occur in the ammonia cloud?
- What do the numerical flow models tell us about the depth of the flow, the source of energy for the flow, and the processes that operate below the tops of the clouds?

Jupiter/exoplanet studies

- What do ISS measurements of disk-integrated polarization of Jupiter and Saturn tell us about what can be learned from exoplanet polarization measurements (cloud and haze particle properties)?
- What do ISS measurements of disk-integrated reflected flux from Jupiter and Saturn tell us about what can be learned from time-series measurements of flux from exoplanet flux (rotation rates, differential rotation)?
- What can ISS measurements of Jupiter and Saturn tell us about the amplitudes of flux and polarization variations for giant planets, providing insight for signal/noise estimates for exoplanet time-series measurements?

Jupiter's satellites

- What are the masses and densities of the small inner satellites Metis, Adrastea and Thebe?
- What are the rotational periods of the irregular satellites? So far, a reliable spin period is only available for Himalia. For the other 60 known irregulars, none has been published to date. An inventory is highly desired.
- Determine to good accuracy the sizes, albedos, colors, pole-axis orientations, object shapes, phase curves of the Jovian irregulars.
- What are the densities, composition and internal structure of the Jovian irregulars?
- Does Jupiter have binary or contact-binary satellites?

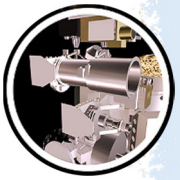

- For the Saturnian irregulars, likely non-random correlations were found between ranges to the planet, orbit tilts, object sizes, and rotation periods. Do the Jovian irregulars show something similar as well?
- Origin—are the irregulars former Jupiter Trojans, or do they come from the inner solar system, or the outer solar system? Was it the same source that also fed Saturn's irregular moon system?
- Origin—how many progenitor objects did Jupiter capture, and when? How massive were they? What is their collisional history?

Science Objectives and Traceability Matrices

Table ISS-1 is the Cassini Solstice Mission Science Objectives. Tables ISS-2 through ISS-6 are the Saturn, Rings, Magnetospheres, Icy Satellites, and Titan Cassini Solstice Mission detailed Traceability Matrices.

Cell codes for Table ISS-1 through Table ISS-6 are as follows:

- First letter = discipline (**S**aturn, **R**ings, **M**agnetospheric and Plasma Science (**M**APS), **I**cy Satellites, **T**itan)
- Second letter = objective type (**C**hange related or **N**ew question)
- Third number = priority level (**1**, **2**)
- Fourth letter = distinction within priority level (**a**, **b**, **c**, etc.)

Color key for Table ISS-1 through Table ISS-6 are as follows:

- Not an ISS objective
- Measurement objectives satisfied
- Measurement objectives partially satisfied
- Measurement objectives not satisfied

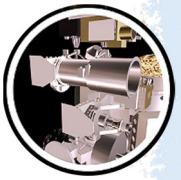

Table ISS-1. Cassini Solstice Mission Science Objectives—Prioritized Summary. Goal: Observe seasonal change in the Saturn system, to understand the underlying process and prepare for future missions.

Saturn	Rings	MAPS	Icy Satellites	Titan
Seasonal-Temporal Change				
Priority 1				
SC1a: Observe seasonal variation in temperature, clouds, and composition in three spatial dimensions.	**RC1a:** Determine the seasonal variation of key ring properties and the microscale properties of ring structure, by observing at the seasonally maximum opening angle of the rings near Solstice.	**MC1a:** Determine the temporal variability of Enceladus' plumes.	**IC1a:** Identify long-term secular and seasonal changes at Enceladus, through observations of the south polar region, jets, and plumes.	**TC1a:** Determine seasonal changes in the methane-hydrocarbon hydrological cycle: of lakes, clouds, aerosols, and their seasonal transport.
SC1b: Observe seasonal changes in the winds at all accessible altitudes coupled with simultaneous observations of clouds, temperatures, composition, and lightning.	**RC1b:** Determine the temporal variability of ring structure on all timescales up to decadal for regions including Encke gap, D-ring, F-ring, and ring edges by substantially increasing the cadence and time baseline of observations.	**MC1b:** Observe Saturn's magnetosphere over a solar cycle, from one solar minimum to the next.		**TC1b:** Determine seasonal changes in the high-latitude atmosphere, specifically the temperature structure and formation and breakup of the winter polar vortex.
Priority 2				
SC2a: Observe the magnetosphere, ionosphere, and aurora as they change on all time scales—minutes to years—and are affected by seasonal and solar cycle forcing.	**RC2a:** Focus on F-ring structure, and distribution of associated moonlets or clumps, as sparse observations show clumps, arcs, and possibly transient objects appearing and disappearing.	**MC2a:** Observe seasonal variation of Titan's ionosphere, from on Solstice to the next.		**TC2a:** Observe Titan's plasma interaction as it goes from south to north of Saturn's solar-wind-warped magnetodisk from one solstice to the next.
New Questions				
Priority 1				
SN1a: Determine Saturn's rotation rate and internal structure despite the planet's unexpected high degree of axisymmetry.	**RN1a:** Constrain the origin and age of the rings by direct determination of the ring mass, and of the composition of ring ejects trapped on field lines.	**MN1a:** Determine the dynamics of Saturn's magnetotail.	**IN1a:** Determine the presence of an ocean at Enceladus as inferred from induces magnetic field and plume composition, search for possible anomalies in the internal structure of Enceladus as associate with plume sources, and constrain the mechanisms driving the endogenic activity by in situ observations and remote sensing.	**TN1a:** Determine the types, composition, distribution, and ages, of surface units and materials, most notably lakes (i.e., filled versus dry and depth; liquid versus solid and composition; polar versus other latitudes and lake basin origin).

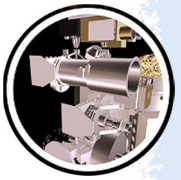

Table ISS-1. Cassini Solstice Mission Science Objectives—Prioritized Summary. Goal: Observe seasonal change in the Saturn system, to understand the underlying process and prepare for future missions.

Saturn	Rings	MAPS	Icy Satellites	Titan
SN1b: Observe the aftermath of the 2010–2011 storm. Study the life cycles of Saturn's newly discovered atmospheric waves, south polar hurricane, and rediscovered north polar hexagon.	**RN1b:** Determine the composition of the close-in ring moons as targets of opportunity.	**MN1b:** Conduct in situ and remote sensing studies of Saturn's ionosphere and inner radiation belt.	**IN1b:** Complete the comparative study of Saturn's mid-sized satellites, their geological and cratering histories, and interactions with the Saturn system, with remote sensing of Mimas at the highest resolution possible in order to understand the mechanisms behind its unique thermal properties discovered by Cassini.	**TN1b:** Determine internal and crustal structure: Liquid mantle, crustal mass distribution, rotational state of the surface with time, intrinsic and/or internal induced magnetic field.
SN1c: Measure the spatial and temporal variability of trace gases and isotopes.	**RN1c:** Determine structural and compositional variations at high-resolution across selected ring features of greatest interest, using remote and in situ observations.	**MN1c:** Investigate magnetospheric periodicities, their coupling to the ionosphere, and how the SKR periods are imposed from close to the planet (3–5 R_S) out to the deep tail.	**IN1c:** Determine whether Dione exhibits evidence for low-level activity, now or in recent geological time.	**TN1c:** Measure aerosol and heavy molecule layers and properties.
		Priority 2		
SN2a: Monitor the planet for new storms and respond with new observations when the new storms occur.	**RN2a:** Conduct in-depth studies of ring microstructure such as self-gravity wakes, which permeate the rings.	**MN2a:** Determine the coupling between Saturn's rings and ionosphere.	**IN2a:** Determine whether there is ring material orbiting Rhea, and if so, what its spatial and particle size distribution is.	**TN2a:** Resolve current inconsistencies in atmospheric density measurements (critical to a future Flagship mission).
	RN2b: Perform focused studies of the evolution of newly discovered propeller objects.		**IN2b:** Determine whether Tethys contributes to the E-ring and the magnetospheric ion and neutral population.	**TN2b:** Determine icy shell topography and viscosity.
			IN2c: Determine the extent of differentiation and internal inhomogeneity within the icy satellites, especially Rhea and Dione.	**TN2c:** Determine the surface temperature distribution, cloud distribution, and tropospheric winds.

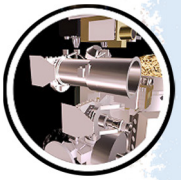

Table ISS-1. Cassini Solstice Mission Science Objectives—Prioritized Summary. Goal: Observe seasonal change in the Saturn system, to understand the underlying process and prepare for future missions.

Saturn	Rings	MAPS	Icy Satellites	Titan
			IN2d: Observe selected small satellites to quantify the movement of Enceladus material through the system, the history of satellite collisions/breakup, interaction with ring material as indicated by surface properties/ composition, and cratering rates deep in the Saturnian system.	

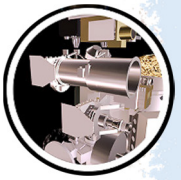

Table ISS-2. Cassini Solstice Mission Saturn Traceability Matrix.

Science Objective	Science Investigation	Measurement	Instrument(s)	Geometric Contraint(s)	Science Investigation Achieved? If No, Explain Further. New/Open Questions.
Seasonal-Temporal Change					
Priority 1					
SC1a - Observe seasonal variations in temperature, clouds, and composition in three spatial dimensions.	1. Investigate seasonal distribution of clouds.	1a. Observations at medium spatial resolution of visible-near-infrared cloud reflectivity, cloud-top altitude, and opacity. Full global daylit and nightside views (10.5 hrs continuous for each dayside and nightside observation) every ~6 months.	1a. VIMS (may be combinable with ISS designs).	1a. Dayside views: phase angle lower than 80 deg; distance between 12 and 20 R_S; Nightside views: phase angle greater than 120 degrees; Distance between 12 and 20 R_S. Polar views every ~6 months during high-inclination revs.	
		1b. Apoapse imaging every ~6 months in ~10 filters. May or may not be combined with part of 1a. Spread out over an orbit to get ~10 uniformly spaced phase angles from 0 to 165 degrees.	1b. ISS/WAC (may or may not be combined with VIMS/UVIS).	1b. Must be done over one almost complete rev to get phase angle coverage. Needs to be done in the range 20-40 R_S.	Phase angle coverage in the F-ring and proximal orbits was sparse due to close proximity to Saturn and fast sweep of phase angle near Periapse.
		1c. Apoapse high-res global map in true color (3 filters) every 2 years for public outreach, 10 hour observation.	1c. ISS/NAC (may or may not be combined with VIMS/UVIS).	1c. At < 90 deg phase angle (dayside). Distance of >30 R_S. From the equatorial plane.	
	2. Characterize seasonal distribution of aerosols.	2c. Observe the sunlight limb from pole to pole every ~6 months.	2c. ISS/NAC	2c. Spacecraft must be in eclipse.	
	4. Determine seasonal changes in the high latitude atmosphere, specifically the north and south polar vortices.	4b. Image both poles every ~6 months at start of Solstice Mission, only the north pole later in Solstice Mission.	4b. ISS (may be combined with other ORS instruments).	4b. Phase angles < 90 degrees. Need duration of ~5 hours for winds. Inclined orbits (i > 20 degrees is sufficient).	

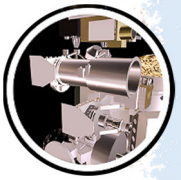

Table ISS-2. Cassini Solstice Mission Saturn Traceability Matrix.

Science Objective	Science Investigation	Measurement	Instrument(s)	Geometric Contraint(s)	Science Investigation Achieved? If No, Explain Further. New/Open Questions.
SC1b - Observe seasonal changes in the winds at all accessible altitudes coupled with simultaneous observations of clouds, temperatures, composition, and lightning.	1. Study the winds at high spatial resolution by observing the planet on successive rotations. Derive thermal winds from temperatures.	1a. Pairs of blocks (each of duration several hours): the second block should begin 11 hours after the first block begins. Cover each latitude every ~6 months.	1a. ISS Observation may be part of the VIMS/UVIS/CIRS template, e.g., 5-6-5 hour template.	1a. At < 100 deg phase angle, equatorial orbits, use 2-9-2 template if time is limited. Need ~8 repetitions to cover all latitudes (fewer than 8 at > 50 R_S).	Study of winds is best done at low phase angle. At high phase angle the contrast is too low. Too little time was available at low phase angle during the F-ring and Proximal orbits.
		1b. 5 µm observations of deep clouds. Pairs of blocks (each of duration several hours): the second block should begin 11 hours after the first block begins. Cover each latitude every ~6 months.	1b. VIMS; observation may be part of the ISS/UVIS template, e.g., 5-6-5 hour template.	1b. Distance between 3 and 15 R_S encompassing both 11 hour observation blocks.	
	3. Study seasonal change in convective storms and lightning.	3a. Night side visible images to see lightning, multiple short exposures to minimize scattered light. Cover each latitude every ~6 months.	3a. ISS; VIMS may ride along.	3a. Phase angle 90 to 130 degrees.	
		3c. Look for sudden appearance of convective storms. Day side imaging at Saturn waypoint. This is a monitoring activity. The idea is to have minimum impact on spacecraft operations.	3c. ISS.	3c. WAC in 1–3 filters whenever pointing at Saturn waypoint, range > 20 R_S, phase angle < 135 deg. Try to repeat every 2 hours, but whenever conflict arises, drop it.	
Priority 2					
SC2a - Observe the magnetosphere, ionosphere, and aurora as they change on all time scales - minutes to years - and are affected by seasonal and solar cycle forcing.	1. Investigate the northern and southern aurora using remote sensing.	1a. High spatial resolution imaging of visible aurora. An 80 hour movie every ~6 months plus ride-alongs.	1a. ISS rides along with UVIS/VIMS/CAPS auroral campaign.	1a. Phase angle > 90 degree (night side).	

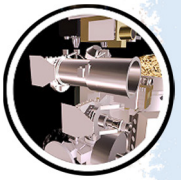

Table ISS-2. Cassini Solstice Mission Saturn Traceability Matrix.

Science Objective	Science Investigation	Measurement	Instrument(s)	Geometric Contraint(s)	Science Investigation Achieved? If No, Explain Further. New/Open Questions.
New Questions					
Priority 1					
SN1b - Observe the aftermath of the 2010-2011 storm. Study the life cycles of Saturn's newly discovered atmospheric waves, south polar hurricane, and rediscovered north polar hexagon.	1. Study Saturn atmospheric features (special features, defined by their latitudes) including the 2010–2011 northern storm region, the north polar vortex and hexagon, the ribbon, donuts, the string of pearls at 30 N, the QXO near the equator, the thunderstorm region at 35 S, and the eye region of the south polar vortex.	1a. High-resolution (few km/pix) visible observations of special latitudes. 11 hour repeat cycle to measure winds. Observe each feature every year.	1a. ISS may be combined with VIMS.	1a. At < 100 deg phase angle.	Study of winds is best done at low phase angle. At high phase angle the contrast is too low. Too little time was available at low phase angle during the F ring and Proximal orbits.
Priority 2					
SN2a - Monitor the planet for new storms and respond with new observations when the new storms occur.	1. Investigate recently active northern storm latitudes and storm alley at 35 S for new lightning storms and other phenomena.	1a. Visible imaging of both hemispheres: 2010–2011 active northern region and southern hemisphere and the "dragon storms" at ~35 S. Take 1–3 images every time the spacecraft is already pointed toward Saturn's center, up to once every 2 hours.	1a. ISS/WAC; VIMS may or may not ride along.	1a. Dayside only (phase angle < 90). ~3.5 Mbits/image.	

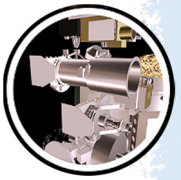

Table ISS-3. Cassini Solstice Mission Rings Traceability Matrix.

Science Objective	Science Investigation	Measurement	Instrument(s)	Geometric Contraint(s)	Science Investigation Achieved? If No, Explain Further. New/Open Questions.
Seasonal-Temporal Change					
Priority 1					
RC1a -Determine the seasonal variation of key ring properties and the microscale properties of ring structure, by observing at the seasonally maximum opening angle of the rings near Solstice.	1. Determine seasonal variability of ring particle temperature.	1c. Measure ring particle albedo at visible-IR wavelengths as a function of radius using radial scans in inclined orbits throughout Solstice Mission.	1c. ISS, VIMS	1c. Take photometric measurements in 3 filters and VIMS plus clear at 5–10 phase angles and 3–5 ring opening angles (lit and unlit face). Distance from Saturn of around 20 R_S is acceptable.	In many or perhaps most cases, there was inadequate data volume to make all the images 12 bits, but this was not a serious problem because the SNR was high. In some cases, allocated time backed us off from 8 filters to maybe 7. But overall, the spirit of them was satisfied. Two of them (RN1b1a and RN1b2c) were more VIMS-emphasis.
	2. Investigate how spoke occurrence varies with season.	2a. Point and Stare observations pointed at a fixed position in the B-ring to look for spokes before they fade in ~2013. Long time baseline needed for accurate measurement of periodicity. 500 h of observation time is required for each of the three types of observations shown in the geometric constraints. (1500 h total.)	2a. ISS	2a. Observations must be performed before the spokes fade out as the ring plane opening angle to the Sun increases beyond 20.5 degrees (~late 2013). Observations must be performed for low phase (less than 50 degrees) lit face, high phase (greater than 100 degrees) lit face and high phase dark face. Spacecraft elevation angle must be greater than 3 degrees.	For the CSM, we were assigned about 1072 hours' worth of observing time, but only about 718 of those hours happened before the spokes faded out. So we roughly got half of the 1500 hours that we were looking for.
	3. Characterize seasonal variation of Saturn's E-ring structure.	3a. Edge-on images of both ansa of the E-ring every 1–2 years to measure changes in sun-driven warp of the rings.	3a. ISS/WAC	3a. Ring opening angle must be less than 0.1 degrees, and range must be greater than 20 R_S, greater than 30 R_S is preferred. There are no strong constraints on the phase angle for these observations. Low (< 30 degrees), high (> 120 degrees) and moderate (~90 degrees) are preferred.	

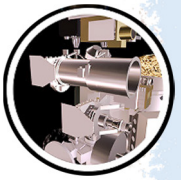

Table ISS-3. Cassini Solstice Mission Rings Traceability Matrix.

Science Objective	Science Investigation	Measurement	Instrument(s)	Geometric Contraint(s)	Science Investigation Achieved? If No, Explain Further. New/Open Questions.
		3b. Imaging of all longitudes in the E-ring at high signal-to-noise in multiple filters every 2 years to measure changes in the spatial distribution of different sized particles.	3b. ISS/WAC	3b. Ideally performed while Cassini is in Saturn's Shadow and more than 10 R_S from the planet. Additional information can be obtained at phase angles between 130 and 145 degrees and ring elevations between 5 and 15 degrees.	We were able to observe all longitudes in 2012 and 2013, and a large fraction of longitudes in 2017 during eclipse periods. We did not have a similar opportunity in the 2014–2016 time frame.
	5. Determine ring microstructure, especially in the optically-thickest regions.	5d. Image rings at 50 meter resolution. One complete lit-face radial profile and one complete unlit-face radial profile are required.	5d. ISS	5d. Range must be less than 0.1 R_S, and spacecraft elevation angle must be greater than 10 degrees. Lit and unlit faces are desired.	Practically no images achieved the stated resolution, much less with full radial coverage. Regions of particular interest were imaged at 400 meter resolution, full coverage at 800 meter resolution.
		5f. Radial profiles of ring brightness of A-ring and B-ring, and Cassini Division over at least 6 longitudes at 3 or more tilt angles to measure amplitude of azimuthal asymmetry at radial resolution better than 5 km. Coverage of the C-ring is desirable, but not required.	5f. ISS	5f. Observations that cover A-rings, Cassini division and B-rings. Sampling is spacecraft relative and should occur over at least 6 longitudes at 3 or more tilt angles (> 20 degrees, 10–20 degrees, and < 20 degrees). Range must be less than 13 R_S, and phase angle must be less than 60 degrees to minimize Saturn-shine.	
	6. Characterize ring properties in geometries that are comparable to Voyager and Earth observations for purposes of cross comparison.	6c. Multi-color radial profiles of lit ring brightness in at least 5 broadband filters in the near-UV, visual wavelengths and near-IR that cover A-rings, Cassini division, B-rings and C-rings at 5 or more solar elevation angles.	6c. ISS	6c. Observations of the lit face of the rings at 5 or more solar elevation angles in the range 5-27 degrees to compare with HST and ground-based observations of the rings. Range must be less than 25 R_S. Phase angles should be as small as possible, preferably < 7 degrees, to allow direct comparison with ground-based data.	

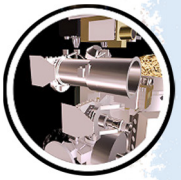

Table ISS-3. Cassini Solstice Mission Rings Traceability Matrix.

Science Objective	Science Investigation	Measurement	Instrument(s)	Geometric Contraint(s)	Science Investigation Achieved? If No, Explain Further. New/Open Questions.
RC1b - Determine the temporal variability of ring structure on all timescales up to decadal for regions including Encke gap, D-ring, F-ring, and ring edges by substantially increasing the cadence and time baseline of observations.	1. Study Encke gap, other gaps and associated ringlets over long-time baseline.	1a. Ansa stare for one full orbital period in each of 5 zones at resolutions of better than 15 km/pixel: i) Inner C/D: Huygens, Russell and Herschel gaps; ii) Outer C/D: Laplace and Jeffreys gaps; iii) Outer C-ring: 1.470, 1.495 R_S gaps; iv) Maxwell gap; v) Columbo gap.	1a. ISS	1a. Phase angle must be less than 60 degrees. Prefer unlit rings, but observation can be performed on lit rings if necessary. Ranges must be between 15 and 40 R_S, and ring opening angles must be greater than 5 degrees.	
		1b. Image multiple longitudes in Laplace Gap, Huygens Gap, Maxwell Gap and D68 at resolutions of better than 15 km/pixel every 1–2 years to measure time evolution of eccentric and heliotropic features.	1b. ISS	1b. For Laplace Gap and D68, no strong constraints on phase angles (although higher phase has higher SNR). For Huygens and Maxwell Gaps, phase angles greater than 130 degrees are preferred. Ranges must be between 15 and 40 R_S and ring opening angles must be greater than 5 degrees.	
	2. Study the D-ring over long-time baseline.	2a. High-Resolution (3-5 km/NAC pixel) imaging of the outer part of the D-ring every year to measure time evolution of corrugation.	2a. ISS	2a. No strong constraints on phase angle. Range must be between 8 and 15 R_S. Both low (0.3–5 degree) and high (5–20 degree) ring opening angles are useful.	
		2b. 12-hour (1 Saturn Rotation) ansa movies of the D-ring between 71,500–74,500 km and the Roche Division between the A-ring and F-ring where a related pattern appears. Desire 2–3 movies of each region within a time span of 6–12 months every 2–3 years to measure structures in the rings tied to SKR.	2b. ISS	2b. Phase must be above 140 degrees. Ring opening angle must be above 5 degrees, and range must be between 15 and 40 R_S.	

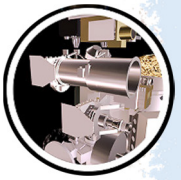

Table ISS-3. Cassini Solstice Mission Rings Traceability Matrix.

Science Objective	Science Investigation	Measurement	Instrument(s)	Geometric Contraint(s)	Science Investigation Achieved? If No, Explain Further. New/Open Questions.
	3. Characterize the G and other narrow faint rings over long time baselines.	3a. Ansa movies of J/E-ring, G-ring, Pallene Ring, Anthe and Methone Rings every 1–2 years. Movies should be longer than 12 hours (1/3 rotation period) and include time when the appropriate moon moves through the ansa.	3a. ISS	3a. No strong constraints on phase angle. Range must be greater than 20 R_S, and ring opening angle must be less than 10 degrees.	For G-ring/ Pallene/Anthe/ Methone the goal was basically achieved, in that we have images around each of these moons with appropriate exposures for the arcs/rings. For the J/E-ring, we made a few attempts to image the relevant region, but it was not clearly visible outside of the HIPHASE/ eclipse periods. We therefore have more limited data on this, but we do have looks in 2013 and 2016/2017.
	4. Determine the temporal evolution of individual propeller.	4a. Scan the outer A-ring (from 133700-136700 km from Saturn Center) at all longitudes at least annually.	4a. ISS	4a. Range must be between 3.5 and 10 R_S. Sub-S/C latitude must be greater than 10 degrees. Observations must be at least 16–18 hours in duration. Observations need not be contiguous, but must be in the same periapse and configured such that all co-rotating longitudes can be sampled.	
		4b. Perform follow-up images of known propellers roughly twice monthly during RTWT segments.	4b. ISS	4b. Range must be less than 15 R_S. (Less than 23 R_S is acceptable for one of the known targets.) Sub-spacecraft latitude must be greater than 10 degrees. Duration of observations require at least 5 minutes (actual dwell time) per target. No connection with 4a is required.	For the J/E-ring, we made a few attempts to image the relevant region, but it was not clearly visible outside of the HIPHASE/ eclipse periods. We therefore have more limited data on this, but we do have looks in 2013 and 2016/2017.

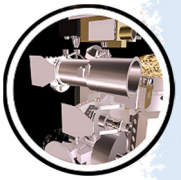

Table ISS-3. Cassini Solstice Mission Rings Traceability Matrix.

Science Objective	Science Investigation	Measurement	Instrument(s)	Geometric Contraint(s)	Science Investigation Achieved? If No, Explain Further. New/Open Questions.
Priority 2					
RC2a - Focus on F-ring structure, and distribution of associated moonlets or clumps, as sparse observations show clumps, arcs, and possibly transient objects appearing and disappearing.	1. Study apse anti-alignment (F-ring/ Prometheus).	1a. Follow Prometheus for one orbital period (15 hours) twice per year, 4–6 times in all, to observe one complete cycle of streamer-channel feature raised in F-ring.	1a. ISS	1a. Range must be between 13 and 22 R_S. Spacecraft elevation angle must be greater than 15 degrees. Execute once early in IN1, the rest later.	
		1b. Ansa stare observations with a duration of 15 hours once per apoapse. Observe complete co-rotating 360 degrees of F-ring as material passes through the NAC field of view.	1b. ISS, VIMS	1b. Range must be less than 30 R_S, and spacecraft elevation angle must be greater than 15 degrees.	We had > 100 FMOVIE observations over the duration of the tour but only ~30 covered the full 360 degrees. Some of the FMOVIEs were intentionally split between ansae to highlight effect of eccentricity. It was impossible to make the "once per apoapse" requirement on every orbit.
	2. Search for and characterize new clumps/strands.	2a. Ansa stare observations with a duration of approximately 15 hours once per apoapse. Observe complete co-rotating 360 degrees of F-ring material as it passes through the NAC field of view.	2a. ISS, VIMS, CIRS	2a. Range must be less than 30 R_S, and spacecraft elevation angle must be greater than 15 degrees.	We had > 100 FMOVIE observations over the duration of the tour but only ~30 covered the full 360 degrees. Some of the FMOVIEs were intentionally split between ansae to highlight effect of eccentricity. It was impossible to make the "once per apoapse" requirement on every orbit.

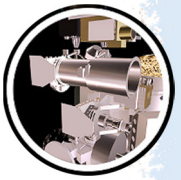

Table ISS-3. Cassini Solstice Mission Rings Traceability Matrix.

Science Objective	Science Investigation	Measurement	Instrument(s)	Geometric Contraint(s)	Science Investigation Achieved? If No, Explain Further. New/Open Questions.
	3. Investigate clumps and moonlets on short timescales.	3a. Obtain high-resolution maps and movies on short time scales for clump and moonlet tracking purposes. Ansa stare observations with a duration of approximately 15 hours should occur once every 2–3 months. Observe F-ring material as it passes through the NAC field of view.	3a. ISS, VIMS	3a. Range must be less than 15 R_S for both instruments, and spacecraft elevation angle must be greater than 15 degrees. If possible, observations should also capture the A-ring edge into ~136000 km without impacting F-ring science in order to partially address RN1c(4a).	We did obtain partial high-resolution coverage but never for the full 360 degrees in this geometry (given the time constraints at peripase this would have been difficult) and never at a frequency of once every 2–3 months. Nevertheless, we did manage to observe and track moonlets.
New Questions					
Priority 1					
RN1b - Determine the composition of the close-in "ringmoons" as targets of opportunity.	1. Obtain spatially resolved spectral and color maps of ringmoons at UV, visual, and NIR wavelengths.	1a. 12-bit images in multiple filters. RED, GRN, BL1, UV3, IR3 and clear at a minimum. Observational opportunities are rare and will be taken as available.	1a. ISS, VIMS, UVIS, CIRS	1a. Phase angle at the satellite must be less than 90 degrees, and ranges must be less than 50,000 km. VIMS requires a minimum object diameter of 1 mrad in order to get at least one filled pixel on the moon. ISS demands are less restrictive. Target will depend on opportunity.	(RN1b1a and RN1b2c) were more VIMS-emphasis
	2. Characterize radial structure of rings at high-resolution.	2b. Two or more multi-filter (at least 8 filters, 12 bit) radial scans across ansa from 68000 km to 141000 km.	2b. ISS, UVIS rider	2b. Observe lit-side. Range must be less than 15 R_S. Elevation angle must be greater than 15 degrees. Phase angle must be less than 60 degrees.	

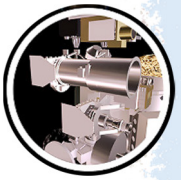

Table ISS-3. Cassini Solstice Mission Rings Traceability Matrix.

Science Objective	Science Investigation	Measurement	Instrument(s)	Geometric Contraint(s)	Science Investigation Achieved? If No, Explain Further. New/Open Questions.
		2c. Radial scans of the entire main ring system during the proximal orbits, supplemented by observations of selected regions such as the outer C-ring and outer B-ring with targeted pointings and/or continuous drift scans. Resolutions better than 30 km/VIMS pixel desired. Require at least two full scans and at least two targeted observations. (RN1b1a and RN1b2c) were more VIMS-emphasis.	2c. VIMS, ISS rider	2c. Range less than 2-3 R_S to observation target and ring opening angles greater than 20 degrees. Lit side preferred. Only proximal orbits will provide these geometries.	
		2d. Radial scans of entire main ring system: 4 lit face and 4 unlit face, at multiple phase angles in at least 4 filters.	2d. ISS	2d. Range must be less than 20 R_S. At least 4 observations of the lit face *and* 4 observations of the unlit face are required, covering a range of phase angles.	
RN1c - Determine structural and compositional variations at high-resolution across selected ring features of greatest interest, using remote and in situ observations.	3. Study gap edges for azimuthal and temporal variations at varying scales and search for potential wakes produced by gap-embedded satellites.	3c. Map the edges of known empty gaps for one full orbital period at least once each.	3c. ISS	3c. Satisfied by requested surveys for undiscovered moonlets and for propellers. Both the lit and unlit sides are acceptable for mapping gap edges.	
		3d. Image Encke and Keeler Gaps at least three times at all available longitudes at 45 degree intervals in less than two hours to disentangle azimuthal and temporal effects.	3d. ISS	3d. Range must be less than 10 R_S, and spacecraft elevation angle must be greater than 15 degrees.	People freaked out about anything that sounded like an "azscan," so this was not done.

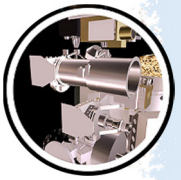

Table ISS-3. Cassini Solstice Mission Rings Traceability Matrix.

Science Objective	Science Investigation	Measurement	Instrument(s)	Geometric Contraint(s)	Science Investigation Achieved? If No, Explain Further. New/Open Questions.
RN2a - Conduct in-depth studies of ring microstructure such as self-gravity wakes, which permeate the rings.	4. Study A-ring and B-ring outer edge modes to improve our understanding of them.	4a. Ansa-stare movies on the ring edges at least twice per year. B-ring requires at least 12 hours per observation, and A-ring requires at least 15 hours per observation. A minimum of 100 images is required for each movie.	4a. ISS	4a. Observe lit side. Elevation angle must be greater than 15 degrees, and phase angle must be less than 60 degrees. A-ring range must be less than 15 R_S. B-ring range must be less than 30 R_S.	
	1. Study self-gravity wakes and over stabilities in depth.	1c. Perform multi-filter lit face radial drift scan from 74,000 km to 141,000 km during the proximal phase of the tour. At least three scans are required.	1c. ISS	1c. Range less than 1 R_S. Lit face required.	
	2. Study "straw" and other packing effects.	2d. Perform multi-filter radial scans from 74,000 km to 141,000 km during the proximal phase of the tour. At least three scans are required.	2d. ISS	2d. Range less than 1 R_S. Lit and unlit face desired, but lit is preferred.	
Priority 2					
RN2b - Perform focused studies of the evolution of newly discovered "propeller" objects.	1. Investigate propeller structure and photometric properties.	1a. Perform focused studies to refine propeller structure and photometric properties at a range of sizes. Scan the "Propeller Belts" in the mid A-ring (from 127000–130000 km from Saturn center) at all longitudes, at least once. Observations must be at least 16–18 hours in duration.	1a. ISS	1a. Range must be between 3.5 and 10 R_S. Sub-spacecraft latitude must be greater than 10 degrees. Observations need not be contiguous, but must be in the same periapse and configured such that all co-rotating longitudes can be sampled.	
		1b. Obtain very-high-resolution images of propellers in the "Propeller Belts" of the mid A-ring. Use multiple color filters while keplerian tracking. Must target at least 3 different radii, at least once each.	1b. ISS	1b. Range must be less than 4 R_S. Sub-spacecraft latitude must be greater than 10 degrees. Observation length (dwell time) of at least 20 minutes per target location required.	Close-range imaging of the Propeller Belts was done, but color imaging proved impractical.

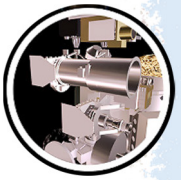

Table ISS-3. Cassini Solstice Mission Rings Traceability Matrix.

Science Objective	Science Investigation	Measurement	Instrument(s)	Geometric Contraint(s)	Science Investigation Achieved? If No, Explain Further. New/Open Questions.
		1c. Obtain very-high-resolution images of known large propellers in the outer A-ring. Use multiple color filters while keplerian tracking. Must target at least 3 known propellers once each.	1c. ISS	1c. Range to the known propeller's position must be less than 4 R_S. Sub-spacecraft latitude must be greater than 10 degrees. Observation length (dwell time) of at least 20 minutes per target required.	Targeted imaging of three propellers was done, but color imaging proved impractical.
		1d. Obtain lit and unlit face images at a range of phase angles and sub-spacecraft latitudes (as shown in the geometric constraints) of known large propellers in the outer A-ring. Use multiple color filters while keplerian tracking. Require at least one observation in each of the eight geometries described.	1d. ISS	1d. Range must be less than 7 R_S. Observe targets for at least 20 minutes when: 1) Sub-spacecraft latitude is between 10 and 20 degrees and phase angle is less than 30 degrees; 2) Sub-spacecraft latitude is between 10 and 20 degrees and phase angle is greater than 130 degrees; 3) Sub-spacecraft latitude is greater than 40 degrees and phase angle is less than 30 degrees; and 4) Sub-spacecraft latitude is greater than 40 degrees and phase angle is greater than 130 degrees. Both lit and unlit faces are desirable.	
		1e. Perform full azimuthal scans of the outer C-ring and Cassini Division, once each.	1e. ISS	1e. Satisfied by the constraints for RC1b(1a).	See RC1b(1a)

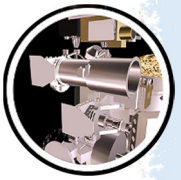

Table ISS-4. Cassini Solstice Mission Magnetospheres Traceability Matrix.

Science Objective	Science Investigation	Measurement	Instrument(s)	Geometric Contraint(s)	Science Investigation Achieved? If No, Explain Further. New/Open Questions.
New Questions					
Priority 1					
MN1b - Conduct in situ and remote sensing studies of Saturn's ionosphere and inner radiation belt.	1. Investigate the effects on aurora of solar wind and seasons.	1a. Sample auroral photon emission, ENA emission, SKR, solar wind conditions.	1a. HST, UVIS, VIMS and/or ISS auroral images; CAPS ions, electrons; MIMI INCA ENA; MAG, RPWS.	1a. In sheath or solar wind, -Y to Saturn aurora.	

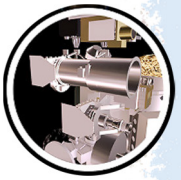

Table ISS-5. Cassini Solstice Mission Icy Satellites Traceability Matrix.

Science Objective	Science Investigation	Measurement	Instrument(s)	Geometric Contraint(s)	Science Investigation Achieved? If No, Explain Further. New/Open Questions.
Seasonal-Temporal Change					
Priority 1					
IC1a - Identify long-term secular and seasonal changes at Enceladus, through observations of the south polar region, jets, and plumes.	1. Understand seasonal changes in Enceladus' south polar region.	1c. Visible imaging of the south polar region illuminated by the sun or Saturn shine with 40 m or better resolution during at least 2 flybys.	1c. ISS	1c. Flybys with views of south pole; 2,000-7,000 km altitude.	As subsolar latitudes moved further north over time, secondary illumination was too poor for imaging surface details except near terminator. However, excellent coverage was obtained early during the CSM. Final high-resolution images of the active SPT region was not obtained in December 2015. However excellent imaging was obtained just outside of the south polar province.
	2. Understand seasonal changes in Enceladus' jets.	2a. High-resolution imaging of jets on temporal scales of at least every 2 months.	2a. ISS	2a. Observations at a range of viewing geometries, including latitudes and longitudes.	As subsolar latitudes moved further north over time, imaging of jets at the surface became problematic due to solar terminator geometry.
	3. Understand seasonal changes in Enceladus' plumes.	3c. Plume imaging, evenly spaced throughout Solstice mission, with observations at a minimum of every two months if possible.	3c. ISS	3c. Very high phase distant views, ideally with spacecraft in Saturn shadow (for plume "tendril" movies).	
		3d. Plume monitoring throughout Solstice mission, with observations at a minimum of every two months if possible.	3d. ISS	3d. Imaging from 60,000 km altitude, 140–165 deg phase, throughout tour.	
	4. Investigate effects on the inner mid-sized and small satellites due to interaction with the E-ring.	4a. Medium and high-resolution imaging and compositional mapping of satellites out to and including Rhea.	4a. ISS, VIMS, UVIS	4a. Medium and high-resolution flybys of leading/trailing hemispheres (1000-100,000 km) at least once per satellite.	

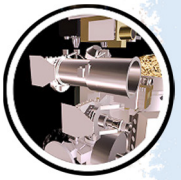

Table ISS-5. Cassini Solstice Mission Icy Satellites Traceability Matrix.

Science Objective	Science Investigation	Measurement	Instrument(s)	Geometric Contraint(s)	Science Investigation Achieved? If No, Explain Further. New/Open Questions.
New Questions					
Priority 1					
IN1a - Determine the presence of an ocean at Enceladus as inferred from induced magnetic field and plume composition, search for possible anomalies in the internal structure of Enceladus as associated with plume sources, and constrain the mechanisms driving the endogenic activity by in situ observations and remote sensing.	3. Determine internal structure and any possible anomalies.	3b. Imaging to determine a more accurate shape model for Enceladus (to determine bulk density and regions of isostatic compensation) on at least 3 compensation) on at least 3.	3b. ISS	3b. Flybys in the 2000-50,000 km range with a range of viewing geometries as available from the mission design.	
	4. Determine mechanisms of activity using in situ observations and remote sensing.	4e. High-resolution (40 m or better in the visible, 0.5 km or better in the IR) imaging, compositional mapping and radiometry of south polar.	4e. ISS, VIMS, RADAR	4e. Flybys with views of south pole; 2,000-7,000 km altitude.	
		4f. Measure dust in plume using visible & IR imaging, every two months if possible.	4f. ISS, VIMS	4f. Long stares (1-2 hours) of plumes.	
IN1b - Complete the comparative study of Saturn's mid-sized satellites, their geological and cratering histories, and interactions with the Saturn system, with remote sensing of Mimas at the highest resolution possible in order to understand the mechanisms behind its unique thermal properties discovered by Cassini.	1. Investigate Mimas' geological and cratering history	1a. Imaging of both leading and trailing hemispheres to complete mapping coverage.	1a. ISS	1a. At least 4 flybys in the 100,000 km range.	

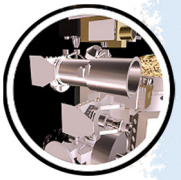

Table ISS-5. Cassini Solstice Mission Icy Satellites Traceability Matrix.

Science Objective	Science Investigation	Measurement	Instrument(s)	Geometric Contraint(s)	Science Investigation Achieved? If No, Explain Further. New/Open Questions.
IN1c - Determine whether Dione exhibits evidence for low-level activity, now or in recent geological time.	1. Investigate Dione's level of current activity.	1f. Seek forward scattered component in solar phase function during flybys by making high phase angle measurements.	1f. VIMS, ISS, UVIS	1f. Observations at large solar phase angles (150-165 degrees; the higher the better).	
		1g. Search for tenuous atmosphere using off-limb.	1g. VIMS, ISS, UVIS	1g. Long integration times off limb.	
	2. Investigate Dione's past geologic activity.	2a. Imaging surface to complete mapping coverage.	2a. ISS	2a. Medium and high-resolution mapping (3000-50,000 km).	
Priority 2					
IN2a - Determine whether there is ring material orbiting Rhea, and if so, what its spatial and particle size distribution is.	1. Investigate Rhea and its environment to search for a ring (or debris disk).	1a. High-resolution imaging of the surface to complete mapping coverage.	1a. ISS	1a. Flybys in 3000-50,000 km altitude range.	
IN2b - Determine whether Tethys contributes to the E ring and the magnetospheric ion and neutral population.	2. Investigate Tethys's level of current activity.	2d. High phase angle measurements to complete phase angle coverage & seek forward-scattered component to the solar phase curve.	2d. VIMS, ISS, UVIS	2d. Observations at large solar phase angles (150-165 degrees, the larger the better).	
	3. Investigate whether Tethys appears to be currently geologically active.	3b. High-resolution imaging of the surface to complete mapping coverage.	3b. ISS	3b. Flybys at 3000-150,000 km.	
	4e. Investigate whether Tethys has a tenuous atmosphere.	4a. Off-limb imaging of Tethys, at least once during Solstice.	4a. VIMS, UVIS, ISS	4a. Long integration time near limb.	
IN2c - Determine the extent of differentiation and internal inhomogeneity within the icy satellites, especially Rhea and Dione.	2. Determine a more detailed shape model for Rhea and Dione.	2a. Medium and high-resolution imaging of Rhea to complete coverage.	2a. ISS	2a. Flybys in the 3000-50,000 km range	
		2b. Medium and high-resolution imaging of Dione to complete coverage.	2b. ISS	2b. Flybys in the 3000-50,000 km range.	

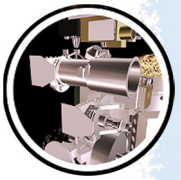

Table ISS-5. Cassini Solstice Mission Icy Satellites Traceability Matrix.

Science Objective	Science Investigation	Measurement	Instrument(s)	Geometric Contraint(s)	Science Investigation Achieved? If No, Explain Further. New/Open Questions.
IN2d - Observe selected small satellites to quantify the movement of Enceladus material through the system, the history of satellite collisions/ breakup, interaction with ring material as indicated by surface properties/compo sition, and cratering rates deep in the Saturnian system	1. Observe Epimetheus, Janus, Methone, Prometheus, and others as opportunities arise.	1a. Visible imaging of surface	1a. ISS	1a. Flybys in the 1000-100,000 km range over solar phase angles 0-120 degrees	Some close flyby images were not obtained due to ephemeris and/or pointing errors especially during very close flybys. This was especially true for close flybys of Helene (2008, 2010), Atlas (2015) and Daphnis (2016).

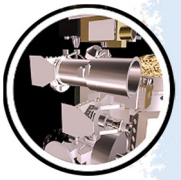

Table ISS-6. Cassini Solstice Mission Titan Traceability Matrix.

Science Objective	Science Investigation	Measurement	Instrument(s)	Geometric Contraint(s)	Science Investigation Achieved? If No, Explain Further. New/Open Questions.
Seasonal-Temporal Change					
Priority 1					
TC1a - Determine seasonal changes in the methane-hydrocarbon hydrological cycle: of lakes, clouds, aerosols, and their seasonal transport.	1. Determine the seasonal distribution of the lakes.	1c. Repeated, as allocated by TOST, medium resolution (≤ 10km/pixel), high-latitude (> 70° N and S; > 50° N for Kraken Mare) observations to look for changes (preferably close (in time) to RADAR observations for comparison and to provide context).	1c. ISS	1c. High latitude (> 70 N and S); > 50° N for Kraken Mare); resolution ≤ 10 km	Limited constraints on the rate of surface changes and extent of seasonal interaction between surface, atmosphere, and subsurface methane reservoirs due to later than predicted onset of summer weather at the north pole. Another question is what is the nature of the bright north-polar surface deposit and how does it relate to the lakes and seas?
	2. Determine the seasonal distribution of clouds.	2b. Repeated, ideally weekly, low-resolution (≤ 50 km/pixel) imaging throughout a seasonal cycle. Desire several opportunities/month throughout the Solstice Mission.	2b. ISS	2b. Phase angle < 120°; any longitude and any latitude—high northern latitudes (> 60°) preferred for development of summer clouds; pixel scale ≤ 50 km (range < 8.4e6 km)	Onset of north-polar cloud activity did not occur before EOM; timing of predicted seasonal weather pattern remains unknown. What causes differences from model predictions and how typical are the weather patterns we observed? What is the nature of the north-polar cloud features VIMS detected at 2.1 μm starting in June 2016 that were not visible at other wavelengths?

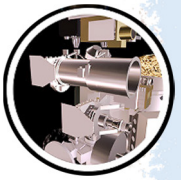

Table ISS-6. Cassini Solstice Mission Titan Traceability Matrix.

Science Objective	Science Investigation	Measurement	Instrument(s)	Geometric Contraint(s)	Science Investigation Achieved? If No, Explain Further. New/Open Questions.
	3. Characterize the seasonal distribution of aerosols.	3c. Repeated limb observations at various latitudes, and resolutions (few to several km) Desire several opportunities/year during distant/non-targeted encounters (or at distant times during targeted encounters) throughout Solstice Mission.	3c. ISS	3c. Variety of phase angles (0–180°) and latitudes (90° S to 90° N) desired	
TC1b - Determine seasonal changes in the high-latitude atmosphere, specifically the temperature structure and formation and breakup of the winter polar vortex.	1. Study wintertime polar vortices.	1b. Repeated polar imaging throughout Solstice Mission at pixel scales of a few to several km. Desire a few opportunities per month throughout the Solstice Mission.	1b. ISS	1b. Latitude > |70°|; resolutions ≤ few to several km	
	2. Understand the tilted pole.	2b. Whole-disk imaging in methane bands, with a frequency of a few opportunities per month throughout the Solstice Mission.	2b. ISS	2b. Phase angles < 90°; latitudes > |60| deg	
New Questions					
Priority 1					
TN1a - Determine the types, composition, distribution, and ages of surface units and materials, most notably lakes (i.e. filled versus dry and depth; liquid versus solid and composition; polar versus other latitudes and lake basin origin).	1. Characterize lakes as liquid or dry and their composition.	1c. ISS context beyond the swaths. ISS/VIMS/RADAR comparisons, i.e. overlapping coverage, for interpretation beyond RADAR swaths/VIMS noodles. (As much ISS coverage overlapping RADAR and VIMS swaths as possible within TOST allocation.)	1c. ISS	1c. Previous RADAR/VIMS observations	Detailed compositions of different geologic surface units and interactions between materials on the surface and in the subsurface remain unknown. What is the bright north-polar surface unit? How does it relate to the lakes and seas? What are the implications of a lack of a comparable surface unit at the south pole?

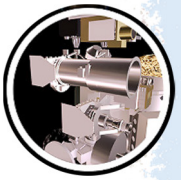

Table ISS-6. Cassini Solstice Mission Titan Traceability Matrix.

Science Objective	Science Investigation	Measurement	Instrument(s)	Geometric Contraint(s)	Science Investigation Achieved? If No, Explain Further. New/Open Questions.
	3. Study surface modifications due to geological activity. Determine the origin of depressions, Xanadu, fluvial features, and crypto-circles	3d. Repeated, as allocated by TOST, medium-high resolution (≤few km) observations throughout the Solstice Mission, especially at high latitudes. Most important to get some observations near equinox and some near northern summer solstice to extend the temporal baseline as long as possible	3d. ISS	3d. Phase < 90 deg; resolutions ≤ few km	Limited constraints on the rate of surface changes and extent of seasonal interaction between surface, atmosphere, and subsurface methane reservoirs due to later than predicted onset of summer weather at the north pole.
TN1c - Measure aerosol and heavy molecule layers and properties.	1. Characterize aerosol properties	1b. Repeated limb observations at various latitudes, and resolutions (few to several km). Desire several opportunities/ year during distant/non-targeted encounters (or at distant times during targeted encounters) throughout Solstice Mission.	1b. ISS	1b. Variety of phase angles (0–180°) and latitudes (90° S to 90° N) desired	
Priority 2					
TN2c - Determine the surface temperature distribution, cloud distribution, and tropospheric winds.	1. Study tropospheric cloud distribution	1a. Repeated (ideally weekly) low-resolution (≤ 50 km/pixel) imaging throughout a seasonal cycle. Desire several opportunities/month throughout the Solstice Mission.	1a. ISS	1a. Phase angle < 120°; any longitude and any latitude—high northern latitudes (> 60°) preferred for development of summer clouds; NAC pixel scale ≤ 50 km (range < 8.4e6 km)	Onset of north-polar cloud activity did not occur before EOM; timing of predicted seasonal weather pattern remains unknown. What causes differences from model predictions and how typical are the weather patterns we observed? What is the nature of the north-polar cloud features VIMS detected at 2.1 μm starting in June 2016 that were not visible at other wavelengths?

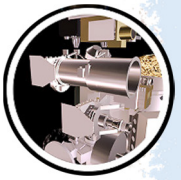

Table ISS-6. Cassini Solstice Mission Titan Traceability Matrix.

Science Objective	Science Investigation	Measurement	Instrument(s)	Geometric Contraint(s)	Science Investigation Achieved? If No, Explain Further. New/Open Questions.
	3. Infer surface and tropospheric winds	3b. Repeated medium-resolution (≤ few to several km/pixel) imaging over several hours; can be distant, e.g. non-targeted encounters (range < 1e6 km)—these are more opportunistic observations than tour/encounter drivers, with as many opportunities as are available throughout the Solstice Mission.	3b. ISS Cloud Tracking	3b. Phase angle < 120°; high northern latitudes (> 60°) preferred for development of summer clouds; resolutions ≤ few to several km (range < 1e6 km)	Onset of north-polar cloud activity did not occur before EOM; timing of predicted seasonal weather pattern remains unknown. What causes differences from model predictions and how typical are the weather patterns we observed? What is the nature of the north-polar cloud features VIMS detected at 2.1 µm starting in June 2016 that were not visible at other wavelengths?

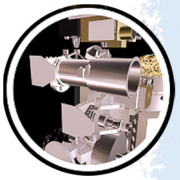

ACRONYMS

Note: For a complete list of Acronyms, refer to Cassini Acronyms – Attachment A.

BIU	Bus Interface Unit
CAPS	Cassini Plasma Spectrometer
CCD	Change Coupled Device
CDS	Command & Data System
CER	Co-rotation-eccentricity Resonance
CIRS	Composite Infrared Spectrometer
CSM	Cassini Solstice Mission
DTM	Digital Terrain Model
EFC	Engineering Flight Computer
FOV	Field of View
GM	Gravitational Mass
ILR	Inner Lindblad Resonance
IR	Infrared
ISS	Imaging Science Subsystem
MAG	Magnetometer
MAPS	Magnetospheric and Plasma Science
MIMI	Magnetospheric Imaging Instrument
NAC	Narrow Angle Camera
RADAR	Titan Radar Mapper
SKR	Saturn Kilometric Radiation
SOI	Saturn orbit insertion
SPT	South Polar Terrain
TPW	True Polar Wander
USGS	United States Geological Survey
UV	Ultraviolet
UVIS	Ultraviolet Imaging Spectrometer
VIMS	Visual and Infrared Mapping Spectrometer
WAC	Wide Angle Camera

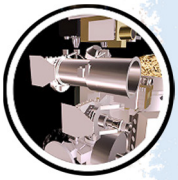

REFERENCES

Disclaimer: The partial list of references below correspond with in-text references indicated in this report. For all other Cassini references, refer to Attachment B – References & Bibliographies; Attachment C – Cassini Science Bibliographies; the sections entitled References contributed by individual Cassini instrument and discipline teams located in Volume 1 Sections 3.1 and 3.2 Science Results; and other resources outside of the Cassini Final Mission Report.

Achterberg, R. K., B. J. Conrath, P. J. Gierasch, F. M. Flasar, C. A. Nixon, (2008), Observation of a tilt of Titan's middle-atmospheric super-rotation, Icarus 197, 549–555.

Annex, A. M., A. J. Verbiscer, P. Helfenstein, C. Howett, P. Schenk, (2013), Photometric properties of thermally anomalous terrains on icy Saturnian satellites, American Astronomical Society DPS meeting #45, 417.02.

Antuñano, A., T. del Rio-Gaztelurrutia, A. Sánchez-Lavega, J. Rodreiguez-Aseguinolaza, (2018), Cloud morphology and dynamics in Saturn's northern polar region, Icarus 299, 117–132.

Antuñano, A., T. del Rio-Gaztelurrutia, A. Sánchez-Lavega, R. Hueso, (2015), Dynamics of Saturn's polar regions, Journal of Geophysical Research, Planets 120, 155–176.

Arregi, J., J. F. Rojas, R. Hueso, A. Sanchez-Lavega, (2009), Gravity waves in Jupiter's equatorial clouds observed by the Galileo orbiter, Icarus, 202, 1, 358–360, doi: 10.1016/j.icarus.2009.03.028.

Asay-Davis, X. S., P. S. Marcus, M. H. Wong, I. de Pater, (2011), Changes in Jupiter's zonal velocity between 1979 and 2008, Icarus, 211(2), 1215–1232, doi: 10.1016/j.icarus.2010.11.018.

Asay-Davis, X. S., P. S. Marcus, M. H. Wong, I. de Pater, (2009), Jupiter's shrinking Great Red Spot and steady Oval BA: Velocity measurements with the 'Advection Corrected Correlation Image Velocimetry' automated cloud-tracking method, Icarus, 203, 1, 164–188, doi: 10.1016/j.icarus.2009.05.001.

Attree, N., C. Murray, G. Williams, N. Cooper, (2014), Survey of low-velocity collisional features in Saturn's F-ring, Icarus 277, 56–66.

Attree, N. O, C. D. Murray, N. J. Cooper, G. A. Williams, (2012), Detection of low-velocity collisions in Saturn's F-ring, The Astrophysical Journal Letters 755, L27–L31.

Barnes, J. W., B. J. Buratti, E. P. Turtle, et al., (2013), Precipitation-induced surface brightenings seen on Titan by Cassini VIMS and ISS, Planetary Science 2, doi: 10.1186/2191-2521-2-1.

Barnes, J. W., R. H. Brown, J. Radebaugh, et al., (2006), Cassini observations of flow-like features in western Tui Regio, Titan, Geophysical Research Letters 33, L16204.

Barnes, J. W., R. H. Brown, E. P. Turtle, et al., (2005), A 5-μm bright spot on Titan: Evidence for surface diversity, Science 310, 92–95.

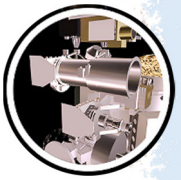

Barrado-Izagirre, N., S. Perez-Hoyos, A. Sanchez-Lavega, (2010), Turbulence in Jupiter's clouds, In Highlights of Spanish Astrophysics V, (eds.) J. M. Diego, L. J. Goicoechea, J. I. GonzalezSerrano, J. Gorgas, pp. 451–451, doi: 10.1007/978-3-642-11250-8_123.

Barrado-Izagirre, N., S. Perez-Hoyos, A. Sanchez-Lavega, (2009), Brightness power spectral distribution and waves in Jupiter's upper cloud and hazes, Icarus, 202, 1, 181–196, doi: 10.1016/j.icarus.2009.02.015.

Barrado-Izagirre, N., A. Sanchez-Lavega, S. Perez-Hoyos, R. Hueso, (2008), Jupiter's polar clouds and waves from Cassini and HST images: 1993–2006, Icarus, 194, 1, 173–185, doi: 10.1016/j.icarus.2007.08.025.

Becker, T. L., M. T. Bland, K. L. Edmundson, L. A. Soderblom, et al., (2016), Completed global control network and basemap of Enceladus, 47th Lunar Planetary Science Conference, p. 2342.

Beddingfield, C. B., D. M. Burr. L. T. Tran, (2016), Polygonal impact craters on Dione: Evidence for tectonic structures outside the wispy terrain, Icarus 274, 163–194.

Behounková, M., G. Tobie, O. Cadek, G. Choblet, C. Porco, F. Nimmo, (2015), Timing of water plume eruptions on Enceladus explained by interior viscosity structure, Nature Geoscience 8, 601–604.

Beurle, K., C. D. Murray, G. A. Williams, M. W. Evans, N. J. Cooper, C. B. Agnor, (2010), Direct evidence for gravitational instability and moonlet formation in Saturn's Rings, Astrophysical Journal Letters 718, L176–L180.

Beuthe, M., A. Rivoldini, A. Trinh, (2016), Enceladus's and Dione's floating ice shells supported by minimum stress isostasy, Geophysical Research Letters 43, no. 19, 10-088.

Birch, S. P. D., A. G. Hayes, W. E. Dietrich, A. D. Howard, et al., (2017), Geomorphologic mapping of Titan's polar terrains: Constraining surface processes and landscape evolution. Icarus, volume 282, p. 214–236.

Burleigh, K. J., P. Helfenstein, B. Carcich, J. Veverka, et al., (2010), Linear polarization and albedo reconnaissance for regolith texture on Saturn's moon Iapetus, 41st Lunar Planetary Science Conference, abstract 1533, p.2607.

Castillo-Rogez, J. C., D. Hemingway, G. Tobie, W. B. McKinnon, G. Schubert, (2018), Origin and evolution of Saturn's midsize moons, In Enceladus and the Icy Moons of Saturn, Part 3: Saturn’s Icy Moons, (eds.) P. M. Schenk, R. N. Clark, C. J. A. Howett, A. J. Verbiscer, J. H. Waite, Space Science Series, The University of Arizona Press, Tucson, AZ, pp. 285–305.

Castillo-Rogez, J. C., T. V. Johnson, P. C. Thomas, M. Choukroun, D. L. Matson, J. I. Lunine, (2012), Geophysical evolution of Saturn's satellite Phoebe, a large planetesimal in the outer Solar System, Icarus 219, 86–109, doi: 10.1016/j.icarus.2012.02.002.

Castillo-Rogez, J. C., D. L. Matson, C. Sotin, T. V. Johnson, J. I. Lunine, P. C. Thomas, (2007), Iapetus’ geophysics: Rotation rate, shape and equatorial ridge, Icarus 190, 179–202.

- - - - - - - - - - - - - -

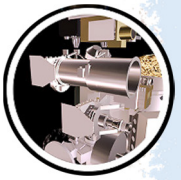

Charnoz S., A. Brahic, P. Thomas, C. Porco, (2007), The equatorial ridges of Pan and Atlas: terminal accretionary ornaments?, Science, vol. 318, issue 5856, pp. 1622–1624, doi: 10.1126/science.1148631.

Charnoz, S., C. C. Porco, E. Deau, A. Brahic, J. N. Spitale, G. Bacques, K. Baillie, (2005), Cassini discovers a kinematic spiral ring around Saturn, Science 310, 1241–1351.

Choi, D. S., A. P. Showman, A. R. Vasavada, A. A. Simon-Miller, (2013), Meteorology of Jupiter's equatorial hot spots and plumes from Cassini, Icarus, 223, 2, 832–843, doi: 10.1016/j.icarus.2013.02.001.

Choi, D. S., and A. P. Showman, (2011), Power spectral analysis of Jupiter's clouds and kinetic energy from Cassini, Icarus, 216, 2, 597–609, doi: 10.1016/j.icarus.2011.10.001.

Choi, D. S., A. P. Showman, A. R. Vasavada, (2010), The evolving flow of Jupiter's white ovals and adjacent cyclones, Icarus, 207, 1, 359–372, doi: 10.1016/j.icarus.2009.10.013.

Cooper, N., S. Renner, C. Murray, M. Evans, (2015), Saturn’s inner satellites: Orbits, masses, and the chaotic motion of Atlas from new Cassini imaging observations, The Astronomical Journal 149, 27.

Cooper, N., C. Murray, V. Lainey, R. Tajeddine, M. Evans, G. Williams, (2014), Cassini ISS mutual event astrometry of the mid-sized Saturnian satellites 2005–2012. Astronomy and Astrophysics 572, A43.

Cooper, N., C. Murray, G. Williams, (2013), Local variability in the orbit of Saturn's F-ring, The Astronomical Journal 145, 161–175.

Cooper, N. J., C. D. Murray, M. W. Evans, K. Beurle, R. A. Jacobson, C. C. Porco, (2008), Astrometry and dynamics of Anthe (S/2007 S 4), a new satellite of Saturn, Icarus, 195, 765–777.

Cooper, N. J., C. D. Murray, C. C. Porco, J. N. Spitale, (2006), Cassini ISS astrometric observations of the inner Jovian satellites, Amalthea and Thebe, Icarus, 181, 223–234.

Ćuk, M., L. Dones, D. Nesvorny, (2016), Dynamical evidence for a late formation of Saturn’s moons, The Astrophysical Journal, 820, 97.

Cuzzi, J. N.,G. Filacchione, E. A. Marouf, M. S. Tiscareno, C. D. Murray, (2018), The Rings of Saturn, Chapter 3, In Planetary Ring Systems: Properties, Structure, and Evolution, (eds.) M. S. Tiscareno, C. D. Murray, Queen Mary University of London, pp. 51–92, doi: 10.1017/9781316286791.003.

Cuzzi, J. N., A. D. Whizin, R. C. Hogan, A. R. Dobrovolskis, L. Dones, M. R. Showalter, J. E. Colwell, J. D. Scargle, (2014), Saturn’s F-ring core: Calm in the midst of chaos?, Icarus 232, 157–175.

Damptz, A. L., A. J. Dombard, M. R. Kirchoff, (2018), Testing models for the formation of the equatorial ridge on Iapetus via crater counting, Icarus 302, 134–144.

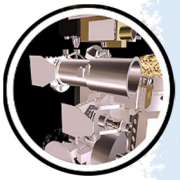

de Kok, R. J., N. A. Teanby, L. Maltagliati, P. G. J. Irwin, and S. Vinatier, (2014), HCN ice in Titan's high-altitude southern polar cloud, Nature, 514, no. 7520, 65, doi: 10.1038/nature13789.

Del Genio, A., and J. Barbara, (2016), An objective classification of Saturn cloud features from Cassini ISS images, Icarus 271, 222–236.

Del Genio, A. D., and J. M. Barbara, (2012), Constraints on Saturn's tropospheric general circulation from Cassini ISS images, Icarus 219, 689–700.

Del Genio, A. D., R. K. Achterberg, K. H. Baines, F. M. Flasar, P. L. Read, Sanchez-Lavega, A., Showman, A. P., (2009), Saturn atmospheric structure and dynamics, Saturn from Cassini-Huygens, (eds.) M. Dougherty, L. Esposito, S. Krimigis, Springer-Verlag, Dordrecht, Netherlands, pp. 113–159.

Del Genio, A. D., J. M. Barbara, J. Ferrier, A. P. Ingersoll, R. A. West, A. R. Vasavada, J. Spitale, C. C. Porco, (2007), Saturn eddy momentum fluxes and convection: First estimates from Cassini images, Icarus 189, 479–492.

del Rio-Gaztelurrutia, T., J. Legarreta, R. Hueso, S. Pérez-Hoyos, A. Sánchez-Lavega, (2010), A long-lived cyclone in Saturn's atmosphere: Observations and models, Icarus 209, 665–681.

Denk, T., S. Mottola, F. Tosi, W. B. Bottke, D. P. Hamilton, (2018), The Irregular satellites of Saturn, In Enceladus and the icy moons of Saturn, (eds.) P. M. Schenk, R. N. Clark, C. J. A. Howett, A. J. Verbiscer, J. H. Waite, Space Science Series, The University of Arizona Press, Tucson, AZ.

Denk, T., G. Neukum, T. Roatsch, C. C. Porco, J. A. Burns, et al., (2010), Iapetus: Unique surface properties and a global color dichotomy from Cassini imaging, Science 327, no. 5964, 435–439, doi: 10.1126/science.1177088.

Denk, T., G. Neukum, N. Schmedemann, T. Roatsch, R. J. Wagner, B. Giese, J. E. Perry, P. Helfenstein, E. P. Turtle, C. C. Porco, (2008), Iapetus Imaging during the targeted flyby of the Cassini spacecraft, 39th Lunar and Planetary Science Conference, abstract 2533.

Denk, T., G. Neukum, P. Helfenstein, P. C. Thomas, E. P. Turtle, A. S. McEwen, T. Roatsch, J. Veverka, T. V. Johnson, J. E. Perry, W. M. Owen, R. J. Wagner, C. C. Porco, Cassini ISS team, (2005a), The first six months of Iapetus observations by the Cassini ISS camera, 36th Lunar and Planetary Science Conference, abstract 2262.

Denk, T., G. Neukum, T. Roatsch, A. S. McEwen, E. P. Turtle, P. C. Thomas, P. Helfenstein, R. J. Wagner, C. C. Porco, J. E. Perry, B. Giese, T. V. Johnson, J. Veverka, Cassini ISS team, (2005b), First imaging results from the Iapetus B/C flyby of the Cassini spacecraft, 36th Lunar and Planetary Science Conference, abstract 2268.

Denk, T., K.-D. Matz, T. Roatsch, U. Wolf, R. J. Wagner, G. Neukum, R. Jaumann, (2000), Iapetus (1): Size, topography, surface structures, craters, 31st Lunar and Planetary Science Conference, abstract 1596.

- - - - - - - - - - - - - -

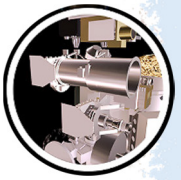

Dones, L., C. R. Chapman, W. B. McKinnon, H. J. Melosh, M. R. Kirchoff, G. Neukum, K. J. Zahnle, (2009), Icy satellites of Saturn: Impact cratering and age determination, Saturn from Cassini-Huygens, (eds.) M. Dougherty, L. Esposito, S. Krimigis, Springer-Verlag, Dordrecht, Netherlands, pp. 613–35.

Dyudina, U., X. Zhang, L. Li, P. Kopparla, A. P. Ingersoll, L. Dones, A. Verbiscer, Y. L. Yung, (2016), Reflected light curves, spherical and bond albedos of Jupiter- and Saturn-like exoplanets, The Astrophysical Journal, 822, 2, 76, doi: 10.3847/0004-637x/822/2/76.

Dyudina, U. A., A. P. Ingersoll, S. P. Ewald, D. Wellington, (2015), Saturn’s aurora observed by the Cassini camera at visible wavelengths, Icarus 263, 32–43.

Dyudina, U. A., A. P. Ingersoll, S. P. Ewald, C. C. Porco, G. Fischer, Y. Yair, (2013), Saturn’s visible lightning, its radio emissions, and the structure of the 2009–2011 lightning storms, Icarus 226, 1020–1037.

Dyudina, U. A., A. P. Ingersoll, S. P. Ewald, C. C. Porco, G. Fischer, W. S. Kurth, R. A. West, (2010), Detection of visible lightning on Saturn, Geophysical Research Letters 37, L09205.

Dyudina, U. A., A. P. Ingersoll, S. P. Ewald, A. R. Vasavada, R. A. West, K. H. Baines, et al., (2009), Saturn's south polar vortex compared to other large vortices in the solar system, Icarus 202, 240–248.

Dyudina, U. A., A. P. Ingersoll, S. P. Ewald, A. R. Vasavada, et al., (2008), Dynamics of Saturn's south polar vortex, Science 319, 1801.

Dyudina, U., A. Ingersoll, S. Ewald, C. Porco, G. Fischer, W. Kurth, et al., (2007), Lightning storms on Saturn observed by Cassini ISS and RPWS during 2004–2006, Icarus 190, 545–555.

Dyudina, U. A., P. D. Sackett, D. D. R. Bayliss, S. Seager, C. C. Porco, H. B. Throop, L. Dones, (2005), Phase light curves for extrasolar Jupiters and Saturns, Astrophysical Journal 618, 973–986.

Dyudina, U. A., A. D. Del Genio, A. P. Ingersoll, C. C. Porco, R. A. West, A. R. Vasavada, J. M. Barbara, (2004), Lightning on Jupiter observed in the H-alpha line by the Cassini imaging science subsystem, Icarus, 172(1), 24–36, doi: 10.1016/j.icarus.2004.07.014.

El Moutamid, M., Nicholson, P., French, R., Tiscareno, M., Murray, C., Evans, M., French, C., Hedman, M., Burns, J., (2016), How Janus' orbital swap affects the edge of Saturn's A-ring?, Icarus 279, 125–140.

Elder, C., P. Helfenstein, P. Thomas, J. Veverka, J. A. Burns, T. Denk, C. Porco, (2007), Tethys’ mysterious equatorial band, Bulletin of the American Astronomical Society 39, p. 429.

Estrada, P. R., R. H. Durisen, and H. N. Latter, (2018), Meteoroid bombardment and ballistic transport in planetary rings, In Planetary Ring Systems: Properties, Structure, and Evolution, (eds.) M. S. Tiscareno, C. D. Murray, Cambridge, United Kingdom, Cambridge University Press, 198–224.

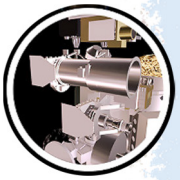

Fischer, G., S. Ye, J. Groene, A. Ingersoll, K. Sayanagi, J. Menietti, W. Kurth, D. Gurnett, (2014), A possible influence of the Great White Spot on Saturn kilometric radiation periodicity, Annales Geophysicae 32, 1463–1476.

Fischer, G., W. S. Kurth, D. A. Gurnett, P. Zarka, U. A. Dyudina, A. P. Ingersoll, S. P. Ewald, C. Porco, A. Wesley, C. Go, M. Delcroix, (2011), A giant thunderstorm on Saturn, Nature 475, 75-77.

Fischer, G., W. Kurth, U. Dyudina, M. Kaiser, P. Zarka, A. Lecacheux, A. Ingersoll, D. Gurnett, (2007), Analysis of a giant lightning storm on Saturn, Icarus 190, 528–544.

Flasar, F. M., K. H. Baines, M. K. Bird, T. Tokano, R. A. West, (2009), Atmospheric dynamics and meteorology, Chapter 13, In Titan from Cassini-Huygens, (eds.) R. Brown, J. P. Lebreton, J. Waite, Springer-Verlag, Dordrecht, Netherlands, pp. 323–353.

Fletcher, L. N., T. K. Greathouse, S. Guerlet, J. I. Moses, and R. A. West, (2018), Saturn's seasonally changing atmosphere: Thermal structure, composition and aerosols, Chapter 10, In Saturn in the 21st Century, (eds.) K. H. Baines, F. M. Flasar, N. Krupp, T. Stallard, Cambridge University Press, pp, 251–294, doi: 10.1017/9781316227220.010.

French, R. S., S. K. Hicks, M. R. Showalter, A. K. Antonsen, D. R. Packard, (2014), Analysis of clumps in Saturn’s F-ring from Voyager and Cassini, Icarus 241, 200–220.

French, R. S., M. R. Showalter, R. Sfair, C. A. Argüelles, M. Pajuelo, P. Becerra, M. Hedman, P. D. Nicholson, (2012), The brightening of Saturn’s F-ring, Icarus 219, 181–193.

Fussner S., A. S. McEwen, J. E. Perry, E. P. Turtle, D. D. Dawson, C. C. Porco, R. A. West, Cassini ISS team,(2005), Dependence of surface contrast on emission angle in Cassini ISS 938-nm images of Titan, Lunar and Planetary Science XXXVI, Part 6.

Galperin, B., R. M. B Young, S. Sukoriansky, N. Dikovskaya, P. L. Read, A. J. Lancaster, D. Armstrong, (2014), Cassini observations reveal a regime of zonostrophic macroturbulence on Jupiter, Icarus, 229, 295–320, doi: 10.1016/j.icarus.2013.08.030.

Gao, P., P. Kopparla, X. Zhang, A. P. Ingersoll, (2016), Aggregate particles in the plumes of Enceladus, Icarus 264, 227–238, doi: 10.1016/j.icarus.2015.09.030.

Garcia-Melendo, E., R. Hueso, A. Sánchez-Lavega, J. Legarreta, T. del Rio-Gaztelurrutia, J. F. Rojas, S. Pérez-Hoyos, J. F. Sanz-Requenna, (2013), Atmospheric dynamics of Saturn’s 2010 giant storm, Nature Geoscience, 6, 525–529.

Garcia-Melendo, E., S. Pérez-Hoyos, A. Sánchez-Lavega, R. Hueso, (2011a), Saturn’s zonal wind profile in 2004–2009 from Cassini ISS images and its long-term variability, Icarus 215, 62–74.

Garcia-Melendo, E., J. Arregi, J. F. Rojas, R. Hueso, N. Barrado-Izagirre, J. M. Gomez-Forrellad, S. Perez-Hoyos, J. F. Sanz-Requena, A. Sanchez-Lavega, (2011b), Dynamics of Jupiter's equatorial region at cloud top level from Cassini and HST images, Icarus, 211, 2, 1242–1257, doi: 10.1016/j.icarus.2010.11.020.

- - - - - - - - - - - - - -

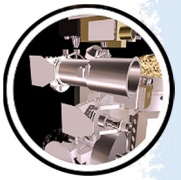

Garcia-Melendo, E., A. Sanchez-Lavega, J. Legarreta, S. Perez-Hoyos, R. Hueso, (2010), A strong high altitude narrow jet detected at Saturn's equator, Geophysical Research Letters, 37, doi: 10.1029/2010gl045434.

Garcia-Melendo, E., A. Sánchez-Lavega, J. F. Rojas, S. Pérez-Hoyos, R. Hueso, (2009), Vertical shears in Saturn's eastward jets at cloud level, Icarus 201, 818–820.

Geissler, P., A. McEwen, C. Porco, D. Strobel, J. Saur, J. Ajello, R. West, (2004), Cassini observations of Io's visible Aurorae, Icarus 172, 127–140.

Giese, B., P. Helfenstein, E. Hauber, H. Hussmann, R. Wagner, (2017), An exceptionally high standing ridge on Enceladus, European Planetary Science Congress 2017, abstract, vol 11, EPSC2017-28-1.

Giese, B., P. Helfenstein, T. A. Hurford, G. Neukum, C. C. Porco, (2011a), Observation of cycloidal features on Enceladus, 42nd Lunar Planetary Science Conference, abstract 1608.

Giese, B., H. Hussmann, T. Roatsch, P. Helfenstein, P. C. Thomas, G. Neukum, (2011b), Enceladus: Evidence for librations forced by Dione, EPSC-DPS Joint Meeting 2011, 976–977.

Giese, B., P. Helfenstein, P. C. Thomas, A. P. Ingersoll, J. Perry, R. Wagner, G. Neukum, C. C. Porco, (2010a), The morphology of an active zone near Enceladus' south pole and implications. In European Geosciences Union General Assembly Conference Abstracts, vol. 12, p. 11085.

Giese, B., and Cassini ISS team, (2010b), The topography of Enceladus, European Planetary Science Congress 2010, abstract, vol. 5, EPSC2010-675.

Giese, B., T. Denk, G. Neukum, T. Roatsch, P. Helfenstein, P. C. Thomas, E. P. Turtle, A. McEwen, C. C. Porco, (2008a), The topography of Iapetus' leading side, Icarus 193, 359–371.

Giese, B., R. Wagner, H. Hussmann, G. Neukum, J. Perry, P. Helfenstein, P. C. Thomas, (2008b), Enceladus: An estimate of heat flux and lithospheric thickness from flexurally supported topography, Geophysical Research Letters 35, Issue 24, CiteID L24204.

Giese, B., R. Wagner, G. Neukum, P. Helfenstein, P. C Thomas, (2007), Tethys: Lithospheric thickness and heat flux from flexurally supported topography at Ithaca Chasma, Geophysical Research Letters 34, L21203.

Giese, B., G. Neukum, T. Roatsch, T. Denk, C. C. Porco, (2006), Topographic modeling of Phoebe using Cassini images, Planetary and Space Science 54, 1156–1166.

Goldstein, D. B., M. Hedman, M. Manga, M. Perry, J. Spitale, B. Teolis, (2018), Enceladus plume dynamics: From surface to space, In Enceladus and the Icy Moons of Saturn, Part 2: Enceladus Plume and the E-ring, (eds.) P. M. Schenk, R. N. Clark, C. J. A. Howett, A. J. Verbiscer, J. H. Waite, Space Science Series, The University of Arizona Press, Tucson, AZ, pp. 175–194.

Hadjighasem, A., and G. Haller, (2016), Geodesic transport barriers in Jupiter's atmosphere: A video-based analysis, Siam Review, 58, 1, 69–89, doi: 10.1137/140983665.

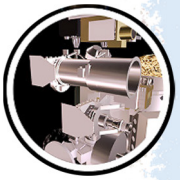

Harbison, R. A., P. C. Thomas, and P. D. Nicholson, (2011), Rotational modeling of Hyperion, Celestial Mechanics and Dynamical Astronomy, vol 110, issue 1, pp. 1–16, doi: 10.1007/s10569-011-9337-3.

Hayes A. G., O. Aharonson, J. I. Lunine, R. L. Kirk, H. A. Zebker, L. C. Wye, R. D. Lorenz, E. P. Turtle, P. Paillou, G. Mitri, S. D. Wall, E. R. Stofan, K. L. Mitchell, C. Elachi, Cassini RADAR team, (2011), Transient surface liquid in Titan's polar regions from Cassini, Icarus 211, 655–671.

Hedman, M. M., F. Postberg, D. P. Hamilton, S. Renner, H.-W. Hsu, (2018), Dusty rings, In Planetary Ring Systems: Properties, Structure, and Evolution, (eds.) M. S. Tiscareno, C. D. Murray, Cambridge, United Kingdom, Cambridge University Press, pp. 308–337.

Hedman, M. M., J. A. Burns, P. D. Nicholson, M. S. Tiscareno, M. W. Evans, E. Baker, (2017), One last look from the dark side: Cassini’s final views of Saturn’s rings from within the planet’s shadow, AAS/DPS Meeting, abstracts 49, 212.01.

Hedman, M. M., and B. J. Carter, (2017), A curious ringlet that shares Prometheus’ orbit but precesses like the F-ring, Icarus 281, 322–333.

Hedman, M. M., J. A. Burns, M. R. Showalter, (2015), Corrugations and eccentric spirals in Saturn’s D-ring: New insights into what happened at Saturn in 1983, Icarus 248, 137–161.

Hedman, M. M., and C. C. Stark, (2015), Saturn’s G- and D-rings provide nearly complete measured scattering phase functions of nearby debris disks, Astrophysical Journal 811, 67.

Hedman, M., and M. Showalter, (2015), A new pattern in Saturn's D-ring created in late 2011, Icarus 279, 155–165.

Hedman, M., J. Burt, J. Burns, M. Showalter, (2014), Non-circular features in Saturn’s D-ring: D68, Icarus 223, 147–162.

Hedman, M., J. Burns, D. Hamilton, M. Showalter, (2013), Of horseshoes and heliotropes, dynamics of dust in the Encke Gap, Icarus, vol. 223, issue 1, pp. 252–276, doi: 10.1016/j.icarus.2012.11.036.

Hedman, M. M., J. A. Burns, D. P. Hamilton, M. R. Showalter, (2012), The three-dimensional structure of Saturn's E-ring, Icarus 217, 322–338.

Hedman, M. M., J. A. Burns, M. W. Evans, M. S. Tiscareno, C. C. Porco, (2011), Saturn's curiously corrugated C-ring, Science 332, 708–711.

Hedman, M. M., J. A. Burt, J. A. Burns, M. S. Tiscareno, (2010a), The shape and dynamics of a heliotropic dusty ringlet in the Cassini Division, Icarus 210, 284–297.

Hedman, M. M., N. J. Cooper, C. D. Murray, K. Beurle, M. W. Evans, M. S. Tiscareno, J. A. Burns, (2010b), Aegaeon (Saturn LIII), a G-ring object, Icarus 207, 433–447.

Hedman, M. M., J. A. Burns, M. S. Tiscareno, C. C. Porco, (2009a), Organizing some very tenuous things: Resonant structures in Saturn's faint rings, Icarus 202, 260–279.

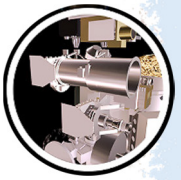

Hedman, M. M., C. D. Murray, N. J. Cooper, M. S. Tiscareno, K. Beurle, M. W. Evans, J.A. Burns, (2009b), Three tenuous rings/arcs for three tiny moons, Icarus 199, 378–386.

Hedman, M. M., J. A. Burns, M. R. Showalter, C. C. Porco, P. D. Nicholson, A. S. Bosh, M. S. Tiscareno, R. H. Brown, B. J. Buratti, K. H. Baines, R. Clark, (2007a), Saturn's dynamic D-ring, Icarus 188, 89–107.

Hedman, M. M., J. A. Burns, M. S. Tiscareno, C. C. Porco, G. H. Jones, E. Roussos, N. Krupp, C. Paranicas, S. Kempf, (2007b), The source of Saturn's G-ring, Science 317, 653–656.

Heimpel, M., J. Aurnou, J. Wicht, (2005), Simulation of equatorial and high-latitude jets on Jupiter in a deep convection model, Nature, 438, 7065, 193–196, doi: 10.1038/nature04208.

Helfenstein, P. and C. C. Porco, (2015), Enceladus' geysers: Relation to geological features, The Astronomical Journal, 150, 96.

Helfenstein, P., (2014), Y-shaped discontinuity, In Encyclopedia of Planetary Landforms, Springer, New York, NY, doi: 10.1007/978-1-4614-9213-9_576-1, pp. 2347–2350.

Helfenstein, P., (2012), Seeing through frost on Enceladus, American Geophysical Union (AGU), Fall Meeting 2012, abstract P32A-09.

Helfenstein, P., (2010), Tectonic overturn on Enceladus, Nature Geoscience, 3, 75–76.

Helfenstein, P., T. Denk, B. Giese, A. Ingersoll, T. V. Johnson, A. S. McEwen, G. Neukum, J. Perry, C. C. Porco, T. Roatsch, P. C. Thomas, E. P. Turtle, A. Verbiscer, J. Veverka, (2008), Enceladus south polar terrain geology: New details from Cassini ISS high resolution imaging, American Geophysical Union (AGU), Fall Meeting 2008, abstract P13D-02.

Helfenstein, P., P. C. Thomas, J. Veverka, J. Rathbun, J. Perry, E. Turtle, T. Denk, G. Neukum, T. Roatsch, R. Wagner, B. Giese, S. Squyres, J. Burns, A. McEwen, C. Porco, T. V. Johnson, Cassini ISS team, (2006), Patterns of fracture and tectonic convergence near the south pole of Enceladus, 35th Lunar Planetary Science Conference, abstract 2182.

Helfenstein, P., P. C. Thomas, J. Veverka, S. Squyres, J. A. Rathbun, T. Denk, G. Neukum, T. Roatsch, R. Wagner, J. Perry, E. Turtle, A. S. McEwen, T. V. Johnson, C. Porco, Cassini ISS team, (2005a), Geological features and terrains on Enceladus as seen by Cassini ISS, Bulletin of the American Astronomical Society 37, p. 701.

Helfenstein, P., P. Thomas, J. Veverka, T. Denk, G. Neukum, R. A. West, B. Knowles, C. C. Porco, Cassini ISS team, (2005b), A Cassini ISS search for regolith-texture variations on Tethys, 36th Lunar Planetary Science Conference, abstract 2399.

Hueso, R., J. Legarreta, E. Garcia-Melendo, A. Sanchez-Lavega, S. Perez-Hoyos, (2009), The jovian anticyclone BA II: Circulation and interaction with the zonal jets, Icarus, 203, 2, 499-515, doi: 10.1016/j.icarus.2009.05.004.

Hurford, T., B. Bills, P. Helfenstein, R. Greenberg, G. Hoppa, D. Hamilton, (2009), Geological implications of a physical libration on Enceladus, Icarus 203, 541–552.

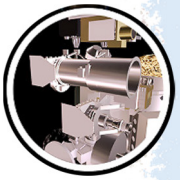

Hurford, T., P. Helfenstein, J. Spitale, (2012), Tidal control of jet eruptions on Enceladus as observed by Cassini ISS between 2005 and 2007, Icarus 220, 896–903.

Ingersoll, A. P., and S. P. Ewald, (2017), Decadal timescale variability of the Enceladus plumes inferred from Cassini images, Icarus 282, 260–275, doi: 10.1016/j.icarus.2016.09.018.

Ingersoll, A. P., and M. Nakajima, (2016), Controlled boiling on Enceladus. 2. Model of the liquid-filled cracks, Icarus 272, 319–326, doi: 10.1016/j.icarus.2015.12.040.

Ingersoll, A. P., and S. P. Ewald, (2011), Total particulate mass in Enceladus plumes and mass of Saturn's E-ring inferred from Cassini ISS images, Icarus 216, 492–506, doi: 10.1016/j.icarus.2011.09.018.

Ingersoll, A. P., and A. A. Pankine, (2010), Subsurface heat transfer on Enceladus: Conditions under which melting occurs, Icarus 206, 594–607, doi: 10.1016/j.icarus.2009.09.015.

Jacobson, R. A., (2014), The small Saturnian satellites—chaos and conundrum, AAS Division on Dynamical Astronomy Meeting Abstracts 45, 304.05, Philadelphia, PA.

Jacobson, R., J. Spitale, C. Porco, K. Beurle, N. Cooper, M. Evans, C. Murray, (2008), Revised orbits of Saturn's small inner satellites, Astronomical Journal 135, 261–263.

Jacobson, R. A., J. Spitale, C. C. Porco, W. M. Owen Jr., (2006a), The GM values of Mimas and Tethys and the libration of Methone, The Astronomical Journal 132, 711–713.

Jacobson, R. A., P. G. Antreasian, J. J. Bordi, K. E. Cridle, R. Ionasescu, J. B. Jones, R. A. Mackenzie, M. C. Meek, D. Parcher, F. J. Pelletier, W. M. Owen, D. C. Roth, I. M. Roundhill, J. R. Stauch, (2006b), The gravity field of the Saturnian system from satellite observations and spacecraft tracking data, The Astronomical Journal 132, 2520–2526.

Jaumann, R., R. N. Clark, F. Nimmo, A. R. Hendrix, B. J. Buratti, T. Denk, J. M. Moore, P. M. Schenk, S. J. Ostro, R. Srama, (2009a), Icy Satellites: Geological evolution and surface processes, In Saturn from Cassini-Huygens, Chapter 20, (eds.) M. Dougherty, L. Esposito, S. Krimigis, Springer, Dordrecht, pp. 637–681, doi: 10.1007/978-1-4020-9217-6_20.

Jaumann R., R. Kirk, R. Lorenz, R. Lopes, E. Stofan, E. P. Turtle, H. U. Keller, C. A. Wood, C. Sotin, L. Soderblom, M. Tomasko, (2009b), Geology and surface processes on Titan, In Titan from Cassini-Huygens, (eds.) R. Brown, J.-P. Lebreton, and H. Waite, Springer, New York, NY, pp. 75–140.

Johnson, T. V., and J. I. Lunine, (2005), Saturn's moon Phoebe as a captured body from the outer solar system, Nature 435, 69–71.

Karkoschka E., A. McEwen, J. Perry, (2017a), Producing the best global mosaic of Titan's surface albedo using Cassini images, LPSC 48 #2518, 48th Lunar and Planetary Science Conference, March 20–24, 2017, The Woodlands, TX.

Karkoschka E., A. McEwen, J. Perry, (2017b), Creating the best global mosaic of Titan's surface albedo using Cassini images, American Astronomical Society, DPS 49, #301.06.

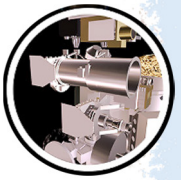

Kirchoff, M. R., E. B. Bierhaus, L. Dones, S. J. Robbins, K. N. Singer, R. J. Wagner, and K. J. Zahnle, (2018), Cratering histories in the Saturnian system, In Enceladus and the Icy Moons of Saturn, (eds.) P. M. Schenk, R. N. Clark, C. J. A. Howett, A. J. Verbiscer, J. H. Waite, Space Science Series, The University of Arizona Press, Tucson, AZ.

Kirchoff, M. R., and P. M. Schenk, (2010), Impact cratering records of the mid-sized, icy Saturnian satellites, Icarus 206, 485–497.

Lainey, V., R. A. Jacobson, R. Tajeddine, N. J. Cooper, C. Murray, V. Robert, G. Tobie, T. Guillot, S. Mathis, F. Remus, J. Desmars, J.-E. Arlot, J.-P. De Cuyper, V. Dehant, D. Pascu, W. Thuillot, C. Le Poncin-Lafitte, J.-P Zahn, (2017), New constraints on Saturn's interior from Cassini astrometric data, Icarus 281, 286–296.

Laraia, A. L., A. P. Ingersoll, M. A. Janssen, S. Gulkis, F. Oyafuso, M. Allison, (2013), Analysis of Saturn’s thermal emission at 2.2-cm wavelength: Spatial distribution of ammonia vapor, Icarus 226, 641–654.

Lavvas P., R. A. West, G. Gronoff, P. Rannou, (2014), Titan’s emission processes during eclipse, Icarus 241, 397–408.

Li, C., and A. P. Ingersoll, (2015), Moist convection in hydrogen atmospheres and the frequency of Saturn’s giant storms, Nature Geoscience 8, 398–403.

Li, J., Q. Xiang, R. Ze, M. Ma, S. Wang, Q. Xie, Y. Xiang (2018), Thermal and electrical analysis of SiGe thermoelectric unicouple filled with thermal insulation materials, Applied Thermal Engineering 134, 266–274.

Li, L., X. Jiang, H. J. Trammell, Y. Pan, J. Hernandez, B. J. Conrath, P. J. Gierasch, et al., (2015), Saturn’s giant storm and global radiant energy, Geophysical Research Letters 42, doi: 10.1002/2015GL063763.

Li, L., R. K. Achterberg, B. J. Conrath, P. J. Gierasch, M. A. Smith, A. A. Simon-Miller, C. A. Nixon, et al., (2013), Strong temporal variation over one Saturnian year: From Voyager to Cassini, Scientific Reports 3, 2410.

Li, L., X. Jiang, A. P. Ingersoll, A. D. Del Genio, C. C. Porco, R. A. West, A. R. Vasavada, et al., (2011), Equatorial winds on Saturn and the stratospheric oscillation, Nature Geoscience 4, 750–752.

Li, L. M., A. P. Ingersoll, A. R. Vasavada, A. A. Simon-Miller, R. K. Achterberg, S. P. Ewald, U. A. Dyudina, C. C. Porco, R. A. West, F. M. Flasar, (2006a), Waves in Jupiter's atmosphere observed by the Cassini ISS and CIRS instruments, Icarus, 185, 2, 416–429, doi: 10.1016/j.icarus.2006.08.005.

Li, L. M., A. P. Ingersoll, A. R. Vasavada, A. A. Simon-Miller, A. D. Del Genio, S. P. Ewald, Porco, C. C., R. A. West, (2006b), Vertical wind shear on Jupiter from Cassini images, Journal of Geophysical Research-Planets, 111(E4), doi: 10.1029/2005je002556.

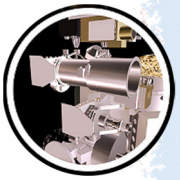

Li, L., Ingersoll, A. P., Vasavada, A. R., Porco, C. C., Del Genio, A. D.,Ewald, S. P., (2004), Life cycles of spots on Jupiter from Cassini images, Icarus, 172, 1, 9–23, doi: 10.1016/j.icarus.2003.10.015.

Lopes R. M. C, M. J. Malaska, A. Solomonidou, A. Le Gall, M. A. Janssen, C. D. Neish, E. P. Turtle et al., (2016), Nature, distribution, and origin of Titan's undifferentiated plains, Icarus 270, pp. 162–182.

Lora, J. M., J. I. Lunine, J. L. Russell, (2015), GCM simulations of Titan's middle and lower atmosphere and comparison to observations, Icarus, volume 250, pp. 516–528.

Martens, H. R., A. P. Ingersoll, S. P. Ewald, P. Helfenstein, B. Giese, (2015), Spatial distribution of ice blocks on Enceladus and implications for their origin and emplacement, Icarus 245, pp. 162–176.

Matson, D. L., J. C. Castillo-Rogez, G. Schubert, C. Sotin, W. B. McKinnon, (2009), The thermal evolution and internal structure of Saturn’s mid-sized Icy satellites, In Saturn from Cassini-Huygens, (eds.) M. K. Dougherty, L. W. Esposito, S. M. Krimigis, Springer, Dordrecht, pp. 577–612 doi: 10.1007/978-1-4020-9217-6_18.

McEwen A. S., E. P. Turtle, J. E. Perry, S. Fussner, C. C. Porco, R. A. West, T. V. Johnson, G. C. Collins, T. del Genio, J. Barbara, Cassini ISS team, (2005a), Cassini Imaging results at Titan, Lunar and Planetary Science XXXVI, Part 13, LPI-Contrib-1234-Pt-13.

McEwen A., E. Turtle, J. Perry, D. Dawson, S. Fussner, G. Collins, C. Porco, T. Johnson, L. Soderblom, (2005b), Mapping and monitoring the surface of Titan, Bulletin of the American Astronomical Society, vol. 37, p. 739.

Mitchell, C., C. Porco, J. Weiss, (2015), Tracking the geysers of Enceladus into Saturn's E-ring, The Astronomical Journal 149, 156.

Mitchell, C., C. Porco, H. Dones, J. Spitale, (2013), The behavior of spokes in Saturn's B-ring, Icarus 225, 446–474.

Mitchell J. L., M. Ádámkovics, R. Caballero, E. P. Turtle, (2011), Locally enhanced precipitation organized by planetary-scale waves on Titan, Nature Geoscience 4, doi: 10.1038/NGEO1219.

Mitchell, C. J., M. Horanyi, O. Havnes, C. C. Porco, (2006), Saturn's spokes: Lost and found, Science 311, 1587–1589.

Morales-Juberías, R., K. M. Sayanagi, A. A. Simon, L. N. Fletcher, R. G. Cosentino, (2015) Meandering shallow atmospheric jet as a model of Saturn’s north-polar hexagon, The Astrophysical Journal 806, L18.

Morales-Juberias, R., and T. E. Dowling, (2013), Jupiter's Great Red Spot: Fine-scale matches of model vorticity patterns to prevailing cloud patterns, Icarus, 225, 1, 216–227, doi: 10.1016/j.icarus.2013.03.026.

Morales-Juberías, R., K. M. Sayanagi, T. E. Dowling, A. P. Ingersoll, (2011), Emergence of polar-jet polygons from jet instabilities in a Saturn model, Icarus 211, 1284–1293.

- - - - - - - - - - - - - -

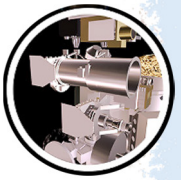

Morrison, S. J., P. C. Thomas, M. S. Tiscareno, J. A. Burns, J. Veverka, (2009), Grooves on small Saturnian satellites and other objects: Characteristics and significance, Icarus 204, 262–270.

Movshovitz N., F. Nimmo, D. G. Korycansky, E. Asphaug, J. M. Owen, (2015), Disruption and reaccretion of midsized moons during an outer solar system Late Heavy Bombardment, Geophysical Research Letters 42, 256–263.

Murray, C. D., and R. S. French, (2018), The F-ring of Saturn, In Planetary Ring Systems: Properties, Structure, and Evolution, (eds.) M. S. Tiscareno, C. D. Murray, Cambridge, United Kingdom, Cambridge University Press, 338–362.

Murray, C. D., N. J. Cooper, G. A. Williams, N. O. Attree, J. S. Boyer, (2014), The discovery and dynamical evolution of an object at the outer edge of Saturn's A-ring, Icarus 236, 165–168.

Murray, C. D., K. Beurle, N. J. Cooper, M. W. Evans, G. A. Williams, S. Charnoz, (2008), The determination of the structure of Saturn's F-ring by nearby moonlets, Nature 453, 739–744.

Murray, C. D., N. Cooper, M. W. Evans, K. Beurle, (2005a), S/2004 S5: A New co-orbital companion for Dione, Icarus 179, 222–234.

Murray, C. D., C. Chavez, K. Beurle, N. Cooper, M. W. Evans, J. A Burns, C. C. Porco, (2005b), How Prometheus creates structure in Saturn's F-ring, Nature 437, 1326–1329.

Nakajima, M., and A. P. Ingersoll, (2016), Controlled boiling on Enceladus. 1. Model of the vapor-driven jets, Icarus 272, 309–318, doi: 10.1016/j.icarus.2016.02.027.

Nicholson, P., R. French, and J. Spitale, (2018), Narrow rings, gaps, and sharp edges. In Planetary Ring Systems: Properties, Structure, and Evolution, (eds.) M. Tiscareno and C. Murray, Cambridge, United Kingdom, Cambridge University Press, pp. 276–307, doi: 10.1017/9781316286791.011.

Nimmo, F., C. Porco, C. Mitchell, T. Van Hoolst, M. Hedman, (2016), The tidally-modulated plume of Enceladus: An update, AGU abstract P33A-2118 presented at 2016 Fall Meeting, AGU, San Francisco, CA, 12–16 Dec.

Nimmo, F., C. Porco, C. Mitchell, (2014), Tidally modulated eruptions on Enceladus: Cassini ISS observations and models, The Astronomical Journal 148, 46.

Nimmo, F., B. C. Bills, and P. C. Thomas, (2011), Geophysical implications of the long-wavelength topography of the Saturnian satellites, Journal of Geophysical Research, 116, E11001, doi: 10.1029/2011JE003835.

NASA/JPL/Space Science Institute, (2007), Released February 27, 2007, Giant Lake on Titan, PIA 08363, 08364, http://ciclops.org/view.php?id=2607.

NASA/JPL/Space Science Institute, (2007), Released March 15, 2007, Exploring the wetlands of Titan, PIA 08365, http://ciclops.org/view.php?id=2631.

NASA/JPL/Space Science Institute, (2005), Land of lakes, Released June 28, 2005 and March 15, 2007, PIA 06240, http://ciclops.org/view.php?id=1161.

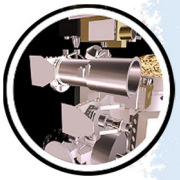

NASA/JPL/Space Science Institute, (2005), NASA'S Cassini reveals lake-like feature on Titan, Released June 28, 2005, http://ciclops.org/view.php?id=1194.

Nixon, C. A., R. D. Lorenz, R. K. Achterberg, A. Buch, P. Coll, R. N. Clark, R. Courtin, et al., (2018), Titan's cold case files-outstanding questions after Cassini-Huygens, Planetary and Space Science 155, 50–72.

O'Neill, C. & F. Nimmo, (2010), The role of episodic overturn in generating the surface geology and heat flow on Enceladus, Nature Geoscience 3, 88–91.

Ordonez-Etxeberria, I., R. Hueso, A. Sanchez-Lavega, S. Perez-Hoyos, (2016), Spatial distribution of Jovian clouds, hazes and colors from Cassini ISS multi-spectral images, Icarus, 267, 34–50, doi: 10.1016/j.icarus.2015.12.008.

Patterson, G. W., S. J. Kattenhorn, P. Helfenstein, G. C. Collins, R. T. Pappalardo, (2018), The geology of Enceladus, In Enceladus and the Icy Moons of Saturn, (eds.) P. M. Schenk, R. N. Clark, C. J. A. Howett, A. J. Verbiscer, J. H. Waite, Space Science Series, The University of Arizona Press, Tucson, AZ.

Pérez-Hoyos, S., J. F. Sanz-Requena, A. Sánchez-Lavega, P. G. J. Irwin, A. Smith, (2016), Saturn's tropospheric particles phase function and spatial distribution from Cassini ISS 2010-11 observations, Icarus 277, 1–18, doi: 10.1016/j.icarus.2016.04.022.

Pérez-Hoyos, S., and A. Sánchez-Lavega, (2006), On the vertical wind shear of Saturn's equatorial jet at cloud level, Icarus 180, 161–175.

Perry, J., E. P. Turtle, A. S. McEwen, D. D. Dawson, C. C. Porco, (2007), Cassini ISS observations of Titan's trailing hemisphere, Bulletin of the American Astronomical Society, 39, #44.04.

Perry J. E., A. S. McEwen, S. Fussner, E. P. Turtle, R. A. West, C. C. Porco, B. Knowles, D. D. Dawson, Cassini ISS team, (2005), Processing ISS images of Titan's surface, Lunar and Planetary Science XXXVI, Part 16, LPI-Contrib-1234-Pt-16.

Porco, C., C. Mitchell, F. Nimmo, M. Tiscareno, (2018), Enceladus' plume temporal variability from analysis of Cassini ISS images, 49th Lunar and Planetary Institute Conference, abstract 2083.

Porco, C., L. Dones, C. Mitchell, (2017), Could it be snowing microbes on Enceladus? Assessing conditions in its plume and implications for future missions, Astrobiology 17, 876–901.

Porco, C., F. Nimmo, and D. DiNino, (2015), Enceladus' 101 Geysers: Phantoms? Hardly, In American Geophysical Union (AGU) Fall Meeting, San Francisco, CA, 14–18 December, abstract P13A-2118.

Porco, C., D. DiNino, F. Nimmo, (2014), How the geysers, tidal stresses, and thermal emissions across the south polar terrain of Enceladus are related, The Astronomical Journal 148, 45.

Porco, C., J. Weiss, D. Richardson, L. Dones, T. Quinn, H. Throop, (2008), Simulations of the dynamical and light-scattering behavior of Saturn's rings and the derivation of ring particle and disk properties, The Astronomical Journal 136, 2172–2200.

- - - - - - - - - - - - - -

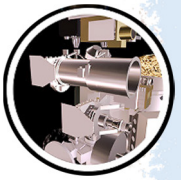

Porco, C., P. Thomas, J. Weiss, D. Richardson, (2007), Saturn's small inner satellites: Clues to their origins, Science 318, 1602–1607.

Porco, C. C., P. Helfenstein, P. C. Thomas, A. P. Ingersoll, J. Wisdom, R. West, G. Neukum, et al., (2006), Cassini observes the active south pole of Enceladus, Science 311, 1393–1401.

Porco, C. C., E. Baker, J. Barbara, K. Beurle, A. Brahic, et al., (2005a), Cassini Imaging Science: Initial results on Saturn's atmosphere, Science 307, 1243–1247.

Porco, C. C., E. Baker, J. Barbara, K. Beurle, A. Brahic, et al., (2005b), Imaging of Titan from the Cassini spacecraft, Nature 434, pp. 159–168.

Porco, C. C., E. Baker, J. Barbara, K. Beurle, A. Brahic, et al., (2005c), Cassini Imaging Science: Initial results on Saturn's rings and small satellites, Science 307, 1226–1236.

Porco, C. C., E. Baker, J. Barbara, K. Beurle, A. Brahic, et al., (2005d), Cassini Imaging Science: Initial results on Phoebe and Iapetus, Science 307, 1237–1242.

Porco, C. C., (2005), Cassini Imaging Science: Saturn's rings and small satellites, Geological Society of America, 2005 annual meeting, Salt Lake City, UT, Oct. 16-19, vol 37, 7, p. 236

Porco, C. C., R. A. West, S. Squyres, A. McEwen, P. Thomas, C. D. Murray, A. Delgenio, et al., (2004), Cassini Imaging Science: Instrument characteristics and anticipated scientific investigations at Saturn, Space Science Reviews 115, 363–497.

Porco, C. C., R. A. West, A. McEwen, A. D. Del Genio, A. P. Ingersoll, P. Thomas, S. Squyres et al., (2003), Cassini imaging of Jupiter's atmosphere, satellites, and rings, Science, 299, 5612, 1541–1547, doi: 10.1126/science.1079462.

Postberg, F., R. N. Clark, C. J. Hansen, A. J. Coates, C. M. D. Ore, F. Scipioni, M. M. Hedman, J. Hunter Waite, (2018), Plume and surface composition of Enceladus, In Enceladus and the Icy Moons of Saturn, (eds.) P. M. Schenk, R. N. Clark, C. J. A. Howett, A. J. Verbiscer, J. H. Waite, Space Science Series, The University of Arizona Press, Tucson, AZ.

Rathbun, J. A., E. P. Turtle, P. Helfenstein, S. W. Squyres, P. Thomas, J. Veverka, T. Denk, G. Neukum, T. Roatsch, R. Wagner, J. Perry, D. Smith, T. V. Johnson, C. C. Porco, (2005), Enceladus' global geology as seen by Cassini ISS, American Geophysical Union (AGU), Fall Meeting 2005, abstract P32A-03.

Read, P. L., P. J. Gierasch, B. J. Conrath, A. Simon-Miller, T. Fouchet, Y. H. Yamazaki, (2006), Mapping potential-vorticity dynamics on Jupiter. I: Zonal-mean circulation from Cassini and Voyager 1 data, Quarterly Journal of the Royal Meteorological Society, 132, 618, 1577–1603, doi: 10.1256/qj.05.34.

Renner, S., N. Cooper, M. El Moutamid, B. Sicardy, A. Vienne, C. Murray, M. Saillenfest, (2016), Origin of the chaotic motion of the Saturnian satellite Atlas, The Astronomical Journal 151, 122–129.

Roatsch, T., R. J. Wagner, N. Schmedemann, P. Helfenstein, K. Stephan, J. Voigt, R. Jaumann, B. Giese, C. Porco, (2016), Stratigraphy in the Samarkand Sulci Region of Enceladus, American Geophysical Union (AGU), Fall Meeting 2016, abstract P33A-2125.

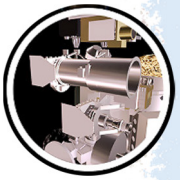

Roatsch T., E. Kersten, A. Hoffmeister, M. Wählisch, K.-D. Matz, C. C. Porco, (2013), Recent improvements of the Saturnian satellites atlases: Mimas, Enceladus, and Dione. Planetary Space Science 77, 118–125.

Roatsch, T., E. Kersten, M. Wählisch, A. Hoffmeister, K.-D. Matz, F. Scholten, R. Wagner, T. Denk, G. Neukum, C. C. Porco, (2012), High resolution atlas of Rhea as derived from Cassini ISS Images, Planetary and Space Sciences 61, 135–141.

Roatsch, T., R. Jaumann, K. Stephan, P.C. Thomas, (2009a), Cartographic mapping of the Icy Satellites using ISS and VIMS data, In Saturn from Cassini-Huygens, (eds.) M. Dougherty, L. Esposito, S. Krimigis, Springer, Dordrecht, pp. 763–781, doi: 10.1007/978-1-4020-9217-6_24.

Roatsch, T., M. Wählisch, A. Hoffmeister, E. Kersten, K.-D. Matz, F. Scholten, R. Wagner, T. Denk, G. Neukum, P. Helfenstein, C. C. Porco, (2009b), High resolution atlases of Mimas, Tethys, and Iapetus derived from Cassini ISS images, Planetary and Space Science 57, pp. 83–92.

Roatsch, T., M. Wählisch, B. Giese, A. Hoffmeister, K.-D. Matz, F. Scholten, R. Wagner, G. Neukum, P. Helfenstein, C. C. Porco, (2008a), High resolution Enceladus atlas derived from Cassini ISS Images, Planetary and Space Sciences 56, 109–116.

Roatsch, T., M. Wählisch, A. Hoffmeister, K.-D. Matz, F. Scholten, E. Kersten, R. Wagner, T. Denk, G. Neukum, C. C. Porco, (2008b), High resolution Dione atlas derived from Cassini ISS Images, Planetary and Space Science 56, 1499–1505.

Roatsch, T., M. Wählisch, F. Scholten, A. Hoffmeister, K.-D. Matz, T. Denk, G. Neukum, P.C. Thomas, P. Helfenstein, C.C. Porco, (2006), Mapping of the icy Saturnian satellites: First results from Cassini ISS, Planetary and Space Science 54, 1137–1145.

Roman, M. T., R. A. West, D. J. Banfield, P. J. Gierasch, R. K. Achterberg, C. A. Nixon, P. C. Thomas, (2009), Determining a tilt in Titan's north-south Albedo asymmetry from Cassini Images, Icarus 203, 242–249.

Salyk, C., A. P. Ingersoll, J. Lorre, A. Vasavada, A. D. Del Genio, (2006), Interaction between eddies and mean flow in Jupiter's atmosphere: Analysis of Cassini imaging data, Icarus, 185, 2, 430–442, doi: 10.1016/j.icarus.2006.08.007.

Sánchez-Lavega, A., E. García-Melendo, S. Perez-Hoyos, R. Hueso, M. H. Wong, A. Simon, J. Francisco Sanz-Requena, et al., (2016), An enduring rapidly moving storm as a guide to Saturn’s equatorial jet’s complex structure, Nature Communications 7, 13262.

Sánchez-Lavega, A., T. del Río-Gaztelurrutia, R. Hueso, S. Pérez-Hoyos, E. García-Melendo, et al., (2014), The long-term steady motion of Saturn’s hexagon and the stability of its enclosed jet stream under seasonal changes, Geophysical Research Letters 41, 1425–1431.

Sánchez-Lavega, A., T. del Río-Gaztelurrutia, R. Hueso, J. M. Gómez-Forrellad, J. F. Sanz-Requena, J. Legarreta, E. García-Melendo, et al., (2011), Deep winds beneath Saturn’s upper clouds from a seasonal long-lived planetary-scale storm, Nature 475, 71–74.

- - - - - - - - - - - - - -

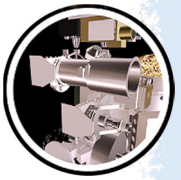

Sánchez-Lavega, A., R. Hueso, S. Pérez-Hoyos, (2007), The three-dimensional structure of Saturn's equatorial jet at cloud level, Icarus 187, 510–519.

Sánchez-Lavega, A., R. Hueso, S. Pérez-Hoyos, J. F. Rojas, (2006), A strong vortex in Saturn's South Pole, Icarus 184, 524–531.

Sato, T. M., T. Satoh, Y. Kasaba, (2013), Retrieval of jovian cloud structure from the Cassini ISS limb-darkening data I. Continuum scattering phase functions for cloud and haze in the south tropical zone, Icarus, 222, 1, 100–121, doi: 10.1016/j.icarus.2012.09.035.

Sayanagi, K. M., K. H. Baines, U. A. Dyudina, L. N. Fletcher, A. Sanchez-Lavega, R. A. West, (2018), Saturn's polar atmosphere, In Saturn in the 21st Century, (eds.) Baines et al., in press.

Sayanagi, K. M., J. J. Blalock, U. A. Dyudina, S. P. Ewald, A. P. Ingersoll, (2017), Cassini ISS observation of Saturn's north polar vortex and comparison to the south polar vortex, Icarus 285, 68–82.

Sayanagi, K., U. Dyudina, S. Ewald, G. Muro, A. Ingersoll, (2014), Cassini ISS observation of Saturn's string of pearls, Icarus 229, 170–180.

Sayanagi, K., U. Dyudina, S. Ewald, G. Fischer, A. Ingersoll, W. Kurth, G. Muro, C. Porco, R. West, (2013), Dynamics of Saturn's great storm of 2010–2011 from Cassini ISS and RPWS, Icarus 223, 460–478.

Sayanagi, K. M., R. Morales-Juberias, and A. P. Ingersoll, (2010), Saturn's northern hemisphere ribbon: Simulations and comparison with the meandering gulf stream, Journal of the Atmospheric Sciences 67, 2658–2678.

Sayanagi, K. M., and A. P. Showman, (2007), Effects of a large convective storm on Saturn's equatorial jet, Icarus 187, 520–539.

Schenk, P., O. White, P. K. Byrne, J. M. Moore, (2018), Saturn's other icy moons: Geologic entities in their own right, In Enceladus and the Icy Moons of Saturn, (eds.) P. M. Schenk, R. N. Clark, C. J. A. Howett, A. J. Verbiscer, J. H. Waite, Space Science Series, The University of Arizona Press, Tucson, AZ, doi: 10.2458/azu_uapress_9780816537075-ch012.

Schenk, P., B. Buratti, P. Helfenstein, S. Kempf, J. Schmidt, (2017), Colors of Enceladus: Plume redeposition and lessons for Europa, 48th Lunar and Planetary Science Conference, LPI Contribution No. 1964, id. 2601.

Schenk, P. M., B. J. Buratti, P. K. Byrne, W. B. McKinnon, F. Nimmo, F. Scipioni, (2015), Blood stains on Tethys: Evidence for recent activity? European Planetary Science Congress 2015, vol. 10, EPSC2015-893.

Schenk, P. M., D. P. Hamilton, R. E. Johnson, W. B. McKinnon, C. Paranicas, J. Schmidt, M. R. Showalter, (2011), Plasma, plumes and rings: Saturn system dynamics as recorded in global color patterns on its midsize icy satellites, Icarus 211, 740–757.

Schmedemann, N., A. Neesemann, F. Schulzeck, K. Krohn, I. van der Gathen, K. A. Otto, R. Jaumann, R. J. Wagner, G. Michael, C. A. Raymond, C. T. Russell, (2017), How the

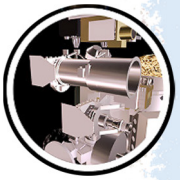

distribution of impact Ejecta may explain surface features on Ceres and Saturnian satellites. European Planetary Science Congress, EPSC2017-119, Riga, 17–22 Sep 2017.

Schmedemann, N., R. J. Wagner, G. Michael, T. Denk, T. Kneissl, (2015), The crater production functions for Mimas. Workshop on Early Solar System Impact Bombardment III, abstract 3021, Houston, TX, 4–5 Feb 2015.

Schmedemann, N., and G. Neukum, (2011), Impact crater size-frequency distribution (SFD) and surface Ages on Mimas. 42nd Lunar and Planetary Science Conference, abstract 2772.

Shetty, S., and P. S. Marcus, (2010), Changes in Jupiter's Great Red Spot (1979–2006) and Oval BA (2000–2006), Icarus, 210, 1, 182–201, doi: 10.1016/j.icarus.2010.06.026.

Simon-Miller, A. A., J. H. Rogers, P. J. Gierasch, D. Choi, M. D. Allison, G. Adamoli, H. J. Mettig, (2012), Longitudinal variation and waves in Jupiter's south equatorial wind jet, Icarus, 218, 2, 817–830, doi: 10.1016/j.icarus.2012.01.022.

Simon-Miller, A. A., and P. J. Gierasch, (2010), On the long-term variability of Jupiter's winds and brightness as observed from Hubble, Icarus, 210, 1, 258–269, doi: 10.1016/j.icarus.2010.06.020.

Singer, K. N., W. B. McKinnon, P. M. Schenk, J. M. Moore, (2012), Massive ice avalanches on Iapetus mobilized by friction reduction during flash heating. Nature Geoscience 5, 574–578.

Singer, K. N., and W. B. McKinnon, (2011), Tectonics on Iapetus: Despinning, respinning, or something completely different? Icarus 216, 198–211.

Spahn, F., H. Hoffmann, H. Rein, M. Seiß, M. Sremcevic, M. S. Tiscareno, (2018), Moonlets in dense planetary rings, In Planetary Ring Systems: Properties, Structure, and Evolution, (eds.) M. S. Tiscareno, C. D. Murray, Cambridge, United Kingdom Cambridge University Press, 157–197.

Spencer, J. R., and T. Denk, (2010), Formation of Iapetus's extreme albedo dichotomy by exogenically-triggered thermal ice migration, Science 327, no. 5964, 432–435, doi: 10.1126/science.1177132).

Spencer, J. R., et al., (2009), Enceladus: An active cryovolcanic satellite, In Saturn from Cassini-Huygens, Springer, Netherlands, 683–724.

Spilker, L. J., A. C. Barr, L. W. Esposito, P. Helfenstein, A. P. Ingersoll, R. Jaumann, C. P. McKay, F. Nimmo, J. H. Waite, (2018), Thermal properties of rings and ring particles, In Planetary Ring Systems: Properties, Structure, and Evolution, (eds.) M. S. Tiscareno, C. D. Murray, Cambridge, United Kingdom, Cambridge University Press, 399–433.

Spitale, J. N., (2017), Saturn’s misbegotten moonlets, AAS/DDA Meeting, abstracts 48, 400.04.

Spitale, J. N., and J. M. Hahn, (2016), The shape of Saturn’s Huygens ringlet viewed by Cassini ISS, Icarus 279, 141–154.

Spitale, J. N., T. A. Hurford, A. R. Rhoden, E. E. Berkson, and S. P. Symeon, (2015), Curtain eruptions from Enceladus’ south-polar terrain, Nature 521, 57.

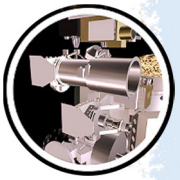

Spitale, J. N., and M. S. Tiscareno, (2012), Cassini images a propeller in Saturn's B-ring, AAS/DPS Meeting, abstracts 44, 414.04.

Spitale, J. N., and C. C. Porco, (2010), Free unstable modes and massive bodies in Saturn's Outer B-ring, The Astronomical Journal 140, 1747–1757.

Spitale, J. N., and C. C. Porco, (2009), Time variability in the outer edge of Saturn's A-ring revealed by Cassini Imaging, The Astronomical Journal 138, 1520–1528.

Spitale, J., and C. Porco, (2007), Association of the jets of Enceladus with the warmest regions on its south polar fractures, Nature 449, 695–697.

Spitale, J. N., R. A. Jacobson, C. C. Porco, W. M. Owen Jr., (2006), The orbits of Saturn's small Satellites derived from combined historic and Cassini imaging observations, The Astronomical Journal 132, 692–710.

Stephan, K., R. Jaumann, R. Wagner, R. N. Clark et al., (2010), Dione's spectral and geological properties, Icarus 206, 631–652.

Stephan K., R. Jaumann, E. Karkoschka, R. L. Kirk, J. W. Barnes, M. G. Tomasko, E. P. Turtle, L. LeCorre, M. Langhans, S. Le Mouélic, R. D. Lorenz, J. Perry, (2009), Mapping products of Titan's surface, In Titan from Cassini-Huygens, (eds.) R. Brown, J.-P. Lebreton, and H. Waite, Springer, New York, NY, pp. 489–510.

Sussman, M. G., N. J. Chanover, A. A. Simon-Miller, A. R. Vasavada, R. F. Beebe, (2010), Analysis of Jupiter's Oval BA: A streamlined approach, Icarus, 210, 1, 202–210, doi: 10.1016/j.icarus.2010.06.044.

Tajeddine, R., K. M. Soderlund, P. C. Thomas, P. Helfenstein, M. M. Hedman, J. A. Burns, P.M. Schenk, (2017a), True polar wander of Enceladus from topographic data, Icarus 295, pp. 46–60.

Tajeddine, R., P. Nicholson, M. Tiscareno, M. Hedman, J. Burns, M. El Moutamid, (2017b), Dynamical phenomena at the inner edge of the Keeler gap, Icarus 289, 80–93.

Tajeddine, R., P. D. Nicholson, P.-Y. Longaretti, M. El Moutamid, J. A. Burns, (2017c), What confines the rings of Saturn?, The Astrophysical Journal Supplement 232, 28.

Tajeddine, R., V. Lainey, N. Cooper, C. Murray, (2015), Cassini ISS astrometry of the Saturnian satellites: Tethys, Dione, Rhea, Iapetus, and Phoebe 2004–2012, Astronomy & Astrophysics 575, A73.

Tajeddine, R., N. J. Cooper, V. Lainey, S. Charnoz, C. D. Murray, (2013), Astrometric reduction of Cassini ISS images of the Saturnian satellites Mimas and Enceladus, Astronomy & Astrophysics 551, A129–A139.

Tamayo, D., S. R., Markham, M. M. Hedman, J. A. Burns, D. P. Hamilton, (2016), Radial profiles of the Phoebe ring: A vast debris disk around Saturn, Icarus 275, 117–131.

Tamayo, D., M. M. Hedman, J. A. Burns, (2014), First observations of the Phoebe ring in optical light, Icarus 233, 1–8.

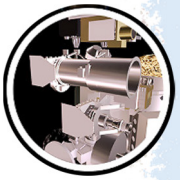

Teolis, B., M. Perry, C. Hansen, H. Waite, C. Porco, J. Spencer, C. Howett, (2017), Enceladus plume structure and time variability: Comparison of Cassini observations, Astrobiology 17, 9, 926–940.

Thomas, P. C., M. S. Tiscareno, P. Helfenstein, (2018), The inner small satellites of Saturn and Hyperion, In Enceladus and the Icy Moons of Saturn, (eds.) P. M. Schenk, R. N. Clark, C. J. A. Howett, A. J. Verbiscer, J. H. Waite, Space Science Series, The University of Arizona Press, Tucson, AZ.

Thomas, P., R. Tajeddine, M. Tiscareno, J. Burns, J. Joseph, T. Loredo, P. Helfenstein, C. Porco, (2016), Enceladus's measured physical libration requires a global subsurface ocean, Icarus 264, 37–47.

Thomas, P., J. Burns, M. Hedman, P. Helfenstein, S. Morrison, M. Tiscareno, J. Veverka, (2013), The inner small satellites of Saturn: A variety of worlds, Icarus 226, 99–1019.

Thomas, P. C., (2010), Sizes, shapes, and derived properties of the Saturnian satellites after the Cassini nominal mission, Icarus 208, 395–401, doi: 10.1016/j.icarus.2010.01.025.

Thomas, P. C., J. A. Burns, P. Helfenstein, S. Squyres, J. Veverka, C. Porco, E. P. Turtle, A. McEwen, T. Denk, B. Giese, T. V. Roatsch, R. A. Jacobson, (2007a), Shapes of the Saturnian icy satellites and their significance, Icarus 190, 573–584.

Thomas, P., J. Armstrong, S. W. Asmar, J. A. Burns, T. Denk, B. Giese, P. Helfenstein, L. Iess, T. V. Johnson, A. McEwen, L. Nicolaisen, C. Porco, N. Rappaport, J. Richardson, L. Somenzi, P. Tottora, E. P. Turtle, J. Veverka, (2007b), Hyperion's sponge-like appearance, Nature 448, 50–53.

Throop, H. B., C. C. Porco, R. A. West, J. A. Burns, M. R. Showalter, P. D. Nicholson, (2004), The Jovian rings: new results derived from Cassini, Galileo, Voyager, and Earth-based observations, Icarus 172, 59–77.

Tiscareno, M., and B. Harris, (2018), Mapping spiral waves and other radial features in Saturn's rings, Icarus, 312, 157–171, doi: 10.1016/j.icarus.2018.04.023.

Tiscareno, M. S., (2017), Imaging of Saturn's main rings during the Cassini Ring-Grazing Orbits and Grand Finale, EPSC Meeting, abstracts, EPSC2017-996.

Tiscareno, M., M. Hedman, J. Burns, J. Weiss, C. Porco, (2013a), Probing the inner boundaries of Saturn's A-ring with the Iapetus -1:0 nodal bending wave, Icarus 224, 221.

Tiscareno, M., C. Mitchell, C. Murray, D. Di Nino, M. Hedman, J. Schmidt, J. Burns, J. Cuzzi, C. Porco, K. Beurle, M. Evans, (2013b), Observations of ejecta clouds produced by impacts onto Saturn's rings, Science 340, 460.

Tiscareno, M. S., J. A. Burns, J. N. Cuzzi, M. W. Hedman, (2010a), Cassini imaging search rules out rings around Rhea, Geophysical Research Letters 37, L14205.

Tiscareno, M. S., J. A. Burns, M. Sremcevic, K. Beurle, M. M. Hedman, N. J. Cooper, A. J. Milano, M. W. Evans, C. C. Porco, J. N. Spitale, J. W. Weiss, (2010b), Physical characteristics

---

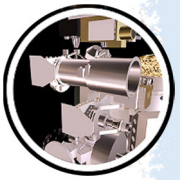

and non-Keplerian orbital motion of propeller, Moons Embedded in Saturn's Rings, Astrophysical Journal Letters 718, L92–L96.

Tiscareno, M., P. C. Thomas, J. A. Burns, (2009), The rotation of Janus and Epimetheus, Icarus 204, 254–261.

Tiscareno, M. S., J. A. Burns, M. M. Hedman, C. C. Porco, (2008), The population of propellers in Saturn's A-ring, The Astronomical Journal 135, 1083–1091.

Tiscareno, M. S., J. A. Burns, P. D. Nicholson, M. M. Hedman, C. C. Porco, (2007), Cassini imaging of Saturn's rings II: A wavelet technique for analysis of density waves and other radial structure in the rings, Icarus 189, 14–34.

Tiscareno, M. S., J. A. Burns, M. M. Hedman, C. C. Porco, J. W. Weiss, L. Dones, D. C. Richardson, C. D. Murray, (2006a), 100-metre-diameter moonlets in Saturn's A-ring from observations of propeller structures., Nature 440, 648–650.

Tiscareno, M. S., P. D. Nicholson, J. A. Burns, M. M. Hedman, C. C. Porco, (2006b), Unraveling temporal variability in Saturn's spiral density waves: Results and predictions, Astrophysical Journal Letters 651, L65–L68.

Tomasko, M. G., R. A. West, (2009), Aerosols in Titan's atmosphere, In Titan from Cassini-Huygens, (eds.) R. Brown, J. P. Lebreton, H. Waite, Springer, Dordrecht, pp. 297–322.

Trammell, H. J., L. Li, X. Jiang, Y. Pan, M. A. Smith, et al., (2016), Vortices in Saturn’s northern hemisphere (2008–2015) observed by Cassini ISS, Journal of Geophysical Research: Planets 121, 1814–1826.

Trammell, H. J., L. Li, X. Jiang, M. Smith, S. Hörst, A. Vasavada, (2014), The global vortex analysis of Jupiter and Saturn based on Cassini Imaging Science Subsystem, Icarus 242, pp. 122–129.

Turtle E. P., J. E. Perry, J. M. Barbara, A. D. Del Genio, C. Sotin, S. Rodriguez, J. M. Lora, S. Faulk, R. A. West, E. Karkoschka, A. S. McEwen, M. Mastrogiuseppe, J. D. Hofgartner, P. Corlies, J. Kelland, A. G. Hayes, J. Pitesky, T.L. Ray, (2018a), Titan insights during the final year of the Cassini Mission, LPSC 49, #1656.

Turtle E. P., J. E. Perry, J. M. Barbara, A. D. Del Genio, S. Rodriguez, S. Le Mouélic, C. Sotin, J. M. Lora, S. Faulk, P. Corlies, J. Kelland, S. M. MacKenzie, R. A. West, A. S. McEwen, J. I. Lunine, J. Pitesky, T. L. Ray, M. Roy, (2018b), Titan's meteorology over the Cassini mission: Evidence for extensive subsurface methane reservoirs, Geophysical Research Letters 45, no. 11, 5320–5328.

Turtle E .P., J. W. Barnes, J. E. Perry, J. M. Barbara, A. G. Hayes, P. Corlies, J. Kelland, R. A. West, A. D. Del Genio, J. M. Soderblom, A. S. McEwen, C. Sotin, (2016), Cassini ISS and VIMS observations of Titan's north polar region during the T120 and T121 flybys: The Curious case of the clouds, Fall Meeting American Geophysical Union (AGU), abstract P33F-05.

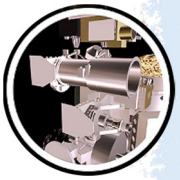

Turtle E. P., J. E. Perry, A. S. McEwen, A. G. Hayes, J. W. Barnes, R. A. West, (2013), ISS observations of Titan's northern lakes and evidence for a north-polar surface unit, Fall Meeting American Geophysical Union (AGU), 9–13 Dec. 2013, abstract P53D-1897.

Turtle E. P., A. D. DelGenio, J. M. Barbara, J. E. Perry, E. L. Schaller, A. S. McEwen, R. A. West, T. L. Ray, (2011a) Seasonal changes in Titan's meteorology, Geophysical Research Letters 38, L03203, doi: 10.1029/2010GL046266.

Turtle E. P., J. E. Perry, A. G. Hayes, R. D. Lorenz, J. W. Barnes, A. S. McEwen, R. A. West, A. D. Del Genio, J. M. Barbara, J. I. Lunine, E. L. Schaller, T. L. Ray, R. M. C. Lopes, E. R. Stofan, (2011b), Rapid and extensive surface changes near Titan's equator: Evidence of April Showers, Science 331, 1414–1417, doi: 10.1126/science.1201063.

Turtle E. P., J. E. Perry, A. G. Hayes, A. S. McEwen, (2011c), Shoreline retreat at Titan's Ontario Lacus and Arrakis Planitia from Cassini Imaging Science Subsystem observations, Icarus 212, 957–959, doi: 10.1016/j.icarus.2011.02.005.

Turtle E. P., J. E. Perry, A. S. McEwen, A. D. DelGenio, J. Barbara, R. A. West, D. D. Dawson, C. C. Porco, (2009), Cassini imaging of Titan's high-latitude lakes, clouds, and south-polar surface changes, Geophysical Research Letters 36, L02204, doi: 10.1029/2008GL036186.

Vasavada, A. R., S. M. Hörst, M. R. Kennedy, A. P. Ingersoll, C. C. Porco, A. D. Del Genio, R. A. West, (2006), Cassini imaging of Saturn: Southern hemisphere winds and vortices, Journal of Geophysical Research-Planets 111, E05004.

Verbiscer, A. J., P. Helfenstein, B. J. Buratti, E. Royer, (2018), Surface properties of Saturn's Icy Moons from optical remote sensing, In Enceladus and the Icy Moons of Saturn, (eds.) P. M. Schenk, R. N. Clark, C. J. A. Howett, A. J. Verbiscer, J. H. Waite, Space Science Series, The University of Arizona Press, Tucson, AZ.

Verbiscer, A. J., P. Helfenstein, C. Howett, A. Annex, P. Schenk, (2014), Spectrophotometric properties of thermally anomalous terrain on Mimas, American Astronomical Society DPS meeting #46, 502.08.

Wagner, R. J., B. Giese, N. Schmedemann, K. Stephan, J. Voigt, P. Helfenstein, E. Kersten, T. Roatsch, R. Jaumann, C. C., (2017), Samarkand Sulci, Enceladus: Topography and geology from the data of the Cassini 2 Porco, 28EN Non-Targeted Flyby in Global Context, 48th Lunar & Planetary Science Conference, LPI Contribution no. 1964, id. 2262.

Wagner, R. J., G. Neukum, U. Wolf, N. Schmedemann, T. Denk, K. Steohan, T. Roatsch, C. C. Porco, (2011), Bright ray craters on Rhea and Dione, 42nd Lunar and Planetary Science Conference, abstract 2249.

Wagner, R. J., G. Neukum, B. Giese, T. Roatsch, T. Denk, U. Wolf, C. C. Porco, (2010), The Geology of Rhea: A first look at the ISS camera data from Orbit 121 (Nov. 21, 2009) in Cassini's Extended Mission, 41st Lunar and Planetary Science Conference, abstract 1672, LPI, The Woodlands (Texas), 1–5 March 2010.

Wagner, R. J., G. Neukum, K. Stephan, T. Roatsch, U. Wolf, and C. C. Porco, (2009), Stratigraphy of tectonic features on Saturn's satellite Dione derived from Cassini ISS camera

- - - - - - - - - - - - - -

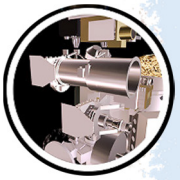

data. 40th Lunar and Planetary Science Conference, abstract 2142, LPI, Houston (Texas), 23-37 March 2009.

Wagner, R., G. Neukum, B. Giese, T. Roatsch, and T. Denk, (2007), Geology and geomorphology of Rhea: A first look at the high-resolution Cassini ISS images from the targeted flyby on Aug. 30, 2007, EOS Transactions American Geophysical Union (AGU), Fall Meeting Supplement, abstract P12B-06.

Wagner, R. J., G. Neukum, B. Giese, T. Roatsch, U. Wolf, T. Denk, Cassini ISS team, (2006), Geology, ages, and topography of Saturn's satellite Dione observed by the Cassini ISS camera, 37th Lunar and Planetary Science Conference, abstract 1805, LPI, Houston (Texas), 13–17 March 2006.

Weiss, J. W., C. C. Porco, M. S. Tiscareno, (2009), Ring edge waves and the masses of nearby satellites, The Astronomical Journal 138, 272–286.

West, R. A., B. Seignovert, P. Rannou, P. Dumont, E. P. Turtle, J. E. Perry, M. Roy, A. Ovanessian, (2018), Titan’s detached haze seasonal cycle, Nature Astronomy vol. 2, pp. 495-500, doi: 10.1038/s41550-018-0434-z.

West, R. A., A. D. Del Genio, J. M. Barbara, D. Toledo, P. Lavvas, P. Rannou, E. P. Turtle, J. Perry, (2016), Cassini Imaging Science subsystem observations of Titan's south polar cloud, Icarus 270, 399–408, doi: 10.1016/ j.icarus.2014.11.038.

West, R. A., P. Yanamandra-Fisher, V. Korokhin, (2015), Gas giant planets, Saturn’s rings, and Titan, In Polarimetry of Stars and Planetary Systems, (eds.) L. Kolokolova, J. Hough, A.-C. Levasseur-Regourd, Cambridge University Press.

West, R., P. Lavvas, C. Anderson, H. Imanaka, (2014), Titan haze, Titan: Surface, atmosphere and magnetosphere 285–321, http://ciclops.org/media/sp/2015/8014_19222_0.pdf.

West, R. A., J. M. Ajello, M. H. Stevens, D. F. Strobel, G. R. Gladstone, J. S. Evans, E. T. Bradley, (2012), Titan airglow during eclipse, Geophysical Research Letters 39, L18204, doi: 10.1029/2012GL053230.

West R. A., J. Balloch, P. Dumont, P. Lavvas, R. Lorenz, P. Rannou, T. Ray, E. P. Turtle, (2011), The evolution of Titan’s detached haze layer near equinox in 2009, Geophysical Research Letters 38, L06204, doi: 10.1029/2011GL046843.

West, R. A., B. Knowles, E. Birath, S. Charnoz, D. Di Nino, M. Hedman, P Helfenstein, A. McEwen, J. Perry, C. Porco, J. Salmon, H. Throop, D. Wilson, (2010), In-flight calibration of the Cassini Imaging Science Subsystem cameras, Planetary and Space Science 58, 1475–1488, doi 10.1016/j.pss.2010.07.006.

West, R. A., K. H. Baines, E. Karkoschka and A. Sánchez-Lavega, (2009), Clouds and aerosols in Saturn's atmosphere, In Saturn from Cassini-Huygens, (eds.) M. K. Dougherty, L. W. Esposito and S. M. Krimigis, Springer, Dordrecht, pp. 161–179.

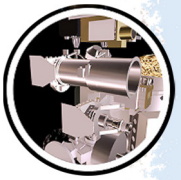

West, R. A., K. H. Baines, A. J. Friedson, D. Baneld, B. Ragent, and F. Taylor, (2004), Jovian clouds and haze, In Jupiter - The Planet, Satellites and Magnetosphere, (eds.) F. Bagenal, T. Dowling, W. McKinnon, Cambridge University Press.

White, O. L., P. M. Schenk, A. W. Bellagamba, A. M. Grimm, A. J. Dombard, V. J. Bray, (2017), Impact crater relaxation on Dione and Tethys and relation to past heat flow, Icarus 288, 37–52.

Young, R. M. B., and P. L. Read, (2017), Forward and inverse kinetic energy cascades in Jupiter's turbulent weather layer, Nature Physics, 13, 11, 1135.